

3D Failure Analysis of UD Fibre Reinforced Composites: Puck's Theory within FEA

H. Matthias Deuschle

INSTITUT FÜR
STATIK UND DYNAMIK
DER LUFT- UND
RAUMFAHRTKONSTRUKTIONEN

UNIVERSITÄT STUTTGART

3D Failure Analysis of UD Fibre Reinforced Composites: Puck's Theory within FEA

A thesis accepted by the Faculty of Aerospace Engineering and Geodesy
of the Universität Stuttgart in partial fulfilment of the requirements
for the degree of Doctor of Engineering Sciences (Dr.-Ing.)

by

Dipl.-Ing. H. Matthias Deuschle

born in Karlsruhe

Main referee: Prof. Dr.-Ing. habil. Bernd-Helmut Kröplin
Co-referee: Prof. Dr. rer. nat. Siegfried Schmauder
Date of defence: September 6, 2010

Institute of Statics and Dynamics of Aerospace Structures
Universität Stuttgart

2010

Herausgeber: Prof. Dr.-Ing. Bernd Kröplin

D93

ISBN 3-930683-99-7

Dieses Werk ist urheberrechtlich geschützt. Die dadurch begründeten Rechte, insbesondere die der Übersetzung, des Nachdrucks, des Vortrags, der Entnahme von Abbildungen und Tabellen, der Funksendung, der Mikroverfilmung oder der Vervielfältigung auf anderen Wegen und der Speicherung in Datenverarbeitungsanlagen, bleiben, auch bei nur auszugsweiser Verwertung, vorbehalten. Eine Vervielfältigung dieses Werkes oder von Teilen dieses Werkes ist auch im Einzelfall nur in den Grenzen der gesetzlichen Bestimmungen des Urheberrechtsgesetzes der Bundesrepublik Deutschland vom 9. September 1965 in der jeweils geltenden Fassung zulässig. Sie ist grundsätzlich vergütungspflichtig. Zuwiderhandlungen unterliegen den Strafbestimmungen des Urheberrechtsgesetzes.

© Institut für Statik und Dynamik der Luft- und Raumfahrtkonstruktionen,
Universität Stuttgart, Stuttgart, 2010

Dieser Bericht kann über das Institut für Statik und Dynamik der Luft- und Raumfahrtkonstruktionen, Universität Stuttgart, Pfaffenwaldring 27, 70569 Stuttgart, Telefon: (0711) 6856-63612, Fax: (0711) 6856-63706, bezogen werden.

Preface

The present work is the achievement of my activity as a research associate with the Institut für Statik und Dynamik der Luft- und Raumfahrtkonstruktionen (ISD) at the Universität Stuttgart. The completion of this dissertation has been possible thanks to the support of many people I would like to acknowledge:

Neither the participation in the WWFE-II nor the present thesis could have been realised without the continuous support of Professor Alfred Puck. The phase-wise daily cooperation has been of inestimable value for both, me personally and for the project. Thank you for your tireless effort to promote, generously share and impartially discuss your ideas. Your intellectual and literal hospitality will be a shining example to me.

I am deeply indebted to Professor Bernd-H. Kröplin who created and preserved an atmosphere of free thinking, mutual trust, independence and personal responsibility at his institute. These values have turned out to be precious in times of an increasing economisation and schoolification of the academic landscape. I am extremely grateful for the opportunity to benefit from as well as to contribute to the character of his outstanding institute.

Special thanks to Günther Lutz and the Institute of Plastics Processing at RWTH Aachen University who generously provided the opportunity to introduce myself to the "Puck community" in 2008. The daily backing of my ISD colleagues has however been just as important. I am particularly grateful to Dr. Thomas Wallmersperger and Manfred Hahn who have repeatedly delved deeply into my numerical and fracture mechanical problems. Thanks to the colleagues who made the effort to influence my way of thinking and formed the particular spirit of the ISD and to all undergraduate students who worked on relevant subjects within their theses.

I wish to express particular gratitude to my parents for providing a loving and respectful parental home. They have constantly striven to open new worlds of experience to me besides reliably funding my education. Eventually they have handed me over to my personal materials science consultant, my beloved wife who patiently takes excellent care of me in all aspects.

Stuttgart, September 2010

H. Matthias Deuschle

Abstract

Unidirectionally fibre reinforced composites (UD FRCs) are an aspiring material where high strength, adjustable stiffness, extraordinary durability and low weight is required. Their layer-wise processing into laminates enables the realisation of complex geometries with locally strongly differing properties. The design concept of integral construction makes use of this feature and combines different tasks in just one component. The increasing proportion of integral components brings significant savings in terms of structural weight and maintenance cost of the overall system. This development is currently opposed by an enormous experimental effort which comes along with the application of FRCs. The dimensioning of FRC laminates in terms of stiffness and strength has only hesitantly been included into efficient, computer-aided design processes. For the three-dimensional prediction of failure and post-failure behaviour there is currently no failure theory available, which would have been implemented into a powerful design tool like Finite Element Analysis (FEA) up to application maturity.

With Puck's fracture criteria for unidirectionally fibre reinforced polymer composites (UD FRPCs), however, there is a per se three-dimensional failure hypothesis, which has proven its capability in the case of plane states of stress and which is successfully applied within the according restrictions. The present work aims on the verification of this failure model for a general three-dimensional load case, its appropriate extension and the combination with the capabilities of a commercial FE software package. The result is an implementation which covers the layer-wise failure of a lamina and the successive damage evolution within the laminate. Together with the interlaminar damage analysis which is already comprised in such software packages, a comprehensive prediction tool for the damage process in UD FRC composites is generated.

The present work contains problems and approaches which are related to the achievement of the above mentioned goal. Starting with the representation of the nonlinear constitutive behaviour of an isolated lamina there occur specific three-dimensional problems. For example the material bears much more shear load under hydrostatic pressure, than comprised in the uniaxially determined experimental stress-strain relation. Such cases are treated by the self-similar scaling of the experimental curves. Being a stress-based criterion Puck's Theory requires the full spacial stress tensor, as soon as a three-dimensional prediction is striven for. It is shown that only few of the commercially implemented finite element formulations are capable of providing these results in the case of shell-like

structures. The quality of the results is evaluated by means of the analytical solution following Pagano. Puck's criteria for fibre and inter-fibre fracture (IFF) include some extensions which gain importance particularly in the three-dimensional stress case. The influences of fibre-parallel stress on the inter-fibre fracture and vice versa are presented in the present work and their fracture-mechanical basis is demonstrated. In particular the influence of stresses, which are not acting on the fracture plane, strongly increases in the three-dimensional case. The versatility of Puck's inter-fibre fracture criterion is proved by its adjustment to the application to isotropic and not intrinsically brittle materials. Regarding the successive three-dimensional damage after the occurrence of an inter-fibre fracture the existing degradation methods have been identified as insufficient. A fracture angle-dependent approach is developed, which homogenises the effect of the fractures and defines the impact on the several stiffnesses. Virtual material tests on representative laminate sections which contain discrete cracks prove the applicability of the developed relations. The described failure and post-failure degradation models are prepared for the application within an implicit Finite Element Analysis. Their implementation into the commercial software package ABAQUS is modular whereas the post-processing of conventionally derived or existing stress fields is sufficient for a pure failure prediction. Only if the post-failure degradation process is to be analysed, deeper manipulations of the FE analysis in form of a user-defined material subroutine are necessary. The applicability of the generated implementation is proved by the analysis of twelve test cases which are provided by the second World Wide Failure Exercise (WWFE-II). The given test cases comprise the failure and post-failure analysis of pure matrix material, of isolated laminae and of laminates subjected to three-dimensional load. All the test cases are treated with an identical subroutine, hence with a single, consistent failure theory and the results are interpreted regarding the actual material behaviour and the underlying failure prediction approaches. It is shown that the application of Puck's fracture hypotheses within a Finite Element Analysis is a versatile and efficient tool for the three-dimensional failure prediction in UD FRC laminates.

Zusammenfassung

Unidirektional faserverstärkte Verbundwerkstoffe sind überall dort ein zukunftssträchtiges Material, wo hohe Festigkeit, variable Steifigkeit, außerordentliche Haltbarkeit und leichtes Gewicht von Vorteil sind. Ihre schichtweise Verarbeitung zu Laminaten erlaubt es, komplexe Geometrien mit lokal stark unterschiedlichen Eigenschaften zu erzeugen. Das konstruktive Konzept der Integralbauweise macht sich diese Fähigkeiten zunutze und vereint so mehrere Aufgaben in *einem* Bauteil. Der zunehmende Anteil an Integralbauteilen erlaubt bedeutende Einsparungen hinsichtlich Gewicht und Wartungskosten des Gesamtsystems. Dieser Entwicklung steht momentan ein hoher experimenteller Aufwand entgegen, der mit der Verwendung von Faserverbund-Laminaten einher geht. Die Auslegung von Faserverbund-Laminaten hinsichtlich Steifigkeit und Festigkeit hat erst zögerlich Eingang in effiziente, computer-unterstützte Entwurfsprozesse gefunden. Für die dreidimensionale Vorhersage des Versagens- und Nachversagensverhalten steht momentan kein Versagensmodell bereit, das bis zur Anwendungsreife in ein leistungsfähiges Auslegungswerkzeug wie die Finite Elemente (FE) Analyse integriert wäre.

Mit den Puck'schen Bruchkriterien für unidirektional faserverstärkte Polymer-Verbunde steht jedoch eine per se dreidimensionale Versagenshypothese zur Verfügung, deren Leistungsfähigkeit für den ebenen Spannungsfall bereits bewiesen wurde und mit den entsprechenden Einschränkungen erfolgreich eingesetzt wird. Die vorliegende Arbeit verfolgt das Ziel, dieses Versagensmodell für den allgemeinen, dreidimensionalen Spannungsfall zu ertüchtigen, gegebenenfalls zu erweitern und mit der Leistungsfähigkeit einer kommerziellen FE-Software zu verbinden. Ergebnis ist eine Implementierung, die das schichtweise Versagen eines Laminates und die fortschreitende Schädigung des Verbundes umfasst. Zusammen mit den interlaminaren Schädigungsmodellen, die bereits in derartigen Softwarepaketen enthalten sind, ergibt sich so eine umfassende Vorhersagemöglichkeit des Schädigungsprozesses in Faserverbund-Laminaten.

Die vorliegende Arbeit behandelt Probleme und Lösungsansätze, die mit dem Erreichen dieses Ziels verbunden sind. Bereits bei der Abbildung des nichtlinearen konstitutiven Verhaltens einer Einzelschicht treten spezifisch dreidimensionale Probleme auf. Beispielsweise erträgt der Werkstoff unter hydrostatischem Druck weit mehr Schubbeanspruchung, als die einachsig ermittelte Schubspannungs-Scherungskurve umfasst. Solche Fälle werden durch die selbstähnliche Skalierung der experimentellen Kurven behandelt. Als spannungsbasiertes Kriterium benötigt Puck's Theorie den kom-

pletten räumlichen Spannungstensor, sobald eine dreidimensionale Vorhersage getroffen werden soll. Es wird gezeigt, dass nur wenige der kommerziell implementierten finiten Elementformulierungen in der Lage sind, dieses Ergebnis für schalenartige Strukturen bereit zu stellen. Die Güte dieser Ergebnisse wird anhand der analytischen Lösung nach Pagano beurteilt. Die Puck'schen Kriterien für Faser- und Zwischenfaserbruch umfassen eine Reihe von Erweiterungen, die gerade im räumlichen Spannungsfall an Relevanz gewinnen. Die Einflüsse von faserparallelen Spannungen auf den Zwischenfaserbruch und umgekehrt werden in dieser Arbeit dargelegt und ihr bruchmechanischer Hintergrund beleuchtet. Insbesondere der Einfluss der Spannungen, die nicht auf der Bruchebene wirken, nimmt im dreidimensionalen Fall stark zu. Die Vielseitigkeit des Puck'schen Zwischenfaserbruch-Kriteriums wird dadurch bewiesen, dass es an die Anwendung auf isotrope und nicht intrinsisch spröde Werkstoffe angepasst wird. Hinsichtlich der fortschreitenden dreidimensionalen Schädigung nach Eintreten eines Zwischenfaserbruches haben sich die vorhandenen Degradationsmethoden als unzureichend erwiesen. Es wird ein bruchwinkelabhängiges Verfahren entwickelt, mit dem die Auswirkung der Schädigung homogenisiert und den entsprechenden Steifigkeiten zugeschlagen wird. Durch virtuelle Materialtests an Laminat-Ausschnitten, die diskrete Risse enthalten, wird die Anwendbarkeit der entwickelten Zusammenhänge bestätigt. Die beschriebenen Versagens- und Degradationsmodelle werden zur Anwendung innerhalb einer impliziten FE Analyse aufbereitet. Ihre Implementierung in das kommerzielle Programmpaket ABAQUS kann modular erfolgen, wobei für die reine Versagensvorhersage ein Postprocessing von konventionell erzeugten oder bereits vorhandenen Spannungsfeldern ausreicht. Erst wenn das Degradationsverhalten entsprechend abgebildet werden soll, werden tiefere Eingriffe in die FE-Analyse in Form einer benutzerdefinierten Material-Subroutine notwendig. Die Anwendungstauglichkeit der entstandenen Implementierung wird durch die Analyse von zwölf Testfällen bewiesen, die dem World Wide Failure Exercise II entspringen. Die gegebenen Testfälle umfassen die Versagens- und Nachversagensanalyse von reinem Matrixmaterial, von Einzelschichten und Laminaten unter räumlicher Beanspruchung. Alle Testfälle werden mit der selben Subroutine, demnach mit *einem* konsistenten Versagensmodell bearbeitet und die Ergebnisse werden hinsichtlich des Materialverhaltens und modelltheoretisch interpretiert. Es wird gezeigt, dass die Anwendung der Puck'schen Bruchhypothesen im Rahmen der Finite Elemente Methode ein vielseitiges und effizientes Werkzeug zur dreidimensionalen Schadensvorhersage in Faserverbund-Laminaten darstellt.

Contents

1	Introduction	1
1.1	Motivation	1
1.2	Problems and aims	2
1.3	Structure of the present work	3
2	Failure of UD fibre-reinforced composites	7
2.1	Scales and coordinate systems of the material	7
2.1.1	Micro-mechanical level	7
2.1.2	Lamina level	8
2.1.3	Laminate level	8
2.1.4	Structural level	9
2.2	Types of failure	9
2.2.1	Micro-damage	9
2.2.2	Fibre fracture	10
2.2.3	Inter-fibre fracture	11
2.2.4	Delamination	12
2.3	Successive failure	12
2.3.1	Damage evolution in a confined lamina	13
2.3.2	Successive failure of a laminate	14
2.4	Failure on the structural level	15
2.4.1	Torsion spring	15
2.4.2	Integral vehicle rear suspension	16
2.4.3	Pressure vessel	17
3	3D stress analysis in laminates and structures	19
3.1	Constitutive behaviour of a lamina	19
3.1.1	Transverse isotropy and orthotropy	19
3.1.2	Nonlinearities in the constitutive behaviour	21

3.1.3	Interaction between transverse and shear deformation	23
3.2	FE representation of laminates and laminate structures	25
3.2.1	Equivalent single layer approaches	27
3.2.2	Layer-wise approach	28
3.3	Laminate and laminate structures in commercial FE codes	29
3.3.1	Material definitions for laminates	29
3.3.2	Element types for laminate structures	30
3.4	Reference: Analytical solution following Pagano	33
3.5	Generalised laminate behaviour: FEA of an RVE	38
3.6	Geometric nonlinearity	41
3.6.1	Load application	42
3.6.2	Engineering vs. true stresses and strains	42
3.7	Residual stresses	44
4	Puck's failure theory	45
4.1	Introduction to failure prediction	45
4.2	Puck's inter-fibre fracture criterion	47
4.2.1	Action plane-related fracture criterion	47
4.2.2	Application-oriented aspects of Puck's IFF criterion	51
4.2.3	Visual and mathematical representation – the MFB	54
4.2.4	IFF fracture modes classification for 3D analysis	58
4.3	Influences on the IFF beyond Mohr's hypothesis	60
4.3.1	Influences of fibre-parallel stress σ_1	60
4.3.2	Influence of non-fracture plane stresses	63
4.4	Puck's IFF criteria and the Mohr' circle	68
4.5	Confined laminae – the In-Situ Effect	71
4.6	Application of Puck's IFF criterion to special cases	71
4.6.1	Application to isotropic material	71
4.6.2	Application to not intrinsically brittle materials	73
4.7	Puck's fibre fracture criterion	74

5	Post-failure degradation analysis	77
5.1	Stability of the damage evolution in a laminate	77
5.2	Smearred crack representation	78
5.3	Existing degradation procedures	79
5.3.1	Excessive IFF stress exposure	80
5.3.2	Constant IFF stress exposure	82
5.4	Variable IFF stress exposure	84
5.5	3D degradation procedure	84
5.6	RVE-studies on a discrete cracks	88
5.6.1	Derivation of the equivalent stiffness of a damaging lamina	90
5.6.2	Results of the RVE virtual material tests	92
5.7	Application-oriented summary	98
6	Implementation of Puck's Theory in ABAQUS	99
6.1	Implicit and explicit FEA	99
6.2	User-defined material behaviour subroutine	101
7	World Wide Failure Exercise II	105
7.1	Degradation aspects of the WWFE-II	105
7.2	Results of the WWFE-II test cases	106
7.2.1	Homogeneous isotropic matrix test case	108
7.2.2	Lamina test cases	109
7.2.3	Laminate test cases	115
8	Conclusion and Outlook	121
	Appendix	127
A	Derivation of the Pagano analytical solution	127
B	WWFE-II test cases	132
B.1	Given Instructions	132
B.2	Given material parameters	134

B.3	Given load cases	136
C	Material data of HexPly 8551-7 (IM7)	137
	Bibliography	148

Notation

Coordinate Systems

x, y, z	Global coordinate system of a laminate
x_1, x_2, x_3	Coordinate system of a UD lamina, x_1 being fibre-parallel, x_3 in through-thickness direction
x_{\parallel}, x_{\perp}	Cylindrical coordinate system of a UD lamina, x_{\parallel} being fibre-parallel
x_1, x_n, x_t	Coordinate system of an action plane, x_1 being fibre-parallel

Arabic characters

c	Index denoting compression
\underline{E}	Stiffness matrix
f	Index denoting fibres' figures
f_E	Stress exposure
f_S	Stretch factor
f_r, f_p	Index denoting fracture / fracture plane
FF, IFF	Index denoting figures concerning fibre fracture / inter-fibre fracture
m	Minimum of the weakening factor η_{w1}
m_{σ_f}	Magnification factor for matrix stresses
k	Shear impact degradation measure
l	Stress exposure impact degradation measure
n	Orientation impact degradation measure
p	Inclination parameter
R	Strength of the material
R^A	Fracture resistance of the action plane
s	Threshold of the η_{w1} influence
S	Integrated standardised stress exposure
\underline{S}	Compliance matrix
t	Index denoting tension

Greek characters

α	Thermal expansion coefficient
β	Orientation of a lamina within an laminate
γ	Shear strain
δ	Macroscopic crack density
ϵ	Normal strain
η	Degradation progress measure
η_{m+p}	Weakening factor due to m icro-damage and p robabilistics
η_{w1}	W eakening factor due to fibre-parallel stresses σ_1
θ	Orientation of an action plane
ν	Poisson's ratio
σ	Normal stress
τ	Shear stress
φ	Second angle unambiguously defining an action plane in isotropic material
ψ	Direction of the resultant shear in an action plane

Abbreviations

2D	two-dimensional
3D	three-dimensional
BMBF	Bundesministerium für Bildung und Forschung Federal Ministry of Education and research
CAE	computer aided design
CFRC	carbon fibre reinforced composite
CLT	classical laminate theory
CPU	central processing unit
ESL	equivalent single layer
FE	finite element
FEA	finite element analysis
FF	fibre fracture
FRC	fibre reinforced composite
FRPC	fibre reinforced polymer composite
FSDT	first-order shear deformation theory
GFRC	glass fibre reinforced composite
GMC	generalised method of cells
HSDT	higher-order shear deformation theory
IFF	inter-fibre fracture
MFB	Master Fracture Body
LW	layer-wise
PVD	principle of virtual displacement
RMVT	Reissner's mixed variational theorem
RVE	representative volume element
SFB	Sonderforschungsbereich / collaborative research centre
UD	unidirectional / unidirectionally
UMAT	user material behaviour subroutine
WWFE	World Wide Failure Exercise

1 Introduction

1.1 Motivation

Engineering composite materials have been present in research and industry for several decades. Starting in the 1950s designs have been realised which heavily rely on the main features of unidirectionally fibre-reinforced composite (UD FRC) laminates – the low weight to strength ratio and the individually adjustable constitutive characteristics. Along with comprehensive experimental effort extraordinary durable designs of lightweight coverings and casings as well as first structurally integrated parts in sail-planes, wind turbines and yachts have been realised. In the beginning the advantages of UD FRCs in terms of strength, weight, and manufacturing outbalanced the high necessary safety factors due to the lack of predictability of the material's behaviour. Nowadays, however, security factors are opposed to commercial aspects and the material selection is stronger influenced by the expense and reliability of its behaviour prediction than by the material's capabilities itself. In this context numerical predictions gain more and more importance in order to omit expensive experiments.

It is only recently that composites have truly started to replace conventional materials in commercial structural assemblies. The automotive industry starts to incorporate FRC accessories, peripheral structural parts, crash boxes and car bodies. The more weight-sensitive aerospace sector has already dared to build highly security-relevant structures like tails or fuselages and proceeds to primary load-carrying assemblies now. The Airbus A380's wing box, the most important part of the structure since it transfers the load between the wings and the fuselage, is completely made of fibre reinforced composite (FRC) materials (see Fig. 1.1 and [1]). This great advance has been made possible by the massive increase of computing power in the last two decades. Along with being able to use more complex models, the components which can be studied to predict the failure behaviour can also be a lot more detailed. Based on the growing reliability of inplane failure prediction [2] the application of FRC has been extended to complex geometries including primary load transferring components, resulting occasionally in 3D loading of the material. A safe design of such materials and structures requires an efficient and reliable failure prediction under general 3D stress states.

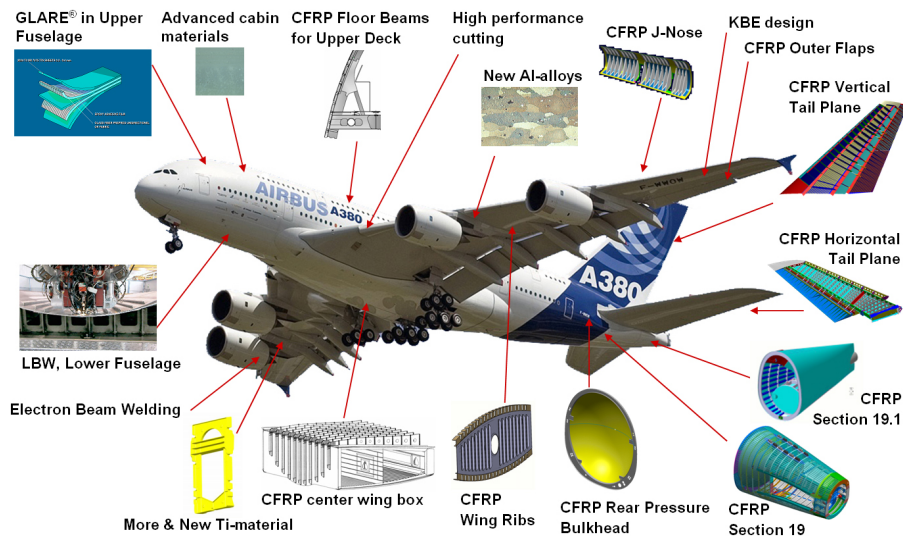


Figure 1.1: The application of composite materials in the Airbus A380. (By courtesy of Airbus)

1.2 Problems and aims

Within the collaborative research centre SFB-381 (1994-2006, [3]) the Universität Stuttgart has generated significant knowledge on the *Characterisation of Damage Development in Composite Materials Using Nondestructive Methods* (SFB title). The project has identified damage mechanisms on different lengths-scales and developed the experimental approaches to detect and monitor their occurrence, evolution and interaction. The revealed relations have been covered by appropriate mathematical descriptions and the associated parameters have been determined for various material systems like wood, short and long fibre reinforced polymer composites or steel reinforced concrete. The resulting theories span from statistical descriptions of the successive fibre fracture (fibre bundle models), over the description of stress concentration fields around successively failing fibres up to macroscopic post-failure degradation models. The sub-project *Numerical simulation of damage evolution* included the implementation of the generated knowledge into application-oriented engineering tools. Aiming on the convenient application within a generally three-dimensional stress analysis, the Institute of Statics and Dynamics of Aerospace Structures (ISD) has evaluated several failure prediction approaches for UD FRPCs. The main requirements were a fracture mechanical basis and an open, accessible structure which allows the incorporation of various actual and future aspects.

Puck's action plane-related failure criteria for unidirectional (UD) fibre reinforced polymer composites [4] are three-dimensional formulations ab initio which have already proven their capability in the first World-Wide Failure Exercise [5, 6]. From the beginning

of their development Puck's key-note has been the fracture mechanical interpretation of numerous experimental results [7]. His decided distinction between fibre and inter-fibre fracture provides efficient access points for systematic enhancements and adjustments. Accordingly Puck's Theory has been chosen as the most promising approach for the prediction of lamina failures and of the post failure load redistribution process in laminates. Being a stress-based theory, the quality of its failure prediction is strongly influenced by the preceding stress analysis. Aiming on complex geometries far beyond a plane layer composition, analytical tools making use of the Classical Laminate Theory (CLT) are obviously falling short of a Finite Element Analysis (FEA). In particular, commercial FEA packages like ABAQUS [8] provide verified user-friendly algorithms for all kinds of nonlinear constitutive behaviour, the simulation of the curing process and the prediction of interface failure (delamination). Joining these capabilities with reliable intralaminar failure criteria results in a comprehensive failure prediction tool for UD FRPC laminates.

Although Puck's Theory is based on fully three-dimensional fracture mechanics, its application on load cases beyond plane states of stress has been neglected in the past. Existing enhancements regarding fibre fracture (see Sec. 4.7) or the interaction between transverse and shear deformation (see Sec. 3.1.3) have not been fully brought to a 3D application maturity whereas the specific 3D enhancement of the η_{m+p} -correction (see Sec. 4.3.2) seemed ignored by the users due to its alleged empirical character. The fracture angle-dependent three-dimensional behaviour of a successively damaging lamina has not been covered by any post failure degradation rule so far. It is the declared aim of the present work to close the gap between Puck's Theory and its unhindered three-dimensional application within contemporary computer aided engineering (CAE) processes. The present work focuses on the three-dimensional work-over and verification¹ of Puck's Theory, the development of an adequate 3D degradation procedure and the application-oriented implementation into the established FEA tool ABAQUS. The second World Wide Failure Exercise (WWFE-II) initiated in 2007 provides the adequate 3D test cases to prove the applicability and versatility of the developed approaches.

1.3 Structure of the present work

The present documentation aims at imparting a profound perception of the mechanisms acting in damaging laminae and laminates and a deep understanding of Puck's Theory, its enhancements and the produced results. Furthermore it intends to encourage the reader to comprehend the presented implementation in order to apply the developed approaches

¹Does the model in 3D cases behave as it was originally intended to?

within his individual design process.

A deliberate application of any failure criteria requires an overview of the material's characteristics, its composition and its inherent failure mechanisms. Chapter 2 describes the scales of UD FRC laminae and laminates (see Sec. 2.1), the different types of failure in a lamina (see Sec. 2.2) and the successive failure of a laminate (see Sec. 2.3.1). Three examples of failure in automotive structures (see Sec. 2.4) complete the chapter.

The basis of any failure analysis, the determination of the stresses acting in a structure, a laminate and eventually every single lamina, is addressed in chapter 3. After the presentation of the constitutive model including nonlinear extensions (see Secs. 3.1.1 to 3.1.3), the sections 3.2 and 3.3 address the theoretical and practical aspects of Finite Element representations of laminates and laminate structures. The different approaches are evaluated by means of the analytical solution for multilayered plates by Pagano (see Sec. 3.4). Regarding the determination of the general behaviour of laminate materials, section 3.5 introduces the Representative Volume Element (RVE) or Unitcell approach before the discussion of geometric nonlinearity (see Sec. 3.6) and of residual stresses (see Sec. 3.7) conclude the chapter.

Chapter 4 presents Puck's Theory for unidirectionally fibre-reinforced polymer composite laminae. Divided into inter-fibre fracture (see Sec. 4.2) and fibre fracture (see Sec. 4.7), the former requires a more detailed description. In addition to application-oriented aspects (see Sec. 4.2.2), section 4.3.1 addresses the influence of fibre-parallel stresses on the inter-fibre fracture (IFF) whereas section 4.3.2 covers the influences of non-fracture plane stresses particular important in the case of 3D load cases. The presented relation between fracture plane stresses and the Mohr's circle demonstrate the meaning of an *action plane-related* fracture criterion (see Sec. 4.4). The application of Puck's IFF criteria to isotropic and not intrinsically brittle materials rounds out the Puck's Theory chapter (see Sec. 4.6).

After a macroscopic inter-fibre fracture has been predicted by Puck's criteria, the post-failure degradation analysis starts (see Ch. 5) and section 5.2 describes the underlying smeared crack representation of the successively damaging lamina. The following section 5.3 provides an overview on existing – mainly two-dimensional – degradation rules before the development of a 3D degradation rule is described in detail (see Sec. 5.5). The approach is validated by virtual material tests on RVEs containing discrete cracks in section 5.6.

The implementation of the introduced and developed material behaviour descriptions is presented in chapter 6 before the generated user material behaviour subroutine is applied

to the twelve test cases of the WWFE-II (see Ch. 7). The experiences and findings gained from the three-dimensional verification and extension of Puck's failure and post-failure theory, the implementation and the application to the test cases is summarised in chapter 8.

2 Failure of UD fibre-reinforced composites

Composites are fixed assemblies of at least two phases of originally separated materials. The present work deals with laminates which are to be categorised as composites in two senses – they are a composition of stacked laminae which themselves are a combination of fibres and an embedding matrix. The present work is based on and valid for materials consisting of idealised infinite glass or carbon fibres and polymer matrices. However, aiming at the physical mechanisms rather than the empirical correlations, the presented findings are expected to be transferable to different material systems with comparable setups. The present chapter provides a definition of terms, scales and coordinate systems of UD fibre-reinforced composites (see Sec. 2.1), an overview on failure mechanisms in laminae and laminates (see Secs. 2.2 and 2.3) and exemplary cases and definitions of failure (see Sec. 2.4). The relevance regarding the material models and failure analysis described in the following chapters is pointed out.

2.1 Scales and coordinate systems of the material

According to the setup of UD fibre-reinforced composites there are four levels on which the composite can be analysed.

2.1.1 Micro-mechanical level

On the smallest, the micro-mechanical level, the fibres and the matrix are treated as separate materials with different constitutive behaviour (see Fig. 2.1a). This is the level, where fibre-matrix and fibre-fibre interactions are studied. For example the bonding between individual fibres and their surrounding matrix has been investigated experimentally and numerically [9]. Furthermore, combined numerical and experimental results concerning the load redistribution due to successive fibre failure [10] have been incorporated into statistical fibre-bundle models [11]. Regarding Puck's failure criteria, the micro-mechanic level is not explicitly analysed but major mechanisms are condensed and transferred to the lamina level (see Sec. 4.3).

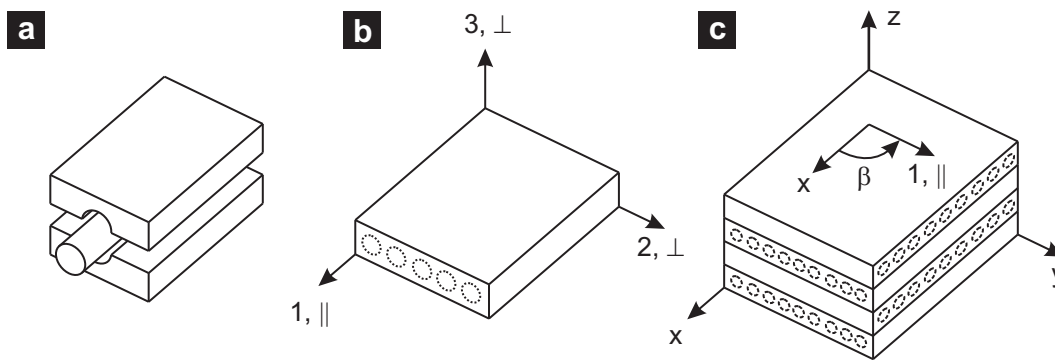


Figure 2.1: Scales of a UD fibre reinforced composite: (a) The micro-mechanical level, (b) the lamina level, and (c) the laminate level.

2.1.2 Lamina level

One scale above – on the lamina¹ level, the fibre-matrix composite is regarded as a homogeneous but anisotropic material (see Fig. 2.1b). With its two inherent directions, fibre-parallel (index \parallel) and fibre-perpendicular (index \perp), a UD-lamina generally behaves transversely isotropic. Using common orthotropic material models this results in an identical behaviour in the transverse (index 2) and through-thickness direction (index 3) and a differing behaviour in the longitudinal direction (index 1) of the lamina. The lamina's constitutive behaviour and strength is either experimentally determined by coupon tests or derived from the individual fibre and matrix behaviour by mixture rules [12, 13], by analytical micro-mechanical models [14, 15] or Representative Volume Element (RVE) approaches [16, 17]. All the methods aim at the characterisation of the lamina by *homogenised* stiffnesses ($E_1, E_2, E_3, G_{12}, G_{13}, G_{23}$) and strengths [18–20]. Most failure criteria, including Puck's Theory, are based on the stresses or strains calculated on the lamina-level. This makes them layer-wise criteria for *intra-laminar* failure.

2.1.3 Laminate level

On the laminate level, the material is regarded as a stacked composition of several laminae including their interfaces (see Fig. 2.1c). The orientation of the individual laminae is given by the angle β between a laminate-related x-axis and the fibre-orientation (1-direction) of the respective lamina. The task of a stress analysis on the lamina level is to provide inter- and intralaminar stresses of the individual laminae and interfaces due to loads applied to the entire laminate. Hence the stress analysis on this level is also the basis for intra-

¹The terms *lamina*, *layer*, and *ply* are used as synonyms within the present work whereas *lamina* is the preferred term. *Layer* and *ply* are only used where required due to the general linguistic usage.

laminar failure analysis and delamination prediction. In contrast to the lamina level, a UD fibre-reinforced lamina may react truly orthotropic when confined within a laminate regarding strength, this is called the *in-situ effect* (see Sec. 4.5).

2.1.4 Structural level

On the structural level, whole components are regarded. These may be of complex geometry and therefore of complex local stacking sequence (see Figs. 2.8 and 2.9). Stress analyses on the structural level provide the local state of stress at an arbitrary position within the component due to the external load applied to the component. The aim of any application-oriented failure analysis has to be a reliable failure prediction within a structural level analysis.

2.2 Types of failure

2.2.1 Micro-damage

The disintegration of any material starts on the micro-mechanical level. In the case of a fibre-polymer lamina, already the manufacturing process of the fibre-matrix composite implicates micro-damage. Due to different thermal expansion coefficients of the fibre and matrix and due to the matrix shrinking during polymerisation, considerable residual stresses exist in the matrix already after the curing [21]. These stresses may lead to flaws in the form of local fibre-matrix debonding and microscopic matrix cracks (see Fig. 2.2b). An increasingly applied load rapidly causes the growth of these micro-defects regarding dimension and quantity. Under applied shear load, microscopic *hackles* develop in the matrix additionally (see Fig. 2.2a). Under an applied fibre-parallel load the early fracture of individual fibres causes the neighbouring matrix to fail due to the locally increased load (see Fig. 2.2c). These micro-defects initiate and develop long before a macroscopic crack is visible, however, their existence has been proven by watching the material turning opaque, by studying the material's reduction in stiffness [22] or its acoustic emission [23]. The micro-damage influences both, the material's stiffness and its strength. In the present work the influence on the stiffness is regarded using nonlinear constitutive material models (see Sec. 3.1.2). The influence on the matrix strength is considered by two weakening factors: One covers the local microscopic fibre-matrix debonding due to a high fibre-parallel load (see Sec. 4.3.1), another accounts for the way in which microscopic matrix cracks merge to a macroscopic inter-fibre fracture (see Sec. 4.3.2).

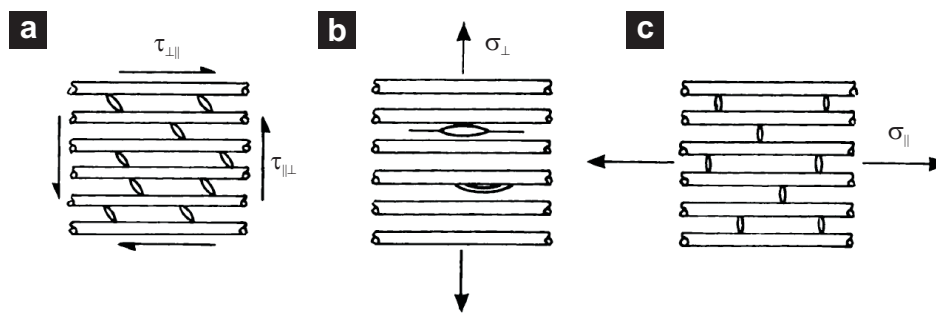


Figure 2.2: Different forms of micro-defects in a UD FRC lamina: (a) Hackles due to shear load $\tau_{\perp\parallel}$, (b) matrix cracks and local fibre-matrix debonding due to fibre-perpendicular tension σ_{\perp} , and (c) local matrix failure due to fibre-parallel tension σ_{\parallel} .

2.2.2 Fibre fracture

The two visible, macroscopic types of failure of a fibre-matrix composite appear on the lamina level: fibre fracture (FF) and inter-fibre fracture. The former term defines the fracture of most or all fibres of a lamina, not the fracture of individual fibres which statistically start to break at some 50% to 70% of the fibre fracture limit. Hence a fibre fracture criterion defines the load case, where the entire lamina abruptly separates in fibre-parallel direction. Regarding the lamina as a homogeneous material, such criteria are defined by the homogenised bearable load in the fibre-parallel, longitudinal direction of the material. In this direction, a lamina behaves significantly different whether subjected to tension or compression. Fibre-parallel tension leads to the separation of the material on a fibre-perpendicular fracture plane. The load bearing capacity in this direction is strongly dominated by the fibres. Accordingly, micro-damage in the matrix due to additionally applied fibre-perpendicular load [24, 25] or shear [26] does not influence the load bearing capacity in fibre direction. However, the load bearing capacity in fibre direction *is* influenced by fibre-perpendicular load due to the differing lateral contraction behaviour of the fibres and the matrix. This effect is covered by Puck's extended fibre fracture criterion (see Sec. 4.7).

In the fibre-parallel compressive load case, the appearance of a FF strongly depends on the material system, i.e. the interaction between fibres and matrix. Perfectly supported and aligned fibres may break due to shear in the fibres which results in an inclined fracture plane and a mutually sliding of the newly emerged surfaces if kinematically possible. This behaviour has been observed rarely and – if at all – for anisotropic carbon fibres exclusively [27, 28]. By far the more common way of the fibres to get rid of their load is to buckle. Depending on the material system and the fibre volume fraction, the scales on which this mechanism is activated spans from micro-buckling to the macroscopic *fibre*

kinking, where the fibres of large continuous regions deflect in a common direction. In contrast to the fibre fractures due to tension, the supporting capacity of the matrix plays a role under compression. Hence the presence of matrix defects due to fibre-perpendicular or shear load influences the compressive load bearing capacity of the lamina [26] but this effect has not yet been incorporated into Puck's Theory. Note that any fibre fracture in one or more laminae is currently defined as the application limit of the laminate.

2.2.3 Inter-fibre fracture

Loaded with fibre-perpendicular tension, fibre-perpendicular compression or any type of shear, the lamina will eventually fail by an inter-fibre fracture (IFF). This term defines a macroscopic crack running through the matrix material or along fibre-matrix boundaries through an entire lamina (see Fig. 2.3). The result is a macroscopically planar *fracture*

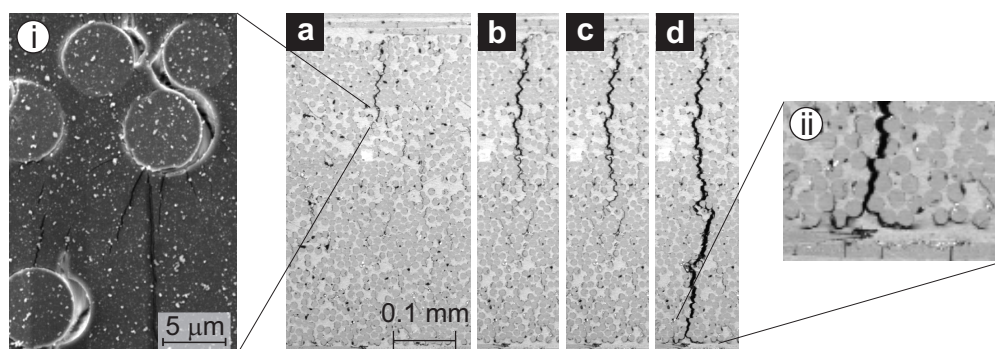


Figure 2.3: In-Situ Laser Scanning Microscope [29] growth observation of a micro-damage (a to c) leading to an inter-fibre fracture due to tensile σ_{\perp} (d) (from [30]), close-ups: (i) Scanning Electron Microscope micrograph of the area in front of the crack tip (from [31]), (ii) Onset of micro-delamination.

plane. The significance of an IFF for the load bearing capacity of a laminate ranges from harmless to fatal, depending on the fracture plane orientation and the transmitted load (see Sec. 2.4). IFFs are a central part of this work and will be discussed in detail in section 4.2.2. Puck's Theory is capable of distinguishing between fibre and inter-fibre fracture and predicts the orientation of the IFF plane as well as the stresses acting on that plane. In the case of IFF, Puck has developed subsequent post-failure degradation rules whereas a fibre fracture in one or more laminae is currently defined as the application limit of the laminate.

2.2.4 Delamination

A laminate as a stacked composition of several laminae may fail by the separation of two or more of these layers. Such a delamination process is caused by inter-laminar stresses namely through-thickness tension, inplane or through-thickness shear. A typical deformation of a laminate leading to significant inter-laminar shear is bending, but also inplane loading may lead to inter-laminar shear depending on the stacking sequence of the laminate [32]. Neglecting the micro-mechanical aspects of delamination, it is a typical problem of fracture mechanics to predict the onset and growth of a crack in a predefined plane [33, 34] depending on the local mixture of fracture modes I, II or III (see Fig. 2.4a). There are several analytical models for delamination onset and growth, mostly based on

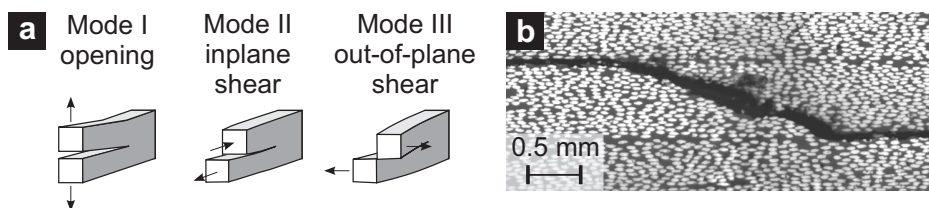


Figure 2.4: (a) Fracture modes following classical fracture mechanics, (b) Delamination jumps between two interfaces via an inter-fibre fracture in a $\pm 45^\circ$ laminate (from [35]).

traction-separation laws and energy terms [36]. Efficient and reliable models have been implemented in Finite Element (FE) formulations [37] and are conveniently available in contemporary commercial FE packages [38]. Hence delamination is not considered in the present work but the developed layer-wise failure and post-failure analysis is expected to join existing delamination analyses in the medium term. It is known that delamination and IFF mutually interact. It has often been observed that delamination starts at that point where a macroscopic inter-fibre crack meets the interface between two laminae (see Fig. 2.3, ii) [39]. On the other hand, IFFs develop and allow the delamination to jump between different interfaces (see Fig. 2.4b). These effects are triggered by local stress concentrations on crack tips and are not covered by Puck's smeared crack representation which does not predict the position of discrete cracks. On the structural level however, IFF-damaged areas do influence the inter-laminar stresses by their declining stiffness and the resulting change in the laminate's overall stress distribution.

2.3 Successive failure

The failure of a composite material is a sequence of the described individual but interacting failure mechanism through the whole range of length scales. This section summarises

the history of events in a damaging lamina and laminate and introduces the relevant terms and definitions regarding Puck's Theory.

2.3.1 Damage evolution in a confined lamina

Using layer-wise failure and post-failure prediction methods like Puck, the study of the successive IFF damage of a confined lamina is of fundamental interest. In the present example, a 0° lamina is confined between two 90° laminae and the material is increasingly loaded in the y -direction (see Fig. 2.5a). At about half the bearable load of the lamina,

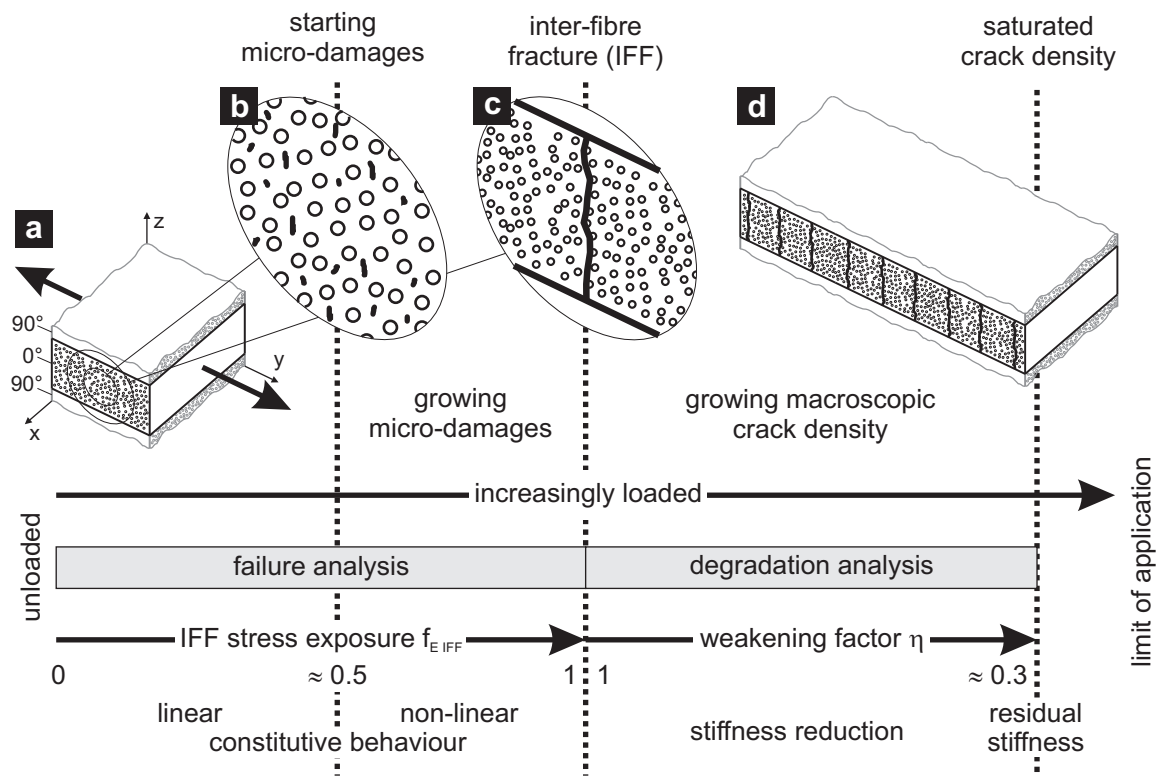


Figure 2.5: Successive IFF damage in a confined lamina (a): Growth of micro-defects (b), micro-defects merge to a macroscopic crack through the entire lamina (c), increasing number of macroscopic cracks in the lamina (d).

existing micro-defects start to grow and new ones are initiated (see Fig. 2.5b). At the same time the material's constitutive behaviour starts to become nonlinear, the lamina's stiffness continuously reduces. The quantity and growth of micro-defects depends on the load case, but load cases – including through-thickness load – generally create more and faster growing micro-defects than inplane load cases. With further increased load, the micro-defects eventually merge to a crack through the entire lamina (c). When loading an isolated lamina this is the load case at which it fails by its complete separation and

loses its entire load bearing capacity. Consistently a layer-wise criterion like Puck defines *inter-fibre fracture* meaning a *macroscopic crack through the entire lamina* as failure of a lamina. Although the arisen fracture plane does no longer transmit any load, in the case of a confined lamina the neighbouring laminae still induce load into the sound sections of the damaging lamina. The result is a growing number of macroscopic cracks if more load is applied (see Fig. 2.5d). The amount of load which is induced into and hence carried by the damaging lamina depends on the size of the sound sections. Accordingly, with a growing macroscopic crack density, the portion of the applied load which is carried by the damaging lamina reduces and more and more load is redistributed to the neighbouring laminae. At a specific crack density – the *saturated crack density*, the sound sections of the damaging lamina have become so small that the induced load is no longer sufficient for producing further cracks. At this point the damage development in the considered lamina is completed, even if more load is applied.

Following Puck's Theory, the prediction of the whole damage development consists of two parts: the *failure analysis* and the post failure *degradation analysis*. The former evaluates a state of stress regarding fibre and – in the present example – inter-fibre fracture. The central parameter is the *IFF stress exposure* $f_{E\ IFF}$ running linearly from 0 (unloaded) to 1 (inter-fibre fracture) with linearly increasing stresses. Micro-damage starts at a value of $f_{E\ IFF} \approx 0.5$ and its influence on the load bearing capacity is regarded by weakening factors (see Sec. 4.3). The failure analysis is preferably based on a nonlinear stress analysis which includes the effects of micro-defects on the material's stiffness (see Sec. 3.1.2). Having reached the IFF limit, in the subsequent post failure degradation analysis the material's stiffness is reduced according to the applied load or the resulting crack density respectively. A central measure is the weakening factor η which develops from 1 (no stiffness reduction) to exemplary 0.3 (residual stiffness) when having reached the saturated crack density. Regarding the numerical realisation the failure analysis is a post-processing of calculated stresses which means it can independently follow any kind of stress analysis. The degradation analysis, however, is constantly changing the material's constitutive behaviour and therefore stress and degradation analysis are two mutually interacting parts of a numerical prediction beyond IFF.

2.3.2 Successive failure of a laminate

The successive damage of a balanced $0^\circ/90^\circ$ laminate loaded in the y-direction (see Fig. 2.6) is representative for the complex and interacting failure process of UD fibre-reinforced composites. Loaded inplane by a tensile load F , the first damage occurs in the 0° laminae where fibre-transverse tensile $\sigma_{2\perp}^t$ produces the first ply failure in form

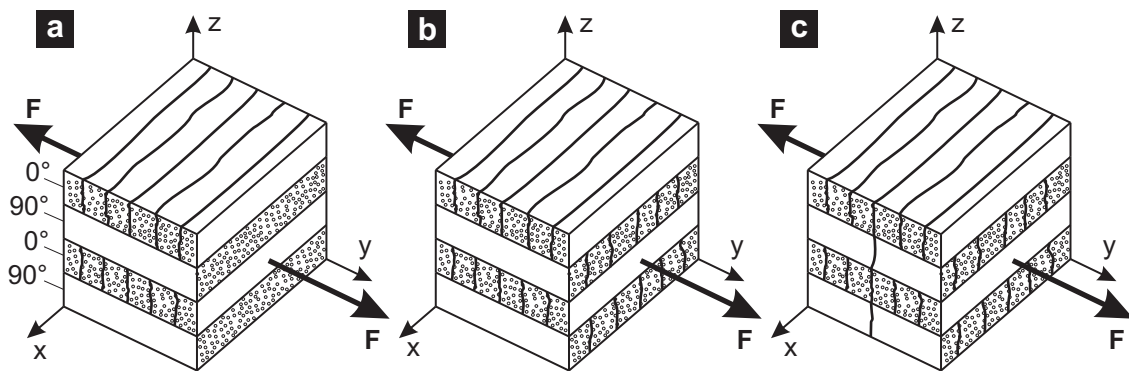


Figure 2.6: Section of a balanced $0^\circ/90^\circ$ laminate increasingly loaded: first ply failure IFFs in the 0° laminae (a), second ply failure IFFs in the 90° laminae (b) and third ply failure FFs in the 90° laminae (c).

of vertical IFFs ($\theta_{fp} = 0^\circ$). Increasingly loaded, in the 0° laminae develop more and more IFFs (see Fig. 2.6a) going along with the decrease of stiffness – the degradation – of these laminae. The result is a load redistribution from the damaging laminae to the neighbouring ones. Accordingly the tensile $\sigma_{1\parallel}^t$ in the 90° laminae increases together with the laminae's lateral contraction due to the Poisson's effect. Impeded by the fibres of the 0° laminae (they carry compressive $\sigma_{1\parallel}^c$), the result is a fibre-transverse tension $\sigma_{2\perp}^t$ in the 90° laminae producing the second ply failure: vertical IFFs in the 90° laminae (b). Still capable of bearing the load F , the laminate may be increasingly loaded until the following fibre fractures in the 90° laminae mark the third ply failure and the final failure of the laminate (c). This example proves the importance of the distinction between fibre fracture (FF) and inter-fibre fracture (IFF) regarding failure analysis in a damage-tolerant design process.

2.4 Failure on the structural level

The aim of any failure analysis is the prediction of when the application limit of a material or a component will be reached. The definitions of these limits are as widespread as the fields of application of fibre-reinforced composites or as their successive modes of failure.

2.4.1 Torsion spring

One of the key geometries for the development of Puck's inter-fibre failure criteria was a short torsion spring for the rear suspension of a passenger car (see Fig. 2.7). Consisting of a $\pm 45^\circ$ laminate, an applied axial momentum M leads to fibre-parallel tension

$\sigma_{1\parallel}^t$ together with fibre-transverse compression $\sigma_{2\perp}^c$ in the outer lamina (white) and to fibre-parallel compression $\sigma_{1\parallel}^c$ together with fibre-transverse tension $\sigma_{2\perp}^t$ in the inner lamina (grey). Repeatedly loaded, the inter-fibre fractures (IFFs) in the inner lamina (see

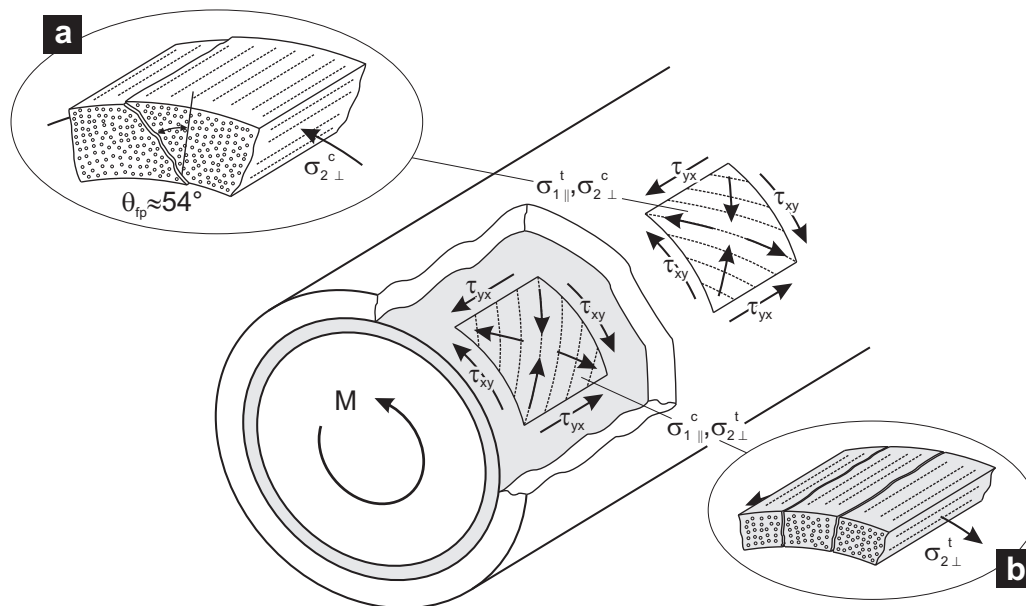


Figure 2.7: Torsion spring made of UD Glass Fibre Reinforced Composite (GFRC): (a) Fatal and (b) tolerable inter-fibre fracture (IFF).

Fig. 2.7b) turned out to be completely harmless for the structure and its load bearing capacity although these fractures had already occurred in large numbers after few cycles. After the crack density of these cracks had reached its saturation, the spring survived 10^6 cycles as long as no IFF in the outer lamina occurred. In contrast to this a single IFF in the outer lamina immediately led to the total failure of the complete structure (see Fig. 2.7a). The inclined fracture plane ($\theta_{fp} \approx 54^\circ$) transmitting pressure leads to the *wedge effect* where parts of the transmitted forces are deflected in trough-thickness direction. In the present case these forces in positive and negative radial direction either cause the inner lamina to collapse or the outer lamina to be blasted – both with the result of an immediate total collapse of the loaded spring [4, 39, 40]. Although the example above is a fatigue experiment and is hence far beyond the failure prediction topic and the scope of the present work, it proves the importance of the distinction between different modes of inter-fibre fracture.

2.4.2 Integral vehicle rear suspension

A contemporary example for the application of failure analysis on UD fibre-reinforced composites is the integral vehicle rear suspension (see Fig. 2.8) developed by the project

Aktives Leichtbaufahrwerk (Active Lightweight chassis) of the German *Bundesministerium für Bildung und Forschung* (BMBF – Federal Ministry of Education and Research). The aim is a lighter chassis due to the application of lightweight, multifunctional and adaptive materials and the integration of currently a large number of structural assemblies into a single suspension component. The fact that one single component is intended to

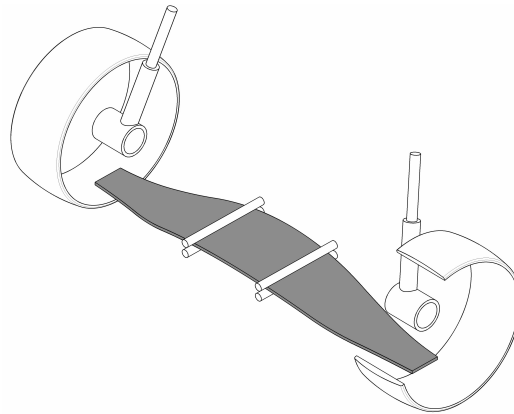


Figure 2.8: Starting point for the future integral vehicle rear suspension: Wheel-guiding transverse leaf spring axle (grey) made of fibre-reinforced composite (FRC), additionally visible suspension components (white) are to be integrated into the final construction (from [41]).

transmit forces between the wheels and the vehicle and at the same time to cushion these forces leads to a particularly narrow design space regarding stiffness [42]. Attached to a passenger car, the customer requires maintenance-free components without the need for health monitoring. Hence the design space regarding strength is also limited since a finite life, damage-tolerant design is excluded. In this project a stress analysis by Finite Element Method (FEM) combined with a failure analysis based on Puck's Theory could identify the overlapping of the two design spaces mentioned. This example proves the need for an accurate damage initiation analysis including reliable information about the safety factor.

2.4.3 Pressure vessel

Another forward-looking application of UD FRC failure analysis is high pressure vessels in fuel cell vehicles (see Fig. 2.9). Opel applies Puck's Theory within a Computer Aided Engineering (CAE) process chain from the laminate design over a filament winding simulation, a quasistatic stress analysis up to a dynamic crash simulation [43]. The failure and post-failure analysis aims at the prediction of the vessel's toughness against inside pressure as well as its behaviour in the case of a dynamic impact – both depending on the

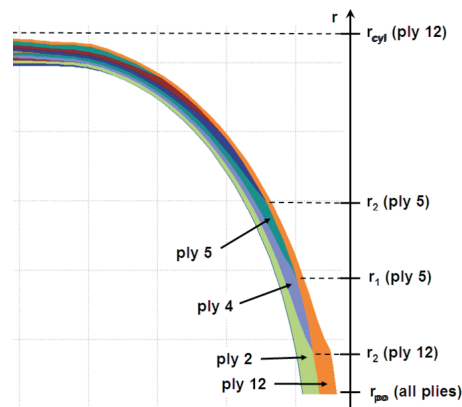


Figure 2.9: Section through the dome area of a wound composite pressure vessel: complex stacking sequence (from [43]).

actual operating temperature. It is obvious that whenever it comes to the failure analysis of a multi-purpose structure, all additionally available information about the predicted failure becomes particularly valuable. In the case of a dynamic crash simulation particular attention is to pay to the amount of energy which is absorbed by the degradation process.

The examples above altogether confirm the pursuit of a mechanism-based failure prediction. Additionally to the information of *when* a failure occurs, information about *what* happens at that particular load case enables the user to predict the limit of use of his individual component. Additionally such failure and post-failure analysis methods allow a systematic design of laminates and structures regarding their successive damage evolution. Puck's action plane-related fibre and inter-fibre failure criteria are regarded as the most promising theories in terms of these requirements.

3 3D stress analysis in laminates and structures

According to the multiscale character of the material (see Sec. 2.1) the task of a stress analysis is related to the respective level. On the lamina level the stress analysis assigns a state of stress to any state of strain or vice versa, i.e. this is the level where the constitutive behaviour of the individual lamina is interpreted (see Sec. 3.1). On the laminate level the stress analysis determines the distribution of load among the involved laminae due to loads which are applied to the laminate material as a whole. This may happen as part of an analysis on the structural level whose task is the determination of the local states of stress and strain at an arbitrary position of the structure due to loads which are applied on specific positions in the form of forces or displacements (see Sec. 3.3.2). The second important application of the stress analysis on the laminate level is the determination of generalised laminate behaviour. In that context the presented RVE approach replaces the established Classical Laminate Theory (CLT) in the case of applied 3D loads (see Sec. 3.5). The mentioned levels are hierarchical in the sense that analysis on a higher level require all those on the levels below. In the following sections the theoretical and practical aspects of the stress analysis are treated whereas the primary attention is drawn to the application within a Finite Element Analysis (see Sec. 3.2) – the commercial FE package ABAQUS [8] in particular (see Sec. 3.3). Furthermore the quality of the presented FE representations is determined by the comparison with the analytical solution following Pagano (see Sec. 3.4) and considerations about geometric nonlinearity (see Sec. 3.6) and thermally induced residual stresses are presented (see Sec. 3.7).

3.1 Constitutive behaviour of a lamina

3.1.1 Transverse isotropy and orthotropy

Neglecting mechanism on smaller scales the individual lamina is regarded as an homogeneous but anisotropic material (see Sec. 2.1). In the undamaged state it behaves equally in the transverse 2-direction and the through-thickness 3-direction which allows to reduce the general anisotropy to a transversely isotropic behaviour with only a fibre-parallel \parallel and fibre-perpendicular \perp direction (see Fig. 2.1b). The constitutive behaviour, i.e. the material law which relates states of stress to states of strain is then defined by the compli-

ance matrix \underline{S} in Voight notation:

$$\begin{bmatrix} \epsilon_1 \\ \epsilon_2 \\ \epsilon_3 \\ \gamma_{12} \\ \gamma_{13} \\ \gamma_{23} \end{bmatrix} = \begin{bmatrix} 1/E_{\parallel} & -\nu_{\perp\parallel}/E_{\perp} & -\nu_{\perp\parallel}/E_{\perp} & 0 & 0 & 0 \\ -\nu_{\parallel\perp}/E_{\parallel} & 1/E_{\perp} & -\nu_{\perp\perp}/E_{\perp} & 0 & 0 & 0 \\ -\nu_{\parallel\perp}/E_{\parallel} & -\nu_{\perp\perp}/E_{\perp} & 1/E_{\perp} & 0 & 0 & 0 \\ 0 & 0 & 0 & 1/G_{\parallel\perp} & 0 & 0 \\ 0 & 0 & 0 & 0 & 1/G_{\parallel\perp} & 0 \\ 0 & 0 & 0 & 0 & 0 & 1/G_{\perp\perp} \end{bmatrix} \cdot \begin{bmatrix} \sigma_1 \\ \sigma_2 \\ \sigma_3 \\ \tau_{12} \\ \tau_{13} \\ \tau_{23} \end{bmatrix} \quad (3.1)$$

A 3D state of stress $\bar{\sigma}$ consists of three normal stresses σ_i and three shear stresses τ_{ij} , accordingly a 3D state of strain $\bar{\epsilon}$ of three normal strains ϵ_i and three shear strains γ_{ij} . The material is characterised by common *engineering constants* namely Young's moduli E_i and shear moduli G_{ij} ¹ and the quantities ν_{ij} . The latter have the physical interpretation of Poisson's ratios that characterise the transverse strain in the j -direction, when the material is stressed in the i -direction. In general, ν_{ij} is not equal to ν_{ji} – they are related by $\nu_{ij}/E_i = \nu_{ji}/E_j$.

For the pure failure analysis of a UD fibre reinforced composite (see Ch. 4), the transversely isotropic material description is generally adequate but within the post-failure degradation process the lamina starts to behave truly orthotropic if not completely anisotropic (see Ch. 5). Whereas the latter behaviour is currently academic (see Sec. 5.6) the orthotropic material model (see Eq. 3.2) is set to the standard for the implementation developed within this work (see Ch. 6) and for 3D stress analyses of laminae in general.

$$\begin{bmatrix} \epsilon_1 \\ \epsilon_2 \\ \epsilon_3 \\ \gamma_{12} \\ \gamma_{13} \\ \gamma_{23} \end{bmatrix} = \begin{bmatrix} 1/E_1 & -\nu_{21}/E_2 & -\nu_{31}/E_3 & 0 & 0 & 0 \\ -\nu_{12}/E_1 & 1/E_2 & -\nu_{32}/E_2 & 0 & 0 & 0 \\ -\nu_{13}/E_1 & -\nu_{23}/E_3 & 1/E_{\perp} & 0 & 0 & 0 \\ 0 & 0 & 0 & 1/G_{12} & 0 & 0 \\ 0 & 0 & 0 & 0 & 1/G_{13} & 0 \\ 0 & 0 & 0 & 0 & 0 & 1/G_{23} \end{bmatrix} \cdot \begin{bmatrix} \sigma_1 \\ \sigma_2 \\ \sigma_3 \\ \tau_{12} \\ \tau_{13} \\ \tau_{23} \end{bmatrix} \quad (3.2)$$

Being a displacement-based approach a FE analysis requires a material description in the form of $\bar{\sigma}(\bar{\epsilon}) = \underline{E} \cdot \bar{\epsilon}$ (see Ch. 6) whereas the stiffness matrix \underline{E} is the inverse of the

¹Within the present work Young's moduli and shear moduli are addressed together by the term *stiffnesses*.

compliance matrix \underline{S} (see Eq. 3.3).

$$\begin{bmatrix} \sigma_1 \\ \sigma_2 \\ \sigma_3 \\ \tau_{12} \\ \tau_{13} \\ \tau_{23} \end{bmatrix} = \begin{bmatrix} D_{1111} & D_{1122} & D_{1133} & 0 & 0 & 0 \\ & D_{2222} & D_{2233} & 0 & 0 & 0 \\ & & D_{3333} & 0 & 0 & 0 \\ & & & D_{1212} & 0 & 0 \\ & \text{sym.} & & & D_{1313} & 0 \\ & & & & & D_{2323} \end{bmatrix} \cdot \begin{bmatrix} \epsilon_1 \\ \epsilon_2 \\ \epsilon_3 \\ \gamma_{12} \\ \gamma_{13} \\ \gamma_{23} \end{bmatrix} \quad (3.3)$$

The components of \underline{E} are

$$\begin{aligned} D_{1111} &= E_1 (1 - \nu_{23}\nu_{32}) \Upsilon \\ D_{2222} &= E_2 (1 - \nu_{13}\nu_{31}) \Upsilon \\ D_{3333} &= E_3 (1 - \nu_{12}\nu_{21}) \Upsilon \\ D_{1122} &= E_1 (\nu_{21} + \nu_{31}\nu_{23}) \Upsilon = E_2 (\nu_{12} + \nu_{32}\nu_{13}) \Upsilon \\ D_{1133} &= E_1 (\nu_{31} + \nu_{21}\nu_{32}) \Upsilon = E_3 (\nu_{13} + \nu_{12}\nu_{23}) \Upsilon \\ D_{2233} &= E_2 (\nu_{32} + \nu_{12}\nu_{31}) \Upsilon = E_3 (\nu_{23} + \nu_{21}\nu_{13}) \Upsilon \\ D_{1212} &= G_{12} \\ D_{1313} &= G_{13} \\ D_{2323} &= G_{23} \end{aligned} \quad (3.4)$$

where

$$\Upsilon = \frac{1}{1 - \nu_{12}\nu_{21} - \nu_{23}\nu_{32} - \nu_{13}\nu_{31} - 2\nu_{21}\nu_{32}\nu_{13}} \quad (3.5)$$

The stability restrictions on the engineering constants are

$$\begin{aligned} E_1, E_2, E_3, G_{12}, G_{13}, G_{23} &> 0 \\ |\nu_{12}| < (E_1/E_2)^{1/2} \quad \text{or} \quad |\nu_{21}| < (E_2/E_1)^{1/2} \\ |\nu_{13}| < (E_1/E_3)^{1/2} \quad \text{or} \quad |\nu_{31}| < (E_3/E_1)^{1/2} \\ |\nu_{23}| < (E_2/E_3)^{1/2} \quad \text{or} \quad |\nu_{32}| < (E_3/E_2)^{1/2} \\ 1 - \nu_{12}\nu_{21} - \nu_{23}\nu_{32} - \nu_{13}\nu_{31} - 2\nu_{21}\nu_{32}\nu_{13} &> 0 \end{aligned} \quad (3.6)$$

3.1.2 Nonlinearities in the constitutive behaviour

In contrast to the nonlinear elastic-plastic behaviour of metals a suitable nonlinear orthotropic material model for glass- or carbon-fibre polymer-matrix composites is not commonly included in contemporary FEA packages. It is however straightforward to include at least those nonlinear stress-strain relations which are determined by uniaxial material

test ². Those experiments result in correlations between stresses and strains, either point-wise or condensed in an analytical relation (see Fig. 3.1). Based on the respective curves

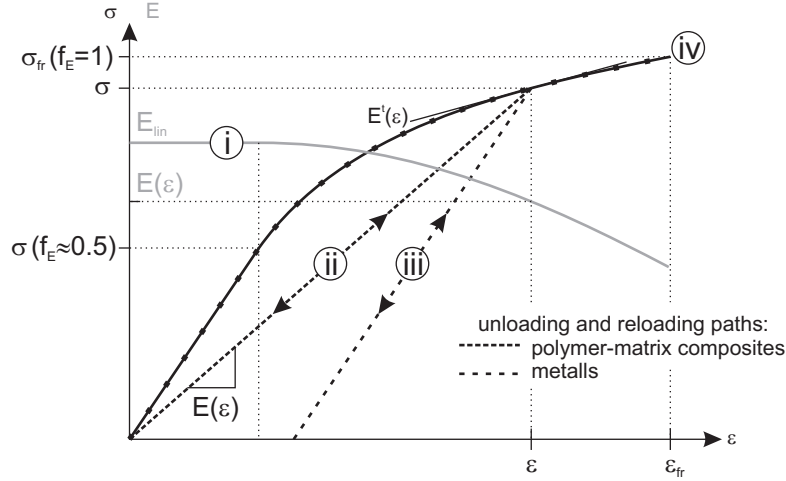


Figure 3.1: Exemplary nonlinear stress-strain relation and the resulting strain-dependent secant modulus E , the tangent modulus E^t is plotted for differentiation purposes only.

any of the stiffnesses in the orthotropic material model (see Eq. 3.3) may be expressed depending on the respective uniaxial strain like exemplary in figure 3.1, i the secant modulus

$$E(\epsilon) = \frac{\sigma(\epsilon)}{\epsilon} \quad (3.7)$$

as long as the stability restrictions (see Eq. 3.6) are met. This allows different stiffnesses for tension or compression as well. In the case of UD FRCs the secant modulus is not only a mathematical term but has the physical meaning of the actual path in the stress-strain diagram on which an intermittent unloading and reloading takes place (see Fig. 3.1, ii). The nonlinearities in the UD FRC's behaviour are attributed to micro-defects (see Sec. 2.3) which are irreversible themselves but in contrast to metal yielding (iii) the micro-damage induced nonlinear strain contribution is reversible. Neglecting strain contributions due to creep [10], the material's strain is expected to return to zero when unloaded. The presented rudimentary approach to include nonlinear behaviour in an orthotropic material model is neglecting known interactions of stresses in producing strains [44]) but qualifies for future developments (see Sec. 3.1.3).

Treating the WWFE-II test cases (see Ch. 7) there is included the nonlinear constitutive behaviour for inplane shear, transverse shear in 1-3-direction and for transverse and through-thickness compression. These stress-strain relations were given for the UD FRC

²Within the present work the term *uniaxial* defines cases where the applied load consists of a single stress or strain component no matter whether this is a normal or a shear component.

material (see App. B). Where the nonlinear constitutive behaviours of the fibres and the matrix were given separately, the application of mixture rules was judged to be less reliable than using the linear relations.

3.1.3 Interaction between transverse and shear deformation

The nonlinear behaviour is commonly entered by the given pointwise correlation between stresses and strains. Generated from uniaxial experiments, these curves end at the fracture due to uniaxial load (see Fig. 3.1, iv). Loaded multiaxially the material possibly bears much higher stresses which widely exceed the given stress-strain relations. The easiest way to ensure that the user material subroutine (UMAT) can still correlate a valid stress to a given strain increment (see Ch. 6) is the extrapolation of the given curve by its last gradient, i.e. by its last tangent modulus. This approach is implemented in all the applied material models and represents a *basic* solution of the problem. As it is completely unphysical and clearly overestimates the resulting strains, the following considerations are necessary.

Based on 2D experiments Puck addressed the interaction between transverse ϵ_2 and shear deformation γ_{12} [4, 45]. The quantification of this finding resulted in two analytical relations for $\gamma_{12}(\tau_{12}, \sigma_2)$ and $\epsilon_2(\sigma_2, \tau_{12})$ expressed by semi-empirical functions for the secant Young's modulus $E_{\perp}(\sigma_2, \tau_{12})$ and shear modulus $G_{\perp\parallel}(\sigma_2, \tau_{12})$:

$$E_{\perp} = E_{\perp}^{lin} - F_{\perp} \cdot \left(E_{\perp}^{lin} - E_{\perp}^{(f_E^{(\sigma_2)}=1)} \right)$$

$$\text{where } F_{\perp} = \left(\frac{f_E^{(\sigma_2)} + C^{(\tau_{12})} \cdot (f_E - f_E^{(\sigma_2)}) - f_E^{thr}}{1 - f_E^{thr}} \right)^{n^{(\sigma_2)}} \quad (3.8)$$

$$G_{\perp\parallel} = G_{\perp\parallel}^{lin} - F_{\perp\parallel} \cdot \left(G_{\perp\parallel}^{lin} - G_{\perp\parallel}^{(f_E^{(\tau_{12})}=1)} \right)$$

$$\text{where } F_{\perp\parallel} = \left(\frac{f_E^{(\tau_{12})} + C^{(\sigma_2)} \cdot (f_E - f_E^{(\tau_{12})}) - f_E^{thr}}{1 - f_E^{thr}} \right)^{n^{(\tau_{12})}} \quad (3.9)$$

In the equations above, the superscript quantities in brackets denominate the stress state at which the associated measures have to be taken rather than powers. Hence E_{\perp}^{lin} and $G_{\perp\parallel}^{lin}$ denote the secant stiffnesses of the linear part of the respective experimentally determined *uniaxial* stress-strain relations whereas $E_{\perp}^{(f_E^{(\sigma_2)}=1)}$ and $G_{\perp\parallel}^{(f_E^{(\tau_{12})}=1)}$ denote the final secant moduli at the fracture due to uniaxial σ_2 or uniaxial τ_{12} , respectively. f_E denotes the common IFF stress exposure due to the applied (σ_2, τ_{12}) -load whereas $f_E^{(\sigma_2)}$ and $f_E^{(\tau_{12})}$

denote the IFF stress exposure due to the isolated σ_2 -component or due to the isolated τ_{12} -component, respectively. The rest of the parameters in equations 3.8 and 3.9 have been experimentally derived [23, 26]:

	CFRC		GFRC	
	(σ_2)	(τ_{12})	(σ_2)	(τ_{12})
$f_{E\ thr}$	0.3	0.3	0.3	0.3
n	2.5	1.7	3.0	2.0
C	0.6	0.6	0.6	0.6

Table 3.1: Parameters for the inplane transverse and shear deformation interaction [4].

These resulting stress-strain-curves perfectly reproduce the experimental results for the stress ratios under consideration $\sigma_2/|\tau_{21}| = [-2; 1]$ and are valid up to fracture due to combined load. The physical background of this approach is the idea that nonlinearities in fibre/polymer composites result from cumulative micromechanical damage [23]. If a combined load leads to higher bearable stresses in terms of macroscopic fracture, it is reasonable to expect the influence of micro-damage also being shifted to higher stress levels. Mainly based on the ratios between the stress exposure due to uniaxial load $f_E^{(\tau_{21})}$ or $f_E^{(\sigma_2)}$, respectively and the stress exposure due to the combined load f_E , the approach is generally transferable into 3D space.

According to Puck's failure theory the presented approach is stress based and therefore not directly applicable for FEA (see Ch. 6). Additionally under 3D loading the IFF stresses can exceed the uniaxial fracture stresses by factors far beyond the verified interval of the presented approach. Hence it is not implemented in the FEA routine but its analytical curves act as a reference for the applied self-similar scaling of the given stress-strain curves. In the present case, the self-similarity is achieved by scaling every point on the curve along its secant modulus by a common factor (see Fig. 3.2). In the case of a lamina, the bearable applied load is mostly independent from its deformation and it is sufficient to scale the given stress-strain relation up to the failure stress after the analysis (see test case 4, Sec. 7.2.2). In the case of a laminate failure analysis, the bearable applied load is depending on the constitutive behaviour of the different laminae. Therefore the failure analysis should be based on stress-strain relations which are scaled to the strain at IFF – which is a result of that very analysis. This circular reference emphasises the need for an iterative adjustment of the respective stress-strain relation. Figure 3.2 exemplarily shows the $\sigma_3(\epsilon_3)$ -relation which the failure analysis of test case 12 is based on (see Sec. 7.2.3). It is scaled up to $\epsilon_3 = -0.065$ which is about the strain at the predicted IFF. Future versions of the user material subroutine (see Ch. 6) should be able to calculate stresses

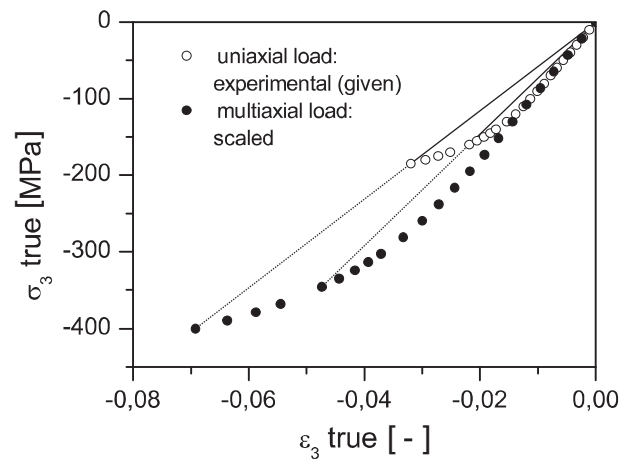


Figure 3.2: Scaled self-similar constitutive behaviour in through-thickness direction for test case 12 (residual stresses neglected).

from stress-strain relations, which have been scaled according to information available from the preceding load increment.

3.2 FE representation of laminates and laminate structures

Laminates and laminate structures commonly have geometries with small thicknesses compared to their lateral expansion. Accordingly there is the legitimate desire to represent the three-dimensional continuum by a condensed two-dimensional structural model [46]. The governing equations and the associated boundary conditions of the reduced model are then derived upon an elimination of the thickness coordinate by integrating along the thickness the partial differential equations of the three-dimensional continuum [47]. A large number of theories and associated finite element definitions have been created over the years to achieve the compliance with the basic requirements for the stress, strain and displacement fields over a laminate's through-thickness direction (see Secs. 3.2.1 and 3.2.2).

The considerations about the slope and the boundary conditions of stress and strain fields throughout the laminate's thickness is based on the perception of a laminate as a stack of different homogeneous and anisotropic layers which are perfectly bonded together. Since the mechanical properties of the interfaces are neglected, the interlaminar boundaries are surfaces of abrupt discontinuities in the material properties. The perfect bond condition requires a continuous displacement field \bar{u} over the bi-material interface and a continuous through-thickness stress and shear stress field σ_z , τ_{xz} and τ_{yz} is required for equilibrium reasons. This results in a discontinuity in the through-thickness strain and shear strain

fields ϵ_z , γ_{xz} and γ_{yz} due to the difference in elastic properties of the adjoining layers. As a consequence the through-thickness displacement u_z has a slope discontinuity across the interface.

The continuous displacement field over the interface results in continuous inplane strains and shear strains ϵ_x , ϵ_y and γ_{xy} which results in discontinuous inplane stresses and shear stresses σ_x , σ_y and τ_{xy} due to the difference in elastic properties of the adjoining layers. Hence through-thickness shear stresses τ_{xz} and τ_{yz} generally have a slope discontinuity in their through-thickness distribution due to equilibrium reasons. On the contrary the continuity of the interlaminar through-thickness shear stresses τ_{xz} and τ_{yz} force the through-thickness stress σ_z to have a continuous derivative along the through-thickness coordinate [48].

behaviour over bi-material interface		slope	slope continuity
displacements	u_x, u_y	cont.	kink
	u_z	cont.	kink
strains	ϵ_x, ϵ_y	cont.	
	ϵ_z	jump	
	γ_{xy}	cont.	
	γ_{xz}, γ_{yz}	jump	
	σ_x, σ_y	jump	
stresses	σ_z	cont.	cont.
	τ_{xy}	jump	
	τ_{xz}, τ_{yz}	cont.	kink

Table 3.2: Allowed discontinuities over the interlaminar boundaries of a stacked layer composition.

Table 3.2 summarises the considerations above whereas figure 3.3 provides a visualisation of the typical situation through a laminate's thickness direction. The values of the through-thickness stress and shear stress at the top or bottom face of the laminate $\sigma_z^{top/bottom}$, $\tau_{xz}^{top/bottom}$ and $\tau_{yz}^{top/bottom}$ equal the applied load.

Following Carrera [49] the requirements above are to be regarded as the basis for the below evaluation of the theories and the associated finite element definitions – no matter whether they appear rather academical or are already user-friendly implemented in commercial FEA codes (see Sec. 3.3.2).

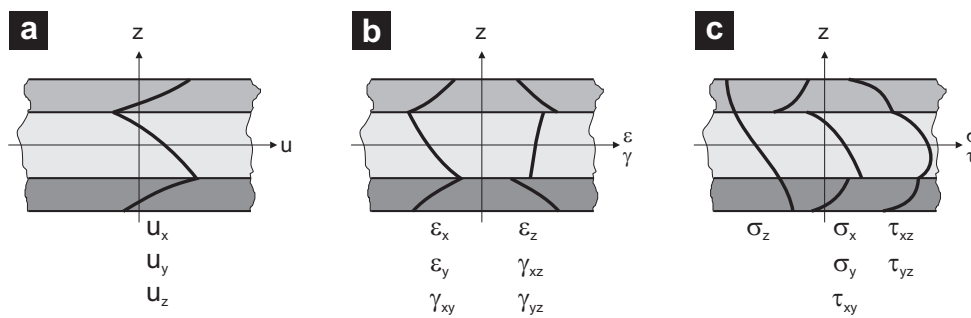


Figure 3.3: Typical behaviours of the displacements (a), strains (b) and stresses (c) throughout a laminate's thickness direction.

3.2.1 Equivalent single layer approaches

The family of Equivalent single layer (ESL) models comprises those models which are to be regarded as direct extensions of approaches established for homogeneous structures to multilayered structures. Without taking explicitly into account the characteristics induced by bi-material interfaces these models commonly introduce through-thickness assumptions for the displacement field. The resulting differential equations are solved by the Principle of Virtual Displacement (PVD) [50] in which the equilibrium equations are fulfilled in a weak sense only – the stress boundary conditions not at all.

The *Classical Laminate Theory* (CLT) is a first-order approximation that relies on the Kirchhoff-Love hypotheses at which linear bending strains are assumed and all transverse deformation effects are neglected ([51]). Main characteristics of the CLT are that the straight cross-section of a laminate under bending deformation remains perpendicular to the mean surface and no transverse shear stresses appear.

The *First-Order Shear Deformation Theory* (FSDT) retains the restriction of a vanishing transverse normal deformation and of a plane cross-section but takes into account the transverse shear deformability typical of FRC materials. Based on a kinematic model originally proposed by Reissner [52] and Mindlin [53] a constant shear deformation is included resulting in additional degrees of freedom referring to the rotations of the cross-section with respect to the normal of the mean surface. The induced through-thickness shear stresses are then interlaminar discontinuous and layer-wise constant.

Higher-Order Shear Deformation Theory (HSDT) release the restrictions of a plane cross-section by the incorporation of additional degrees of freedom for the representation of the through-thickness distribution of the inplane displacement field $u_x(z)$ and $u_y(z)$. A parabolic through-thickness distribution of the through-thickness shear strains is included which allows the warping of the cross-section [54]. This induces a layer-wise parabolic

z -distribution³ of the through-thickness shear stresses whereas the required shear stress conditions at the top and bottom surface of the laminate can be satisfied by an appropriate choice of the thickness polynomials. In particular third-order shear deformation theories have attained a wide acceptance [55].

Theories including *transverse normal deformation* overcome the simplification of the theories presented above concerning $\epsilon_z = 0$. This kind of theories are usually based on HSDT but take into account the full 3D constitutive law [56, 57]. Most kinematic models assume a quadratic through-thickness distribution of the displacement $u_z(z)$ which results in linear through-thickness strain ϵ_z whereas the expansion of the inplane displacements has been based on polynomials of different order.

The approaches presented above either neglect through-thickness strain fields ϵ_z or force them to be continuous in the z -direction and are thus not capable of exactly fulfilling the through-thickness equilibrium at the bi-material interface. Rigorously judged, the application of ESL models is restricted to the analysis of the global response of the laminate [58, 59], but the through-thickness stress and shear predictions of acceptable accuracy can be obtained by post-processing operations [60–62].

3.2.2 Layer-wise approach

Assuming a separate displacement field for each layer – i.e. layer-wise (LW) – is a straightforward approach to explicitly account for the heterogeneous cross-section of a laminate. On the laminate level, the expressions of the layer-wise assumptions are assembled without enforcing a continuous through-thickness strain field. This leaves the possibility for the through-thickness normal and shear stresses to be continuous at the bi-material interfaces. However not all the requirements of table 3.2 are automatically met by *solely displacement-based* layer-wise formulations. For example a layer-wise linear z -distribution of inplane displacements u_x or u_y results in layer-wise constant through-thickness shear stresses which violates the interlaminar equilibrium condition. The fulfilment of the interlaminar equilibrium condition by solely displacement-based LW formulations generally requires higher-order polynomial approximations [60].

The requirements summarised in table 3.2 refer to displacement, strain and stress measures. Accordingly those approaches which exactly fulfil all these conditions are based on displacement and/or stress fields. Lekhnitskii defined a layer-wise *stress-based* function derived the exact solution of the equilibrium equations associated with the two-dimensional problem of a bent cantilever beam. His approach neglects the through-

³i.e. the distribution of a measure along the z -direction.

thickness normal stress [63]. Although the stress-based approach of Ambartsumyan [64] neglects through-thickness stress and strain, his formulations have turned out to be adaptable to many laminate geometries and advanced kinematics [62]. The formulations of the Reissner's Mixed Variational Theorem (RMVT) are based on stress and strain measures, thus allow to fulfil the requirements of table 3.2 a priori [65, 66]. His formulations are regarded to be the most promising [46] but due to their mixed nature they have not yet been implemented in application-ready commercial FEA packages which currently support *displacement-based* element formulations exclusively. The analytical solution following Pagano (see Sec. 3.4 and [67]) is also derived from layer-wise equilibrium equations and completely fulfils the requirements of table 3.2. It is based on the complete 3D orthotropic material law and neglects neither of the stress or strain components of the full 3D space. However its validity is restricted to thin laminate plates because its kinematics neglect the through-thickness shear arising from a bending deformation.

3.3 Laminate and laminate structures in commercial FE codes

The representations of laminate materials and laminate structures available in commercial FE packages like ABAQUS [8] are based on the theories presented above but are not generally attributable to *one* specific theory. Most available approaches are combinations of several aspects mentioned above accepting compromises between accuracy, versatility, applicability and computational cost. The following overview on commonly available approaches enables the user to choose the appropriate material representation (see Sec. 3.3.1) and element type (see Sec. 3.3.2) for his particular problem based on a comparison of their capabilities (see Sec. 3.4). Most presented approaches are available for both implicit and explicit FE analysis. For a differentiation between the both and for an appropriate choice between them please refer to section 6.1.

3.3.1 Material definitions for laminates

Although it has been stated, that the availability of advanced multi-layered plate theories is limited in commercial FE codes, the described fundamental difference between equivalent single layer (ESL) and layer-wise (LW) approach (see Secs. 3.2.1 and 3.2.2) is also reflected in the way in which the laminate behaviour is provided to a commercial FEA. Whereas the ESL approach condenses the inhomogeneity of the material in through-thickness direction in just *one* material description, the LW approach preserves

the different phases of the material thus requires a geometrical through-thickness discretisation.

Equivalent single layer method

Using this approach the laminate stacking sequence is interpreted as part of the material description and consequently entered in the material definition part of the FEA. The commercial code ABAQUS [8] offers convenient graphical user interfaces to create and monitor the stacking sequence information consisting of the material definition (commonly orthotropic, see Sec. 3.1.1), the thickness and the orientation angle β (see Fig. 2.1c) of each individual lamina. The necessary through-thickness integration is controlled by the number of z-integration point at which the requested results (commonly stresses and strains) are output, too. Assigned to the suitable shell or continuum shell elements (see Sec. 3.3.2) the created laminate section represents the whole stacking sequence in just that element. This means that the single-layer equivalent approach requires exactly *one* element for the discretisation of the contained laminate stacking sequence in z-direction. If the resolution in z-direction shall be refined it is possible to increase the number of z-integration points. Alternatively the stacking sequence is in parts condensed in several ESL sections which have to be assigned to the adequate number of elements stacked in thickness direction.

Layer-wise method

The layer-wise method to provide the laminate behaviour is a combination of the separate orthotropic material definitions of each lamina and the geometric representation of the laminate stacking sequence. Hence the effort to describe the laminate behaviour has been transferred from the material definition to the geometrical representation of the laminate. Accordingly the number of elements in thickness direction depends on the number of laminae incorporated in the respective laminate whereas a minimum discretisation by *one* element per layer is required. The resolution in z-direction is defined by the number of elements per layer stacked in through-thickness direction. Generally the LW method results in a greater number of elements associated with a greater computational effort, but the suitable continuum shell and continuum elements provide more accurate results (see Sec. 3.3.2).

3.3.2 Element types for laminate structures

FEA provides a wide variety of elements not only for 3D stress analysis in laminates and laminate structures but also for the analysis of thermal residual stresses (see Sec. 3.7) and delamination (see Sec. 2.2.4). In the following the capabilities and applicability of typical commercial element types for the laminate representation are summarised using

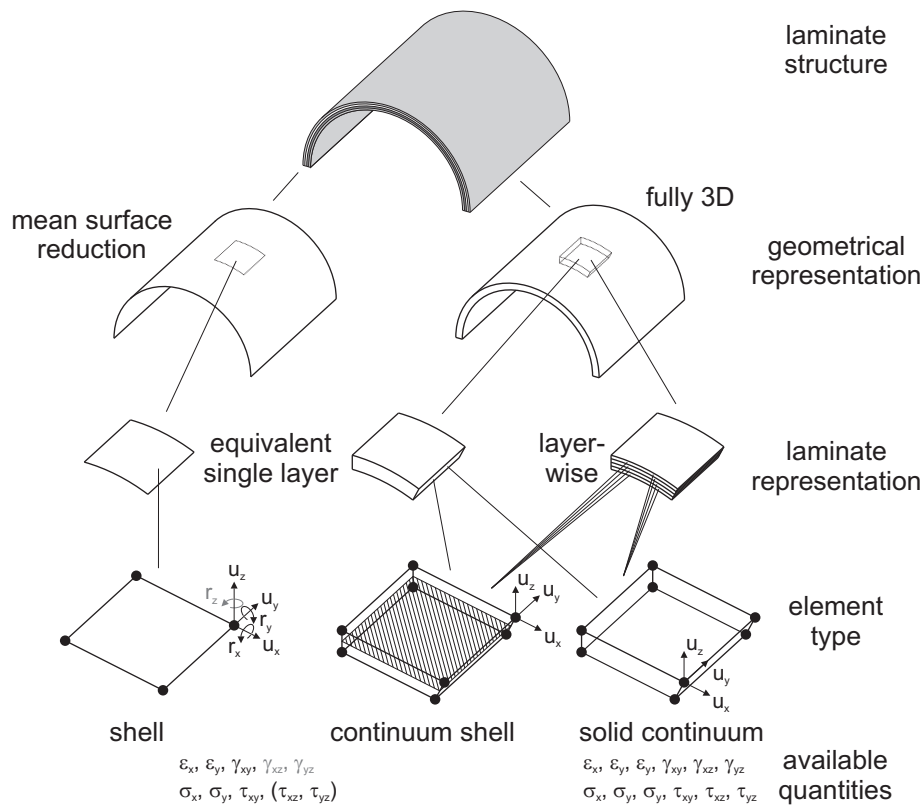


Figure 3.4: FE modelling strategies for laminate structures.

the example of ABAQUS [8]. All the mentioned elements are also provided including a thermo-mechanical coupling for an analysis including residual stresses. The first step in choosing an appropriate element type is the decision how the local thicknesses of the laminate structure shall be represented in the FE model. For the representation of geometries with small thicknesses compared to their lateral extension it may be reasonable to reduce the geometry to its mean surface, thus to a flat, locally 2D geometry without a geometrical extension in through-thickness direction. In this case the local thickness of the structure is interpreted as a material parameter. Alternatively the local thickness of the structure may be retained in the discretised geometry which results in a fully three-dimensional FE representation of the structure (see Fig. 3.4). This decision regarding the geometric representation of the structure influences the choice of element types described below and thus the suitable material definition method (see Sec. 3.3.1).

Shell elements

The most conventional group of element types associated with the representation of geometries with small thicknesses compared to their lateral extension are shell elements.

These elements are used to discretise geometries without any expansion in thickness direction – i.e. locally two-dimensional. The thickness information of the represented structure goes into the material definition. Shell elements are provided for thin structures based on the Kirchhoff kinematics as well as for thick structures based on Reissner kinematics including through-thickness shear contributions due to bending deformation [68]. Applied in a 3D modelling space, thin shell elements feature three translatory degrees of freedom $\bar{u} = [u_x, u_y, u_z]$ but only two rotatoric r_x and r_y from which the inplane strain components ϵ_x , ϵ_y and γ_{xy} are evaluated. Thick shell elements feature the full set of translatory \bar{u} and rotatoric \bar{r} degrees of freedom from which through-thickness the shear strains γ_{xz} and γ_{yz} are derived additionally. In both cases, only the inplane stress components σ_x , σ_y and τ_{xy} are comprised in the governing differential equations, accordingly only these measures are a result of the solution derived by the Principle of Virtual Displacement (PVD). Furthermore ABAQUS provides through-thickness shear stress results τ_{xz} and τ_{yz} which are postprocessed by means of the equilibrium equations

$$\begin{aligned}\frac{\partial \sigma_x}{\partial x} + \frac{\partial \tau_{yx}}{\partial y} + \frac{\partial \tau_{zx}}{\partial z} &= 0 \\ \frac{\partial \tau_{xy}}{\partial x} + \frac{\partial \sigma_y}{\partial y} + \frac{\partial \tau_{zy}}{\partial z} &= 0 \\ \frac{\partial \tau_{xz}}{\partial x} + \frac{\partial \tau_{yz}}{\partial y} + \frac{\partial \sigma_z}{\partial z} &= 0.\end{aligned}\tag{3.10}$$

Neither stress σ_z nor strain components ϵ_z in through-thickness direction are output. Using a shell element any applied boundary condition is related to the mean surface in general. Only if advanced FEA packages offer the possibility to apply boundary conditions to the outmost integration points in z-direction the required continuous displacement field over the bi-material interfaces (see Tab. 3.2) can be enforced in a stacked shell discretisation. If this is not the case, the z-stacking of shell elements for the representation of laminates and laminate structures is not recommended. This interdicts a layer-wise material representation as well.

Continuum shell elements

Continuum shell element are generally based on the kinematics and equations of work defined for conventional shell elements. However they are used to discretise fully 3D geometries. They automatically derive the shell thickness information from geometry if the shell normal has been correctly defined by the user. The necessary shell-analog strain measures are related to the exclusively available translatory degrees of freedom at the eight corner nodes. Continuum shell elements generally provide the same output

information as conventional shell elements – no stress σ_z and no strain components ϵ_z either – but they have an unlimited z-stacking capability. Accordingly they are available for either equivalent single layer or layer-wise laminate descriptions. The laminates z-direction may be discretised by a single continuum shell element comprising an equivalent single layer laminate description or by one or more continuum shell elements per layer together with the orthotropic material descriptions of the respective laminae.

Solid continuum elements

Solid continuum elements are not commonly recommended for the discretisation of geometries with small thicknesses compared to their lateral extension because the accuracy of these groups of elements relies on balanced spatial proportions. In the case of laminate structures this requirement eventually results in a lateral discretisation density which equals at least the lamina thickness. If possible at all this is extremely computationally expensive. The representation of a laminate by solid continuum elements is however free of axiomatic assumptions regarding the displacement, stress or strain field hence the results are expected to converge against the requirements of table 3.2 for a growing number of elements stacked in z-direction. A further unique feature is the availability of stress σ_z and strain components ϵ_z in through-thickness direction. Aiming on a truly 3D failure and post-failure analysis (see Chs. 4 and 5) this output is extremely valuable and suggests the use of solid continuum elements at least for the detailed analysis of generalised laminate behaviour (see Sec. 3.5).

3.4 Reference: Analytical solution following Pagano

The numerous combinations of laminate material definitions and laminate structure representations presented above perform significantly different in terms of output quantities and their quality. In the following a number of modelling strategies are compared to an analytical solution for laminates by Pagano [67]. It is derived from layer-wise equilibrium equations (see App. A) and completely fulfils the requirements of table 3.2. It is based on the complete 3D orthotropic material law and neglects neither of the stress or strain components of the full 3D space. However it does not include the Reissner kinematics [68] regarding through-thickness shear components arising from a bending deformation. Hence the Pagano analytical solution is restricted to thin laminate plates. It is valid for rectangular, simply supported laminate plates under an sinusoidal load applied to the top

surface $z = t/2$ (see Fig. 3.5):

$$q_0(x, y) = 1 \cdot \sin\left(\pi \cdot \frac{x}{a}\right) \cdot \sin\left(\pi \cdot \frac{y}{b}\right) \quad [N/mm^2] \quad (3.11)$$

The laminate plate is supported along all of its edges whereas the whole cross-sections along these edges are vertically fixed:

$$u_z(x = 0) = u_z(x = a) = u_z(y = 0) = u_z(y = b) = 0 \quad \text{for all } z\text{-positions} \quad (3.12)$$

Additionally no longitudinal displacement along the edges is allowed:

$$u_y(x = 0) = u_y(x = a) = u_x(y = 0) = u_x(y = b) = 0 \quad \text{for all } z\text{-positions} \quad (3.13)$$

This results in undisplaceable corners of the laminate plate through its entire thickness.

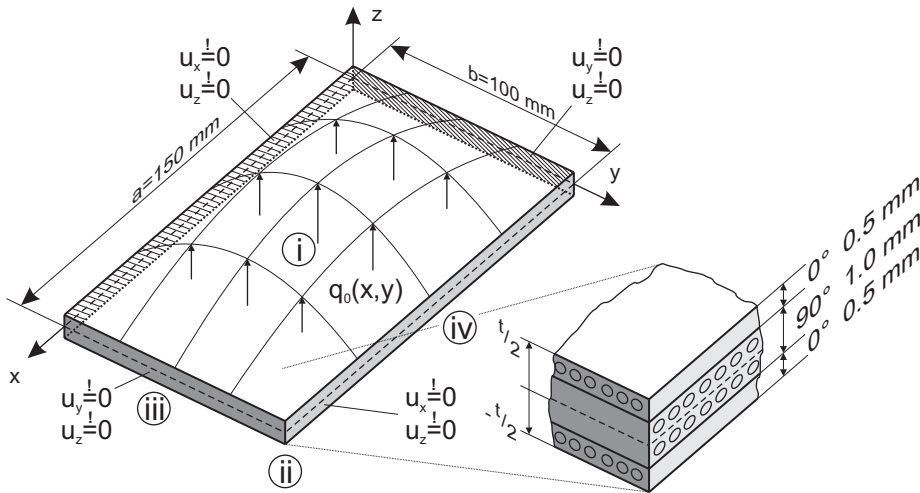


Figure 3.5: Pagano analytical solution: Geometry, stacking sequence, load and displacement boundary conditions of the reference laminate plate.

The FEA results of the reference laminate plate have been derived by ABAQUS Version 6.8. For the material description following the equivalent single-layer approach the material section⁴ has been generated by the composite layup manager whereas the respective lamina materials are of the ortho-type. The section integration has been carried out during analysis by the Simpson thickness integration rule based on five through-thickness integration points per lamina. Such a material section definition may be used in combination with shell, continuum shell and solid continuum elements. The layer-wise material description assigns the respective lamina material behaviour of the ortho-type to a solid, homogeneous material sections if solid continuum elements are to be used. In the case of continuum shell elements the shell, homogeneous section

⁴This font denotes ABAQUS-specific terminology for the sake of reproducibility.

type has been chosen whereas the section integration has been carried out in the same way as described above.

Strictly geometrically linear analyses (`nlgeom=OFF`) have been run where the load quantity is constantly defined on the `undeformed` area and the load direction does not follow `rotation` (see Sec. 3.6). The lamina properties are those of HexPly 8551-7 (IM7) (see App. C). Numerous combinations of material descriptions, element types and through-thickness discretisations have been run (see Tab. 3.3) whereas a constant lateral discretisation of 20 by 30 elements has been retained for the sake of consistency. While this is a reasonable mesh density for the shell representation of the laminate, the resulting volume elements are extremely thin compared to their lateral extensions. Being far away from the desired cube shape [8], the present continuum elements' shape corrupts their accuracy in the case of a linear ansatz – see the corresponding displacement results in table 3.3.

material description	ESL			LW			
<i>z</i> -discretisation	1 per laminate			1 per lamina		4 per lamina	
element family	shell	continuum shell	solid continuum	continuum shell	solid continuum	continuum shell	solid continuum
type	S4R	SC8R	C3D8R	SC8R	C3D8R	SC8R	C3D8R
	22.37	22.25	73.83	22.19	22.61	22.19	3.54
vertical displacement [mm]	1	1.14	2.07	1.78	1.34	8.65	7.35
	S4		C3D8		C3D8		C3D8
	22.34		30.93		18.35		15.46
	1.60		2.76		1.87		9.23
relative CPU time	S8R*		C3D20R*		C3D20R*		C3D20R*
	22.41		22.10		22.24		22.24
	2.01		4.94		7.32		86.37
			C3D20*		C3D20*		C3D20*
			22.19		22.23		22.24
			9.28		9.90		98.02

Table 3.3: Pagano reference FEAs: Combinations of material descriptions, element types and through-thickness discretisations, R denotes *reduced integration*, * a quadratic ansatz. Below the consumed CPU time related to the S4R element and the vertical displacement $u_z(a/2; b/2; -t/2)$ [mm] – the analytical value following Pagano is 22.27 mm.

The following stress results (see Fig. 3.6) provide the through-thickness distribution of

- **a:** $\sigma_x(x = a/2; y = b/2)$, position i in figure 3.5,

- **b:** $\sigma_y(x = a/2; y = b/2)$, position *i* in figure 3.5,
- **c:** $\sigma_z(x = a/2; y = b/2)$, position *i* in figure 3.5,
- **d:** $\tau_{xy}(x = a; y = b)$, position *ii* in figure 3.5,
- **e:** $\tau_{xz}(x = a; y = b/2)$, position *iii* in figure 3.5, and
- **f:** $\tau_{yz}(x = a/2; y = b)$, position *iv* in figure 3.5

for selected discretisations and element types and compares them to the analytical solution. Looking at these analytical solutions provides a deeper understanding of the through-thickness distributions:

- The inplane stresses σ_x and σ_y (see Figs. 3.6a and b) exhibit the expected jumps over the bi-material interfaces due to the required continuous strain fields. The stresses in those laminae are higher, which possess the higher stiffness against the corresponding strain component, i.e. have their fibres oriented in the direction of that strain component.
- The through-thickness stress σ_z (see Fig. 3.6c) takes the value of the externally applied stress on the top surface ($z = 1$) and equals 0 on the bottom face ($z = -1$) according to the free surface condition.
- The inplane shear stress τ_{xy} is a straight line through the plate's whole thickness known from isotropic material (see Fig. 3.6d). As all layers are made of the same lamina material, they possess an identical stiffness against inplane shear no matter what their orientations are.
- Despite their different appearance, the distributions of the two through-thickness shear stresses τ_{xz} and τ_{yz} (see Figs. 3.6e and f) differ in quantity only. They generally show the same continuous slope and fulfil the free surface condition, i.e. no shear stresses, on the top and bottom of the laminate.

For the comparison between different FEA results figure 3.6 concentrates on four model representations:

- **ESL, S4R:** An equivalent single layer discretisation (see Sec. 3.2.1) with four-node linear shell elements with reduced integration. This model representation is computationally extremely cheap and is used for, e.g., complete vehicle simulations. The provided stress results show excellent agreement with the analytical solutions

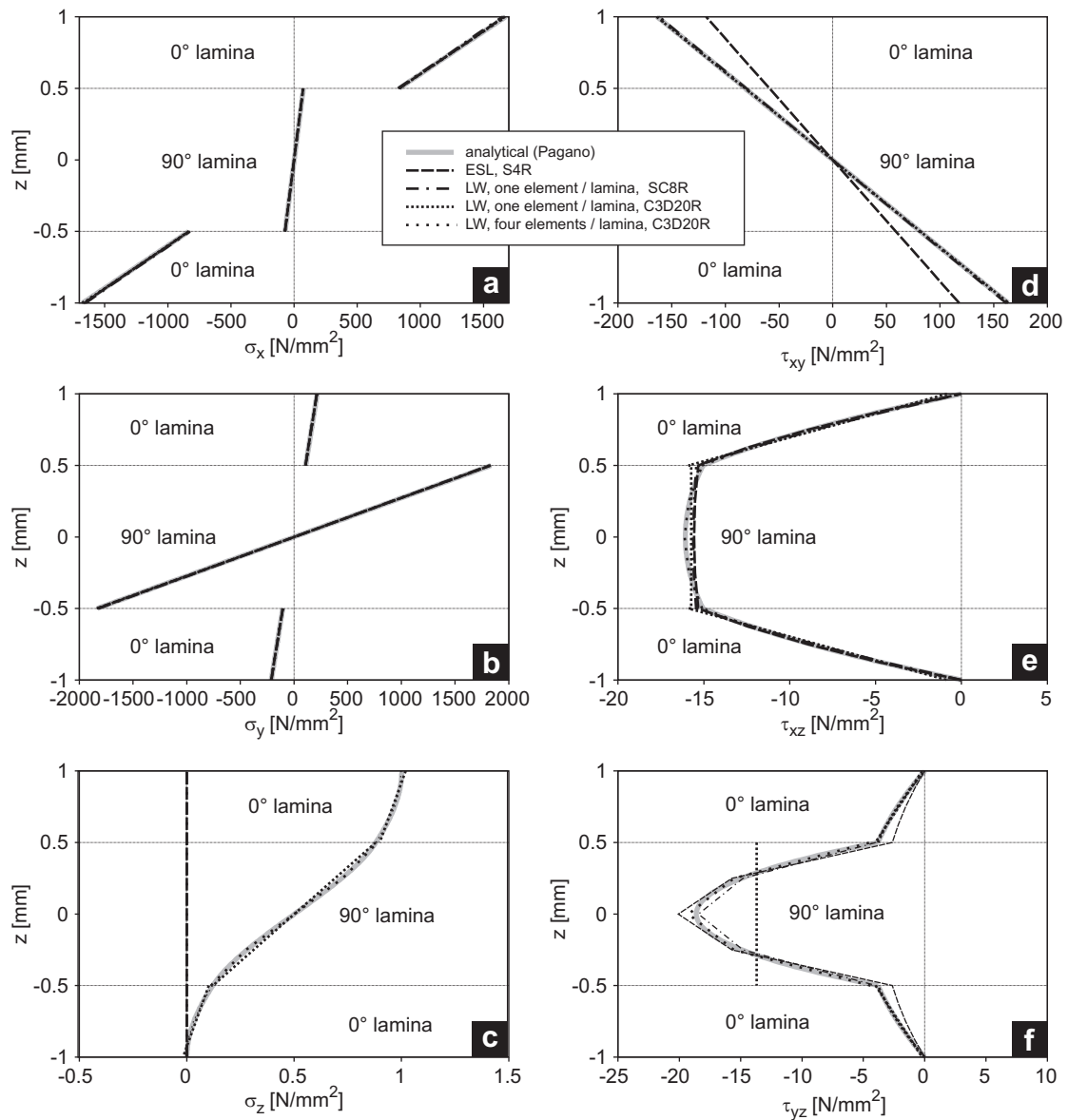


Figure 3.6: Pagano reference FEAs: Through-thickness stress distributions compared with the analytical solutions following Pagano.

whereas the inplane shear results τ_{xy} slightly differ in quantity. Even the post-processed through-thickness shear stress values τ_{xz} and τ_{yz} (see Sec. 3.3.2) are close to the analytical curves but no through-thickness stress σ_z is provided.

- **LW, one element / lamina, SC8R:** A layer-wise discretisation (see Sec. 3.2.2) with one continuum shell element per lamina in through-thickness direction. This representation compares a three-dimensional geometry with computationally cheap two-dimensional kinematics. It performs similar to the above shell elements whereas the more expensive LW representation results in a slightly improved accuracy. Still

there are no σ_z -results provided.

- **LW, one element / lamina, C3D20R:** A layer-wise discretisation with one quadratic solid continuum element per lamina. This geometrically three-dimensional representation offers the full 3D stress result including an accurate σ_z slope. It is computationally extremely expensive (see Tab. 3.3) but still has visible shortcomings where large stress gradients occur within a lamina – here in the τ_{yz} -slope.
- **LW, four elements / lamina, C3D20R:** A layer-wise discretisation with four quadratic solid continuum elements per lamina. At nearly 100 times the computational costs of a plain shell element representation, this model provides excellently accurate fully three-dimensional stress results.

The results generally prove, that a denser and higher-order discretisation produces more accurate results. However, the comparison above is not able to act as an overall guideline. The most favourable compromise between the accuracy and the computational cost depends on numerous factors – last but not least on the requirements of the subsequently applied failure criterion. Rigorously judged, the results above are exclusively significant for the presented laminate, its load and boundary conditions and its lateral discretisation. Different stacking sequences, geometries or loads may lead to qualitatively and quantitatively different stress results for which the individual shortcomings of the respective model representations have to be assessed anew. However, the necessary effort is well-invested regarding the accuracy of a subsequent stress-based failure prediction. Regarding the WWFE-II test cases (see Ch. 7) the assessment had revealed, that a layer-wise discretisation with one linear solid continuum element per lamina is sufficient.

3.5 Generalised laminate behaviour: FEA of an RVE

Besides the analysis of complete laminate structures there is the legitimate interest in the laminate's behaviour in terms of an general material description of the laminate. Such analyses are exemplary demanded in the test cases of the WWFE-II (see Ch. 7 and [69]). This *generalised laminate behaviour* characterises the failure and post-failure degradation behaviour of a laminate due to loads applied to the lamina stacking sequence as a whole. Using a layer-wise failure criterion (see Ch. 4) and post-failure degradation rule (see Ch. 5) the stress analysis on the laminate level is again the crucial part in determining generalised laminate behaviour. The stress analysis' output are the stresses and strains in each involved lamina based on the current – possibly degraded – constitutive behaviour.

The procedure described below is intended to determine a general material behaviour which is independent from the laminate's inplane dimensions. Accordingly in an appropriate stress analysis on the laminate level the laminate's dimension in x- and y-direction may only play a limited role as auxiliary quantities.

While analytical algorithms like Classical Laminate Theory (CLT) are most efficiently used for the prediction of inplane behaviour [70–73], 3D load cases clearly exceed their applicability. Though there are analytical approaches to the 3D-stress analysis of laminates, closed form solutions are only known for few specific cases of rectangular laminates under sinusoidal transverse load (see Sec. 3.4 and [67]). Alternatively the Representative Volume Element (RVE) or *unit cell* approach currently gains more and more importance in the numerical determination of generalised material behaviour of multiphase materials [74, 75]. The basic idea behind RVEs is that the elastic energy stored inside a unit cell is identical to the one stored inside the represented homogenised continuum. The RVE is a volume that is microstructurally typical of the material system. Therefore, it must contain an adequate number of the different material phases, inclusions, defects, voids or cracks. In principle, the inner structure of a unit cell is arbitrary, structured or not, but with the requirement to replicate periodically in space. The method is capable of modelling the material behaviour of multi-phase composites, cellular solids or multi-dissipative materials, e.g., as long as homogenisation is permitted [16].

Within the desired representation the determined behaviour of the material should not depend on the dimension of the analysed material section, accordingly the determined general material behaviour is called *statistically homogeneous* [18–20]. The smallest volume where this condition applies defines the Representative Volume Element (RVE) or *unit cell*. By definition an RVE is microscopically large enough to include the relevant inhomogeneities and macroscopically small enough to be regarded as a single material point. The behaviour of the unit cell represents the average response of the material to the applied loading. This average in form of a macroscopic stress-strain state can be calculated in various manners. Efficient analytical solutions are available for simple cases with respect to geometry, material behaviour and loading conditions [14, 15]. Simple RVEs can be combined to build up more complex microstructures. This procedure calls for a combination of analytical and numerical solutions – the generalised method of cells (GMC). The Structures and Acoustics Division of the NASA implemented this technique to provide a micromechanical analysis tool [17]. Increasing computational power weakened the need for analytical solutions, and *ab-initio* numerical solutions for unit cells became computationally affordable. Since FEA is the standard tool for the structural analysis, its application to the RVE computation is straightforward. Numerical solution techniques entail the advantages to include geometric (see Sec. 3.6) and material nonlin-

earities (see Sec. 3.1.2) as well as complex interface, boundary and loading conditions. Complex non-continuous structures can be represented in a much more refined way as well (see Fig. 5.7).

Whereas FEA is a common tool for the stress analysis on the structural level, the determination of general material behaviour of a laminate or a non-continuous (see Sec. 5.6) or non-homogeneous structure [76] is a field of application which requires further considerations. The abstract aim is the determination of the general behaviour of a volume (here the RVE) independent from interfering effects of clamping or load induction. By definition an RVE has to contain all the material inhomogeneities in a representative manner. Transferring this requirement to a laminate, the material inhomogeneities consist of the different laminae and their stacking sequence in z -direction only (see Fig. 3.7) and the RVEs inplane dimensions are arbitrary. The x - z - and y - z -faces have to fulfil the periodicity requirement whereas the x - y -faces (top and bottom) are except from this because these RVE faces represent free surfaces of the material.

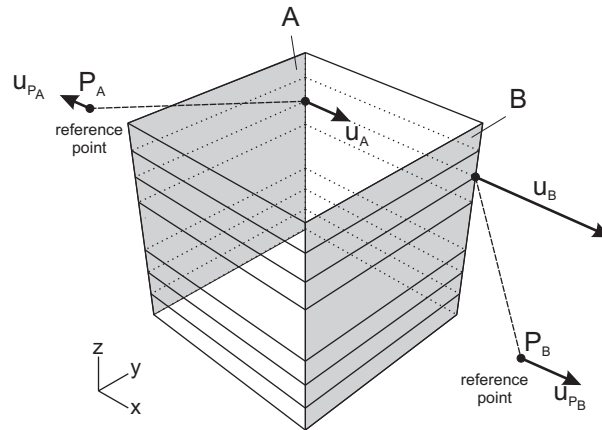


Figure 3.7: FE model: RVE representation of the laminate including exemplary x -displacement constraints for two opposed nodes.

Periodic boundary conditions are not commonly implemented in commercial FEA packages. The requirement that a deformed or undeformed RVE has to allow its periodically assembly to an endless row in any coordinate direction results in the requirement of equal topography of opposed faces. This is achieved by the introduction of one additional reference point per face [77]. The approach is exemplary shown in figure 3.7 for the two y - z -faces of the RVE. The two reference points P_A and P_B are allowed to move in order to enable an overall normal or shear deformation of the RVE. However the relative displacement between an arbitrary node on the surface A and its reference point P_A is set equal to the relative displacement between the respective partner node on the opposite

surface B and its reference point P_B :

$$u_A - u_{P_A} = u_B - u_{P_B} \quad (3.14)$$

This procedure ensures that the deformation of face A is equal to the one of face B whereas the two faces are still allowed the relative motion between each other. The approach requires an equal FE mesh on opposed faces and may result in a large number of displacement constraints in the case of complex geometries (see Sec. 5.6). Earlier applications of the developed approach [78] revealed that the periodicity requirement not only refers to displacements but to stresses as well. Analysing unsymmetric RVE geometries or loads the stress periodicity is not achieved by the measures described above. The definition of stress boundary conditions however requires finite elements with mixed stress-strain-formulations [46] which are currently not available in commercial FEA packages.

Regarding the discretisation of the laminate RVE the FE model needs no discretisation along the two inplane directions due to the RVE's arbitrary inplane dimensions. Neglecting bending load cases and unsymmetric laminates, there are only homogeneous states of stress throughout the lamina's thickness direction expected. Thus only one element per lamina is sufficient for the WWFE-II load cases (see Fig. 3.7). Though commercial FE packages offer various shell elements for the representation of laminates and laminate structures (see Sec. 3.3.2), their 3D capabilities in terms of stress results are still limited (see Sec. 3.4). Thus the RVE model applied to the WWFE-II test cases (see Ch. 7) uses fully integrated linear volume elements.

3.6 Geometric nonlinearity

UD FRC laminae are highly orthotropic materials with considerably different constitutive behaviour in the respective directions. When subjected to a load the material's reaction depends on its orientation towards that load. In the case of UD FRCs very little variances in the orientation may have significant effects – particularly in the case of fibre-parallel applied load. Increasingly loaded the material's orientation might change during the process and therewith changes its orientation towards and its reaction due to this applied load.

A static Finite Element Analysis offers two ways of forming the equilibrium - geometrically linear based on the original geometry or nonlinear based on the actual geometry. The reasons above highly recommend to run geometrically nonlinear analyses when predicting UD FRC's failure and post-failure behaviour, particularly in the case of large deformations above 5% or in shear load cases. This approach automatically includes the

influences due to the change of fibre direction during the loading process. Running geometrically nonlinear analyses requires the following considerations about the direction and quantity of applied loads and about the material description.

3.6.1 Load application

It was stated that during an increasing load process the geometry of a structure, a laminate or a lamina is likely to change. Accordingly in the FE representation the normals of faces and the local coordinate systems of nodes rotate. Furthermore volumes change as well as surface areas.

As far as these measures are used to define the direction or the quantity of applied loads, it's up to the user whether the applied stresses, forces, displacements or rotations are to be constantly based on the original geometry or have to follow the changes going along with the progressive loading. The decision that an applied shear load stays constant in direction during the progressive loading results in a combination of shear and normal stress in the deflected lamina whereas an applied load rotating together with the material's coordinate system constantly produces shear stress only. Applying the load in form of a force distributed over an area the overall applied force stays constant if the load is permanently related to the original area size but the resulting stress on the actual surface changes. Applying such a load related to the actual size of the area the resulting stress stays constant but the overall applied force changes during the progressive loading.

Since it is unknown how the experimental results of the WWFE-II will have been gained [69], the simulated forces have been applied preserving their original orientation. Their magnitude is defined on the undeformed surface which results in true stresses being higher or lower than the applied ones depending on an expansion or contraction of the respective surface. Thus the load applied can be understood as *nominal load* and forms the basis for the presentation of results (see Sec. 7.2).

3.6.2 Engineering vs. true stresses and strains

Running a geometrically nonlinear FE analysis, the original geometry and load configuration is neither available nor relevant for any load increment but the first one. The equilibrium of any successive load increment is based on the actual geometry and load configuration at the beginning of the respective increment, hence stresses and strains related to the original geometry are neither considered during the analysis nor output at the end. Accordingly the underlying material model has to correlate *true* stresses with *true*

strains rather than *engineering* values as they are commonly determined in experiments. Whereas engineering stresses are the quotient of the force F and the original cross-section

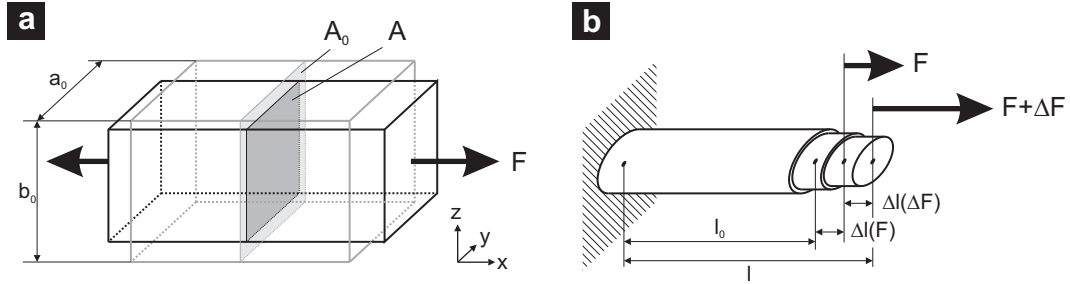


Figure 3.8: Change of material's cross-section area (a) and length (b) due to an uniaxially applied tensile load F .

area A_0 (see Fig. 3.8a), the true stress is derived by using the deformed cross-section area $A(F)$:

$$\sigma^{engin} = \frac{F}{A_0} \quad \text{and} \quad \sigma^{true} = \frac{F}{A(F)} = \frac{F}{A(\epsilon_x)} = \frac{F}{a(\epsilon_x) \cdot b(\epsilon_x)} \quad (3.15)$$

The strain in x-direction ϵ_x induces the two lateral contractions

$$\epsilon_y = -\nu_{xy} \cdot \epsilon_x \quad \text{and} \quad \epsilon_z = -\nu_{xz} \cdot \epsilon_x \quad (3.16)$$

whereas the quantitative effects on the dimensions are

$$a = a_0 \cdot (1 + \epsilon_y) \quad \text{and} \quad b = b_0 \cdot (1 + \epsilon_z) . \quad (3.17)$$

From equations 3.15 to 3.17 the relation between true and engineering stress is

$$\sigma^{true} = \frac{\sigma^{engin}}{1 - (\nu_{xy} + \nu_{xz}) \cdot \epsilon_x + \nu_{xy} \cdot \nu_{xz} \cdot \epsilon_x^2} . \quad (3.18)$$

Note that equation 3.18 differs from the commonly cited Ludwik law $\sigma^{true} = \sigma^{engin} \cdot (1 + \epsilon_x)$ which postulates a constant volume [79]. This relation is valid for fully plastic deformation only, thus is *not* relevant here.

An analogous consideration relates true and engineering strains by means of figure 3.8b where a load increase by ΔF results in an additional elongation $\Delta l(\Delta F)$:

$$\Delta \epsilon^{engin} = \frac{\Delta l(\Delta F)}{l_0} \quad \text{and} \quad \Delta \epsilon^{true} = \frac{\Delta l(\Delta F)}{l(F)} = \frac{\Delta l(\Delta F)}{l_0 + \Delta l(F)} \quad (3.19)$$

Integrating from l_0 to a deformed l represents a summation of infinitesimally small load increments [80] and the result is

$$\epsilon^{true} = \ln \left(\frac{l}{l_0} \right) \quad \text{in contrast to} \quad \epsilon^{engin} = \frac{l - l_0}{l_0} . \quad (3.20)$$

Equation 3.20 points out why *true* strains are often referred to by the term *logarithmic* strains.

3.7 Residual stresses

UD fibre reinforced laminae show orthotropic behaviour in terms of thermal expansion. In the process of curing a laminate, this leads to residual stresses in the final laminate. The process is chemically and thermodynamically challenging. Influences like tempering history, ambient pressure and humidity are hardly to cover in a structural mechanics context. However the representation of the process by a simple cooling from stress free temperature to room temperature using linear thermal coefficients is intuitive but overestimates the resulting residual stresses according to our experience [5, 6]. Puck assumes the true residual stresses to reach half the values calculated from this approach. Accordingly the presented analyses are based on half the temperature drop from the stress free temperature to ambient temperature (see Sec. 7.2).

Including thermal expansion within a thermo-mechanically coupled analysis is a standard procedure in contemporary commercial FE packages and is carried out independently from Puck's Theory contained in the user-defined material description (see Ch. 6). Note that in the case of FEA, the thermally induced residual stresses are automatically subject to the nonlinear constitutive behaviour of the material. In contrast to most analytical approaches, the residual stresses are not calculated at first and then constantly superposed but they are incrementally computed from the residual strains and the current secant stiffness.

4 Puck's failure theory

The present chapter concentrates on the fracture criteria for unidirectionally fibre reinforced polymer composites (UD FRPCs) developed by Puck. As the first World-Wide Failure Exercise [2] encyclopedically compares currently available failure criteria, the present work does not compare Puck's criteria with competitive approaches. After a short introduction to failure hypothesis in general (see Sec. 4.1), the chapter describes Puck's inter-fibre fracture criterion (see Sec. 4.2) and the associated extensions beyond Mohr's hypothesis (see Sec. 4.3). Before the fibre fracture is addressed in section 4.7, the application within a laminate (see Sec. 4.5) and to special cases (see Sec. 4.6) is discussed.

4.1 Introduction to failure prediction

The task of a failure criterion is the determination whether an arbitrary load applied to the lamina leads to a fracture or not. This is commonly achieved by a fracture hypothesis which comprehends the set of all possible states of fracture. It is important to understand the fracture conditions as hypothetical in the sense that they give statements regarding an infinite number of states on the basis of very few known states of fracture. These known – i.e. experimentally accessible, hence determinable states of fracture are referred to as *basic strengths*. In the case of UD FRCs these are the fractures due to applied fibre-parallel or fibre-perpendicular tension and compression (R_{\parallel}^t , R_{\parallel}^c , R_{\perp}^t and R_{\perp}^c) and due to inplane and out-of-plane shear ($R_{\perp\parallel}$ and $R_{\perp\perp}$). These basic strengths may be expressed in terms of stress or strain, but as Puck's criteria are stress-based [21] no strain thresholds are considered within this work. The fracture criterion defines a closed surface in the six-dimensional stress space $(\sigma_1, \sigma_2, \sigma_3, \tau_{12}, \tau_{13}, \tau_{23})$, includes – in the best case – all the available experimental determined strengths and predicts reasonable fractures at all other stress combinations (see Fig. 4.1). This task in mind it becomes evident that a fracture criterion can never be more than an hypothesis – i.e. a model representation – of what happens in cases which are not experimentally proven. As an hypothesis fracture criteria may be proven or contradicted by further experimental results if the criterion is not versatile enough to be adapted to the later findings. The hypothesis may be based on pure mathematical considerations regarding a surface-definition or on fracture-mechanical or physical considerations. The rising number of experimental results has however pointed out the advantage of physically-based fracture conditions of which Puck's Theory is the

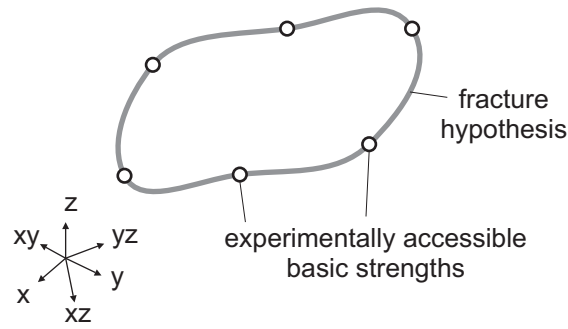


Figure 4.1: Fracture hypothesis (grey line) in the six-dimensional stress or strain space: Its surface contains all those stress or strain combinations presumable leading to fracture, particularly the experimentally determined basic strengths (dots).

first and most elaborated one in the case of UD FRPCs.

Figure 4.2 compares the most known representation of Puck's Theory, the *fracture cigar* (b) with a common Tsai-, Hill- or Wu-like [2, 81, 82] global stress-based criterion (a). Both visualise a fracture condition for plane stress load cases. Without a lookahead to-

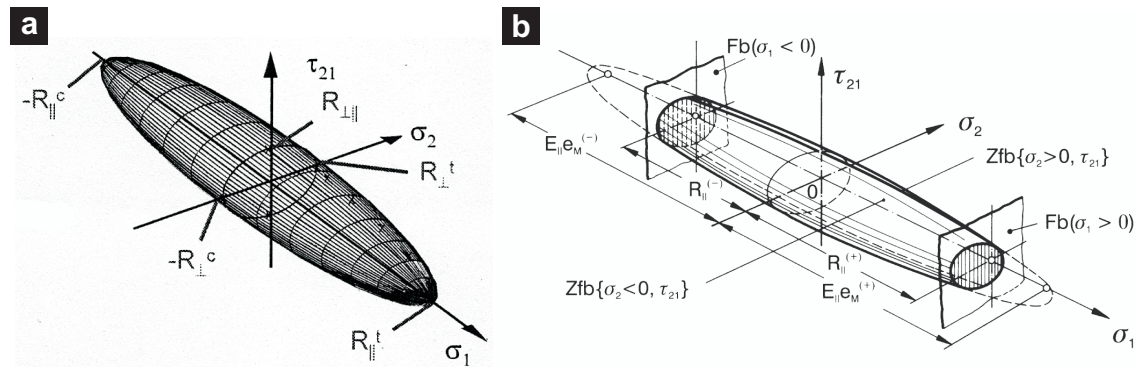


Figure 4.2: Visualisation of UD FRC fracture criteria: Tsai-, Hill- or Wu-like global stress based criterion (a) and the 2D representation of Puck's action plane-related criteria, the *fracture cigar* (b), from [83].

wards the sections below the two main differences between these well-known figures are outlined here: Whereas the left picture actually shows the global stress-based criterion defined in the shown $(\sigma_1, \sigma_2, \tau_{12})$ -stress space, the Puck's fracture cigar is only a result of the actual action plane-related criterion. The second, and visible difference is that Puck's fracture cigar consists of two sub-surfaces which represent two different criteria for fibre fracture (end faces) and inter-fibre fracture (lateral surface). This allows Puck's Theory to respond to the significant differences between both fracture types regarding fracture-mechanical aspects (see Sec. 2.2). Both fracture criteria are described in detail in the following.

4.2 Puck's inter-fibre fracture criterion

The following section describes in detail the elementary thoughts on which Puck's action plane-related fracture criterion is based on (see Sec. 4.2.1) and the aspects of application which are specific to the criterion (see Sec. 4.2.2). The following theoretical part introduces the visual representation of the IFF criterion – the Master Fracture Body (MFB) – and its mathematical description (see Sec. 4.2.3). The presentation of Puck's IFF criterion concludes with considerations about the portability of the common 2D fracture modes classification towards 3D analysis (see Sec. 4.2.4).

4.2.1 Action plane-related fracture criterion

Puck's criteria for fibre fracture (FF) and inter-fibre fracture (IFF) of unidirectionally reinforced (UD) composites are physically based on hypotheses and mathematical formulations appropriate for brittle fracture [4]. Particularly important are formulations of Coulomb [84], Mohr [85] and one of their successors, Paul [86], which have been developed for quasi-isotropic materials such as lime stone or grey cast iron. They have been adapted by Puck to the transversely isotropic UD fibre/polymer composites.

The foundation of all the following formulations is Mohr's fracture hypothesis:

The fracture limit of a material is determined by the stresses on the fracture plane.

Of main importance for inter-fibre fracture (IFF) are the stressing σ_{\perp} transverse to the fibres and the two different shear stressings – inplane shear stressing $\tau_{\perp\parallel}$ and through-thickness shear stressing $\tau_{\perp\perp}$. The term *stress* prevalently implies stresses in the rectangular global or lamina coordinate system. Being a transversely isotropic material however, a UD-lamina is stressed by σ_2 and σ_3 in the same way. Hence the term *stressing* is used to emphasise that values in the cylindrical coordinate system of a UD lamina ($\sigma_{\perp}, \sigma_{\parallel}, \tau_{\perp\parallel}, \tau_{\perp\perp}$) are addressed. Conventional failure criteria are formulated with basic strengths $R_{\perp}^t, R_{\perp}^c, R_{\perp\parallel}$ and $R_{\perp\perp}$ belonging to the basic – i.e. uniaxial¹ – stressings. Every single strength is measured by the application of its particular stressing homogeneously to a UD-volume element up to failure. In a failure criterion without physical basis it is irrelevant where and how failure occurs because the measured uniaxial strengths act as anchor points for an analytical curve or surface without physical meaning only.

¹Within the present work the term *uniaxial* defines cases where the applied load consists of a single stress or strain component no matter whether this is a normal or a shear component.

While the general approach is the same when using action plane-related fracture criteria following Mohr and Puck, the kind and location of a fracture do matter. In this case the combined stresses acting *on a common action plane* have to be related to the *strengths of that action plane*. These strengths are the amount of a single stressing σ_{\perp} or $\tau_{\perp\parallel}$ or $\tau_{\perp\perp}$ that an action plane can bear. Demanding an accurate distinction between these figures and usual strengths, Puck has introduced the term *fracture resistance of the action plane* R^A for the necessary action plane-related material description and has formulated the following definition:

A fracture resistance of the action plane is the resistance (expressed in the dimension of a stress) by which an action plane resists its own fracture due to a stress in the considered action plane caused by one of the basic stressings σ_{\perp} or $\tau_{\perp\perp}$ or $\tau_{\perp\parallel}$.

The adequate question when determining a fracture resistance of an action plane is then (see Fig. 4.3):

To which amount can a single stressing ($\sigma_{\perp}^{t/c}$ or $\tau_{\perp\perp}$ or $\tau_{\perp\parallel}$) be increased before a fracture occurs in exactly that action plane to which the respective stressing is applied?

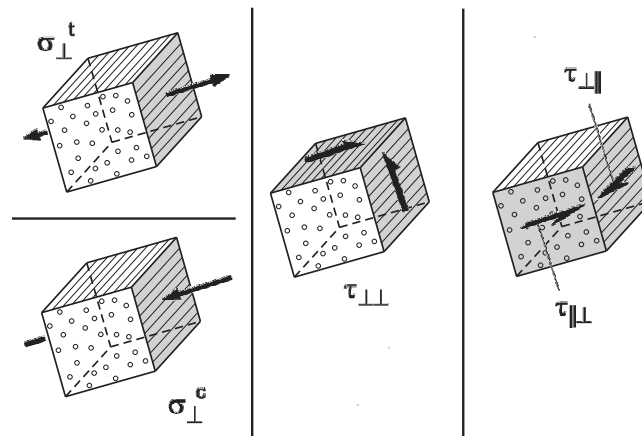


Figure 4.3: Basic stressings of a UD-lamina and their action planes (grey).

Determining the common strength of a material, it is sufficient to divide the maximum bearable load by the cross-section area. Interpreting experimental results in terms of action plane-related fracture criteria, it is important to know whether the fracture has occurred in the action plane of the applied stressing or not. Figure 4.4 shows, that not for all the basic stressings this is the case. In almost all UD-laminae a tensile stressing σ_{\perp}^t leads to a fracture plane perpendicular to the applied stressing – otherwise the material is

classified as not intrinsically brittle (see Sec. 4.6.2). In the former case the fracture plane and the action plane of the applied stressing coincide, thus the strength of the material R_{\perp}^t and the fracture resistance of the action plane $R_{\perp}^{A t}$ have the same value. The same is the case when measuring $R_{\perp\parallel}^A$. An applied single $\tau_{\perp\parallel}$ -stressing leads to a shear fracture on its action plane and thus $R_{\perp\parallel}^A$ has the same value as $R_{\perp\parallel}$. It should be noted that a corresponding $\tau_{\parallel\perp}$ will also be acting. However the fracture resistance of its action plane $R_{\parallel\perp}^A$ is much higher due to the fibre reinforcement and thus this value is irrelevant.

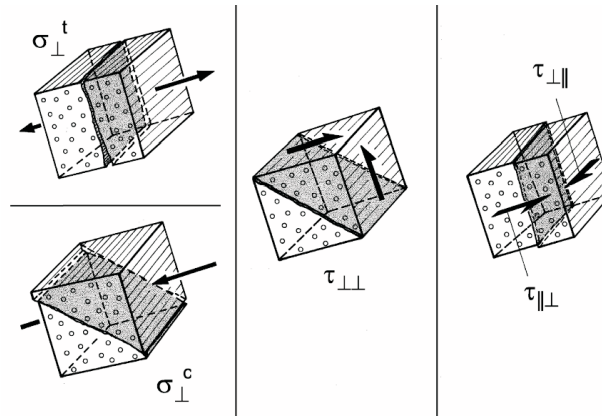


Figure 4.4: Fracture planes of an intrinsically brittle UD-composite under uniaxial or pure shear stressing. (from [4])

In contrast to the two cases above, a single compressive stressing σ_{\perp}^c cannot separate the material in its action plane which is perpendicular to σ_{\perp}^c (see Figs. 4.4 and 4.3). The UD-element fractures due to the resulting shear stressing $\tau_{\perp\perp}$ on an oblique fracture plane. Furthermore it is impossible to produce a fracture in the action plane of an applied $\tau_{\perp\perp}$, the UD-element fractures due to a tensile stressing σ_{\perp}^t on an oblique fracture plane.

A central conclusion from Puck's considerations is that there are no more than three stresses acting on a common action plane ($\sigma_{\perp}, \tau_{\perp\parallel}$ and $\tau_{\perp\perp}$) and thus exactly three fracture resistances of the action plane R^A are needed. Two of them ($R_{\perp}^{A t}$ and $R_{\perp\parallel}^A$) can be derived directly from the usual strengths of the material but $R_{\perp\perp}^A$ needs further consideration (see Sec. 4.2.2) including the following experimental observation: A superposed tensile stress σ_{\perp}^t on an action plane lowers the bearable shear while a superimposed compressive σ_{\perp}^c on an action plane increases its intrinsic fracture resistance against $\tau_{\perp\parallel}$ and/or $\tau_{\perp\perp}$.

To clearly distinguish between applied states of stress and the resulting stresses on an action plane, it is essential to be familiar with the stress components acting on a plane. The most general stress combination on any section plane (and a fracture plane in particular) of an isotropic material consists of one normal stress σ and one shear stress τ . The same situation exists in a UD-composite on a section plane which is parallel to the fibres.

However in a UD lamina, the shear vector is examined by means of its two components τ_{nt} and τ_{n1} . The first index n means that both are acting on the same action plane which is perpendicular to the direction x_n . The second index indicates the direction of the shear stress τ . Its component τ_{nt} is acting transversally and τ_{n1} parallel to the fibre direction x_1 (see Fig. 4.5).

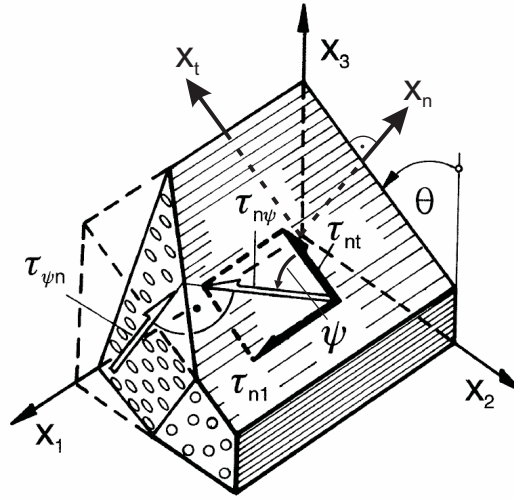


Figure 4.5: Definition of shear stresses in an section plane, from [39].

From a micromechanical aspect these two components of $\tau_{n\psi}$ in either fibre-parallel or fibre-transverse direction certainly behave a little different in terms of shear fracture. This fact is represented by two different fracture resistances of the action plane against shear ($R_{\perp\perp}^A$ and $R_{\perp\parallel}^A$) and therefore, when dealing with strengths, τ_{nt} and τ_{n1} are treated separately. But if only the combined force of τ_{nt} and τ_{n1} is of interest, it is reasonable to look at their resultant shear stress

$$\tau_{n\psi} = \sqrt{\tau_{nt}^2 + \tau_{n1}^2} . \quad (4.1)$$

Schematically then – like in isotropic material – on a common stress action plane exist only one normal stress σ_n and one shear stress $\tau_{n\psi}$. Note that the corresponding $\tau_{\psi n}$ acts in a plane intersecting the fibres (see Fig. 4.5) – the fracture resistances of such planes are much higher than of fibre-parallel action planes hence they do not play a role in the fracture analysis.

The physically based fracture hypotheses outlined above have two severe consequences on the formulation of corresponding fracture criteria:

- Only the three stresses σ_n , τ_{nt} and τ_{n1} acting on a common action plane can appear in the fracture criteria.

- When the fracture hypotheses are dealing exclusively with the fracture in the common action plane of σ_n , τ_{nt} and τ_{n1} , exclusively these stresses have to be related to adequate *action plane-related* strength measures.

4.2.2 Application-oriented aspects of Puck's IFF criterion

In terms of application the consequence of the action plane-related fracture hypotheses is, that in isotropic or transversely isotropic materials there is an infinite number of action planes which are all potential fracture planes. Hence the action plane with the highest risk of fracture has to be identified before the fracture stresses can be calculated. While for 2D states of stress there has been developed an analytical solution by Puck [4], the general 3D state of stress requires the numerical search for the fracture plane.

For this purpose the *stretch factor* f_S is calculated for a large number of sections (normally 180) between $\theta = [-90^\circ; 90^\circ]$. The term f_S is the factor, by which the stress vector $\vec{\sigma} = [\sigma_n(\theta), \tau_{nt}(\theta), \tau_{n1}(\theta)]$ on the considered action plane must be proportionally increased (*stretched*) to cause the fracture of that specific plane (see Fig. 4.6). In other words, f_S is sort of a reserve factor between the stresses acting on a specific action plane and the fracture limit of the respective plane (see Eq. 4.2).

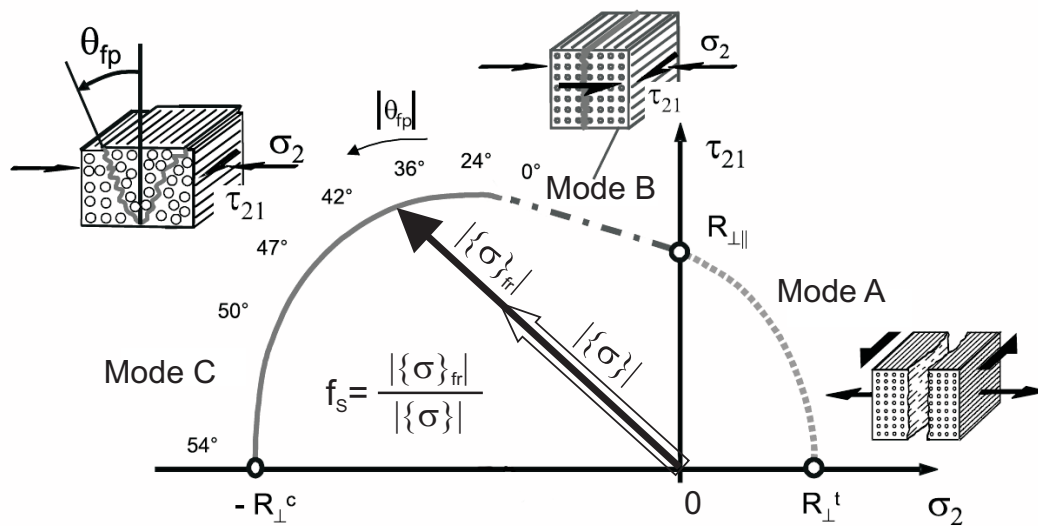


Figure 4.6: Visualisation of the stretch factor f_S in the fracture curve of plane states of stress.

On action planes without stress or only compressive σ_n acting, f_S would take the numerically objectionable value ∞ (see Fig. 4.7, at $\theta = -45^\circ$, i). Thus the reciprocal value of f_S , called the *stress exposure* f_E , is more appropriate for both analysis and graphical

representation (see Eq. 4.2). While the term *stretch factor* is intentionally similar to a *reserve factor*, the *stress exposure* which increases linearly with the applied stress is a direct measure for the risk of fracture.

$$f_E = \frac{1}{f_S} = \frac{\text{length of the actual stress vector } \vec{\sigma}}{\text{length of the vector } \vec{\sigma}_{fr} \text{ of the stresses leading to fracture}} \quad (4.2)$$

The analysis results in the identification of that plane at θ_{fp} which needs the lowest stretch factor $f_{S_{min}}$ to fracture. Obviously this plane will exclusively reach its fracture limit, if the applied external stress is increased by the factor $f_{S_{min}}$ while the rest of the planes with $f_S > f_{S_{min}}$ will stay below (see Fig. 4.7, ii) [87].

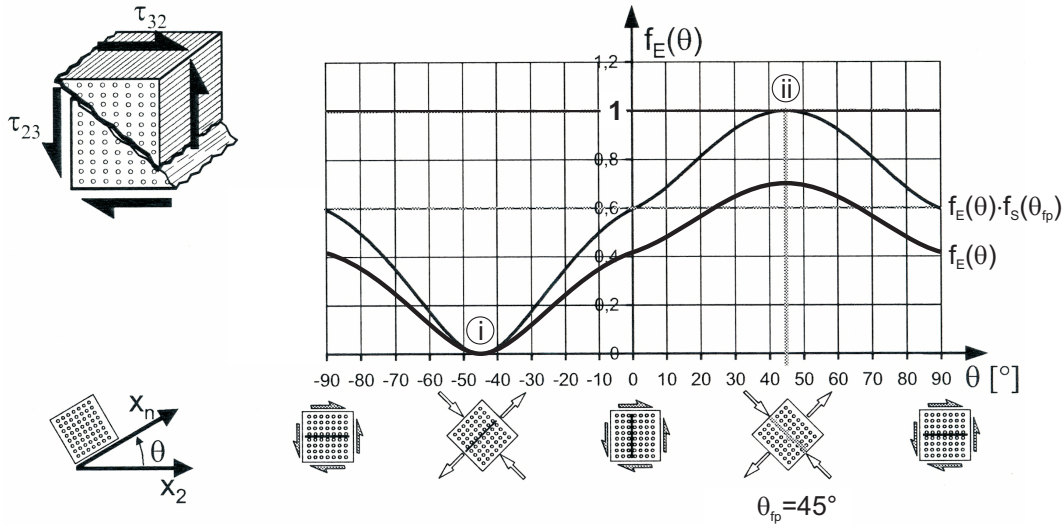


Figure 4.7: Stress exposure $f_E(\theta)$ for an applied τ_{23} , partly from [39].

The applied stresses σ_2 , σ_3 , τ_{23} , τ_{21} and τ_{31} (referring to the UD-lamina system) which have to be transmitted by the matrix and the fibre/matrix interfaces are of main importance for an IFF. If the fibre-parallel stress σ_1 however approaches its fracture limit $R_{||}^t$ or $-R_{||}^c$, it will also influence the IFF (see Sec. 4.3.1).

The action plane-related stresses are derived from the applied stresses as follows:

$$\begin{aligned} \sigma_n(\theta) &= \sigma_2 \cdot \cos^2 \theta + \sigma_3 \cdot \sin^2 \theta + 2\tau_{23} \cdot \sin \theta \cdot \cos \theta \\ \tau_{nt}(\theta) &= -\sigma_2 \cdot \sin \theta \cdot \cos \theta + \sigma_3 \cdot \sin \theta \cdot \cos \theta + \tau_{23} \cdot (\cos^2 \theta - \sin^2 \theta) \\ \tau_{n1}(\theta) &= \tau_{31} \cdot \sin \theta + \tau_{21} \cdot \cos \theta \end{aligned} \quad (4.3)$$

Corresponding to these three stresses which cause a σ_{\perp} , a $\tau_{\perp\perp}$ or a $\tau_{\perp\parallel}$ -stressing respectively, three fracture resistances of the action plane must be known: R_{\perp}^{At} , $R_{\perp\perp}^A$ and $R_{\perp\parallel}^A$.

If for instance a single stressing σ_{\perp}^t is applied to a brittle material it leads to a fracture plane parallel to its action plane in most FRCs. Following Paul [86] this behaviour is called *intrinsically brittle* and Puck's Theory mainly aims on this class of materials. Paul was working with isotropic materials, hence the definition may only be applied to considerations on the isotropic – that is transversal – plane of the UD-lamina. Within the present work intrinsically brittle behaviour is defined as follows: If there are any sections on which the applied stresses lead to tension σ_n^t , the fracture occurs in the section with the largest normal tension σ_n^t . According to that in the case of a pure σ_{\perp}^t -stressing, the applied stress at the time of fracture is the corresponding strength and also the corresponding fracture resistance of the action plane. Assuming that the present composites behave intrinsically brittle the following identity of strength and action plane fracture resistance is valid:

$$R_{\perp}^{At} = R_{\perp}^t \quad (4.4)$$

If a pure $\tau_{\perp\parallel}$ -stressing is applied to a UD-composite the embedded fibres force the fracture to occur in a fibre-parallel section. Thereby the action plane of the $\tau_{\perp\parallel}$ -stressing will experience the highest $\tau_{\perp\parallel}$ -stressing compared to any other action plane inclined by an angle θ . Thus for transverse/longitudinal shear, there is always valid:

$$R_{\perp\parallel}^A = R_{\perp\parallel} \quad (4.5)$$

In contrast to that $R_{\perp\perp}^A$ is extremely different from the transverse shear strength $R_{\perp\perp}$. Up to now, $R_{\perp\perp}^A$ is not accessible experimentally because the fracture of intrinsically brittle materials due to an applied $\tau_{\perp\perp}$ -stressing does neither occur in its action plane nor is it a shear fracture: A single τ_{23} -stress leads to tensile fracture in an action plane which is inclined by 45° to the action plane of the applied τ_{23} (see Fig. 4.7). For the time being $R_{\perp\perp}^A$ is determined from a uniaxial transverse compression test where the applied σ_{\perp}^c leads to a $\tau_{\perp\perp}$ -shear fracture in a fracture plane at about $\theta_{fp} \approx \pm 54^\circ$. While in the action plane at $\theta = 45^\circ$ there obviously acts the highest τ_{nt} there also acts a fracture-obstructing compressive σ_n^c of the same magnitude. This declines towards the actual fracture plane at $\pm 54^\circ$ where the shear fracture due to τ_{nt} occurs. The fact that shear fracture due to τ_{nt} only occurs with superimposed σ_n^c requires the *reconstruction* of $R_{\perp\perp}^A$ using the calibrating inclination parameter $p_{\perp\perp}^c$ (see Eq. 4.6). The meaning and definition of $p_{\perp\perp}^c$ is discussed below (see Sec. 4.2.3).

$$R_{\perp\perp}^A = \frac{R_{\perp}^c}{2(1 + p_{\perp\perp}^c)} \quad (4.6)$$

4.2.3 Visual and mathematical representation – the MFB

The IFF criteria can easily be visualised in the 3D stress space of the action plane $(\sigma_n, \tau_{nt}, \tau_{n1})$ – they accommodate the *Master Fracture Body* (MFB). All the stress vectors which stay inside the MFB can be sustained without fracture, in other words the MFB envelopes all sustainable $(\sigma_n, \tau_{nt}, \tau_{n1})$ -combinations. Due to the different effect of a tensile or compressive σ_n on the development of IFF, the MFB-surface consists of two parts joining at a common cross-section at $\sigma_n = 0$. The known anchor points are R_{\perp}^{At} on the σ_n -axis, $\pm R_{\perp}^A$ on the τ_{nt} -axis and $\pm R_{\perp}^A$ on the τ_{n1} -axis (see Fig. 4.8).

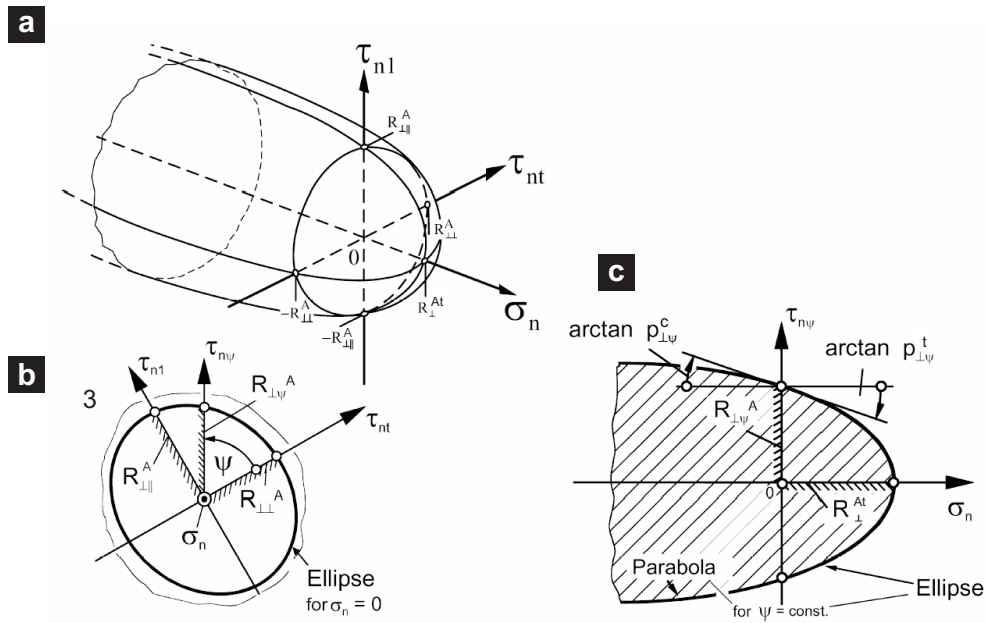


Figure 4.8: The Master Fracture Body (MFB) in the action plane-related $(\sigma_n, \tau_{nt}, \tau_{n1})$ -stress space, from [4].

As τ_{nt} and τ_{n1} both cause a shear stressing acting on a common fibre-parallel action plane (see Fig. 4.5) the corresponding fracture resistances of the action plane R_{\perp}^A and R_{\perp}^A should not differ a lot. Thus it seems reasonable to assume a simple elliptical fracture criterion for combined (τ_{nt}, τ_{n1}) -states of stress $\tau_{n\psi}$ at $\sigma_n = 0$ (see Fig. 4.8b):

$$\left(\frac{\tau_{n\psi}}{R_{\perp}^A}\right)^2 = \left(\frac{\tau_{nt}}{R_{\perp}^A}\right)^2 + \left(\frac{\tau_{n1}}{R_{\perp}^A}\right)^2 = 1 \text{ for } \sigma_n = 0 \quad (4.7)$$

Having fixed the cross-section at $\sigma_n = 0$ Puck decided to describe the MFB by longitudinal sections rather than further cross-sections. The reason is that the tip of a stress

vector, which is proportionally *stretched* by the stretch factor f_S (see Sec. 4.2.2), is moving in a longitudinal section of the MFB. This fact leads to a rather simple equation for a longitudinal section.

Those parts of the MFB surface where an applied plane (σ_2, τ_{21}) -stress combination leads to a fracture in its own action plane ($\theta_{fp} = 0^\circ$), can easily be investigated experimentally. This is the case in the whole positive range of $\sigma_2 > 0$ and a small part of the negative $\sigma_2 \approx [-0.4 R_\perp^c ; 0]$. Within these two ranges there is $\theta_{fp} = 0^\circ$ and accordingly $\sigma_2 = \sigma_n$, $\tau_{21} = \tau_{n1}$ and $\tau_{nt} = 0$. That means that all the resulting IFF fractures are placed on a longitudinal contour line of the MFB in the $(\tau_{nt} = 0)$ -plane.

For positive σ_n the (σ_n, τ_{n1}) -fracture curve can be described well by a branch of an ellipse which cuts the σ_n -axis perpendicularly at $\sigma_n = R_\perp^{At}$ and the positive τ_{n1} -axis at $\tau_{n1} = R_{\perp\parallel}^A$ with a declining slope of about $\frac{\delta\tau_{n1}}{\delta\sigma_n} = -0.3$ (see Fig. 4.8a). According to Coulomb [84] the fracture curve continues in the negative σ_n -region as an inclined straight line. To ensure conservative results however, a *diminishing* dependence of the fracture resistances of the action plane against shear from negative σ_n is assumed. Thus Puck chose a parabolic contour line in this region [4] ^{see p. 54ff}. This assumption follows Mohr's idea that the strengthening effect of compressive σ_n decreases with growing compressive σ_n .

Finally the whole MFB arises from the set of ellipse/parabola-contour lines for all angles ψ . For positive σ_n the result is a calotte with the utmost point on the σ_n -axis at $\sigma_n = R_\perp^{At}$ and $\tau_{n\psi} = 0$. Looking in negative σ_n -direction, the MFB looks like an infinite, slightly widening funnel. This meets the fact that σ_n alone *never* causes fracture. There is always a specific amount of $\tau_{n\psi}$ necessary for fracture and this amount grows with increasing compressive σ_n .

In the following a contour line of the MFB is described by an ellipse in the $\sigma_n \geq 0$ half space and by a parabola in the $\sigma_n < 0$ half space:

$$\left(\frac{\tau_{n\psi}}{R_{\perp\psi}^A}\right)^2 + c_1 \frac{\sigma_n}{R_\perp^{At}} + c_2 \left(\frac{\sigma_n}{R_\perp^{At}}\right)^2 = 1 \text{ for } \sigma_n \geq 0 \quad (4.8)$$

$$\left(\frac{\tau_{n\psi}}{R_{\perp\psi}^A}\right)^2 + c \sigma_n = 1 \text{ for } \sigma_n < 0 \quad (4.9)$$

The ellipse has to include three anchor points (see Fig. 4.8c) which are

$$\begin{bmatrix} \sigma_n \\ \tau_{n\psi} \end{bmatrix} = \begin{bmatrix} R_\perp^{At} \\ 0 \end{bmatrix} \text{ on the } \sigma_n\text{-axis and } \begin{bmatrix} 0 \\ \pm R_{\perp\psi}^A \end{bmatrix} \text{ on the } \tau_{n\psi}\text{-axis.} \quad (4.10)$$

With equation 4.1 and the geometric relations $\tau_{nt} = \tau_{n\psi} \cos \psi$ and $\tau_{n1} = \tau_{n\psi} \sin \psi$ it follows from equation 4.7:

$$R_{\perp\psi}^A = \left[\left(\frac{\cos \psi}{R_{\perp\perp}^A} \right)^2 + \left(\frac{\sin \psi}{R_{\perp\parallel}^A} \right)^2 \right]^{-\frac{1}{2}} \quad (4.11)$$

While the ellipse crosses the σ_n -axis perpendicularly it should cross the $\tau_{n\psi}$ -axis with an inclination which can be chosen within specific limits (see Eq. 4.12). Recommended values will be presented later in this section.

$$\left(\frac{\delta \tau_{n\psi}}{\delta \sigma_n} \right)_{\sigma_n=0}^{ellipse} = \begin{cases} -p_{\perp\psi}^t & \text{for } \tau_{n\psi} > 0 \\ p_{\perp\psi}^t & \text{for } \tau_{n\psi} < 0 \end{cases} \quad (4.12)$$

The parabola describing the contour line of the MFB in areas $\sigma_n < 0$ starts at the anchor points ($\sigma_n = 0, \tau_{n\psi} = \pm R_{\perp\psi}^A$) and its inclination may differ slightly from the inclination of the ellipse joining at that point:

$$\left(\frac{\delta \tau_{n\psi}}{\delta \sigma_n} \right)_{\sigma_n=0}^{parabola} = \begin{cases} -p_{\perp\psi}^c & \text{for } \tau_{n\psi} > 0 \\ p_{\perp\psi}^c & \text{for } \tau_{n\psi} < 0 \end{cases} \quad (4.13)$$

With the above conditions the constants c_1 , c_2 and c (see Eqs. 4.8 and 4.9) become

$$c_1 = 2 \frac{p_{\perp\psi}^t R_{\perp\perp}^{At}}{R_{\perp\psi}^A} \quad (4.14)$$

$$c_2 = 1 - 2 \frac{p_{\perp\psi}^t R_{\perp\perp}^{At}}{R_{\perp\psi}^A} \quad (4.15)$$

$$c = 2 \frac{p_{\perp\psi}^c}{R_{\perp\psi}^A}. \quad (4.16)$$

For the inclination values at $\psi = 90^\circ$, that means the longitudinal section of the MFB where only σ_n and τ_{n1} exist ($\tau_{nt} = 0$), there is some experimental experience concerning the inclination parameters $p_{\perp\psi}^t$ and $p_{\perp\psi}^c$ which are named $p_{\perp\parallel}^t$ and $p_{\perp\parallel}^c$ in that particular case. The present analysis follows the recommendations given in [88, 89] also for the values $p_{\perp\perp}^t$ and $p_{\perp\perp}^c$ valid in the longitudinal section of the MFB at $\psi = 0^\circ$ (see Tab. 4.1).

Having chosen the inclinations of the contour lines at $\psi = 0^\circ$ and 90° , Puck uses the following interpolation procedure (see Eq. 4.17) to define the values of $p_{\perp\psi}^t$ and $p_{\perp\psi}^c$ at

	$p_{\perp\parallel}^t$	$p_{\perp\parallel}^c$	$p_{\perp\perp}^t, p_{\perp\perp}^c$
GFRP	0.30	0.25	0.20 to 0.25
CFRP	0.35	0.30	0.25 to 0.30

Table 4.1: Recommended inclination parameters.

any angle ψ . The procedure ensures a harmonic behaviour of the change in inclination around the circumference of the MFB.

$$\frac{p_{\perp\psi}^{t,c}}{R_{\perp\psi}^A} = \frac{p_{\perp\perp}^{t,c}}{R_{\perp\perp}^A} \cos^2 \psi + \frac{p_{\perp\parallel}^{t,c}}{R_{\perp\parallel}^A} \sin^2 \psi \quad (4.17)$$

with

$$\cos^2 \psi = \frac{\tau_{nt}^2}{\tau_{nt}^2 + \tau_{n1}^2} \quad (4.18)$$

and

$$\sin^2 \psi = \frac{\tau_{n1}^2}{\tau_{nt}^2 + \tau_{n1}^2} \quad (4.19)$$

With equation 4.7 the MFB is completely described by equations 4.8 and 4.9 which are polynomials of second order of the stresses. The right hand side of the equations set to one makes them a *fracture condition*. This means, σ_n and $\tau_{n\psi}$ calculated using these equations are stresses at IFF. If stresses lower than these are inserted in the left hand side of the equations 4.8 and 4.9, the result is a figure lower than one. Though this indicates, that these stresses are bearable without IFF, the figure itself *does not represent* the stress exposure (see Sec. 4.2.2). It was stated that the stress exposure f_E should increase linearly with proportionally increasing stresses – this is *not* the case in the quadratic equations 4.8 and 4.9. Thus they have to be rearranged to form a homogeneous function in the first degree of the stresses. This can be easily achieved by dividing the stress terms of the first order by f_E and those of the second order by f_E^2 . Then the general solution of the resulting quadratic equation for f_E can be written

$$f_E = \frac{1}{2} \left(\sum L + \sqrt{(\sum L)^2 + 4 \sum Q} \right) \quad (4.20)$$

where $\sum L$ is the sum of the stress terms of first order, $\sum Q$ the sum of those of second order. Applying this term to the fracture conditions (Eqs. 4.8 and 4.9) leads to the two central expressions of Puck's IFF criterion:

$$f_{E\ IFF}(\theta) = \sqrt{\left[\left(\frac{1}{R_{\perp}^{At}} - \underbrace{\frac{p_{\perp\psi}^t}{R_{\perp\psi}^A}}_{\text{Eq. 4.23}} \right) \sigma_n(\theta) \right]^2 + \left(\frac{\tau_{nt}(\theta)}{R_{\perp\perp}^A} \right)^2 + \left(\frac{\tau_{n1}(\theta)}{R_{\perp\parallel}^A} \right)^2} + \underbrace{\frac{p_{\perp\psi}^t}{R_{\perp\psi}^A}}_{\text{Eq. 4.23}} \sigma_n(\theta) \quad (4.21)$$

for $\sigma_n \geq 0$ and

$$f_{E\ IFF}(\theta) = \sqrt{\left(\frac{\tau_{nt}(\theta)}{R_{\perp\perp}^A} \right)^2 + \left(\frac{\tau_{n1}(\theta)}{R_{\perp\parallel}^A} \right)^2 + \left(\frac{p_{\perp\psi}^c}{R_{\perp\psi}^A} \sigma_n(\theta) \right)^2} + \underbrace{\frac{p_{\perp\psi}^c}{R_{\perp\psi}^A}}_{\text{Eq. 4.23}} \sigma_n(\theta) \quad (4.22)$$

for $\sigma_n < 0$

where

$$\frac{p_{\perp\psi}^{t,c}}{R_{\perp\psi}^A} = \underbrace{\frac{p_{\perp\perp}^{t,c}}{R_{\perp\perp}^A}}_{\text{Eq. 4.6}} \underbrace{\cos^2 \psi}_{\text{Eq. 4.18}} + \frac{p_{\perp\parallel}^{t,c}}{R_{\perp\parallel}^A} \underbrace{\sin^2 \psi}_{\text{Eq. 4.19}} \quad (4.23)$$

Setting $f_E = 1$ and $\theta = \theta_{fp}$, equations 4.21 and 4.22 are a different form of the fracture condition equations 4.8 and 4.9.

Using these two equations (Eqs. 4.21 and 4.22) the orientation θ_{fp} of the expected fracture plane can be identified:

$$[f_{E\ IFF}(\theta)]_{max} = f_{E\ IFF}(\theta_{fp}) \quad (4.24)$$

The associated value of the stress exposure is generally referred to as $f_{E\ IFF}$ associated with a specific state of applied stress and is also the central parameter for the post-failure degradation analysis (see Ch. 5).

4.2.4 IFF fracture modes classification for 3D analysis

In the design of critical components it is of extraordinary importance to know, which stresses and strengths of the material are of primary relevance for a failure. Regarding IFF, Puck's action plane-related fracture criteria now offer the relevant information by identifying the orientation of the fracture plane and the stresses acting on it.

In his first publication about the new fracture plane-related IFF criteria [21] Puck has extensively discussed the general shape of the experimentally well captured (σ_2, τ_{21}) -fracture curve (see Fig. 4.6) and the basic observations associated with the occurring fracture plane orientations. These observations led to the distinction of three different sections of the fracture curve. Starting from $\sigma_2 = R_{\perp}^t$, via $\tau_{21} = R_{\perp\parallel}$ and ending at $\sigma_2 = -R_{\perp}^c$ (see Fig. 4.6) there consecutively occur different stress combinations on the fracture plane leading to different modes of IFF (see Tab. 4.2).

The most important conclusion from the considerations above is: All the presented fracture modes are described exclusively by equations 4.21 and 4.22. This is possible due to a two-stage analysis: First the criteria are used to identify the orientation of the fracture plane θ_{fp} and in a second step they are used to calculate the fracture stresses on that very plane.

The application of an arbitrary 3D load could potentially produce more states of stress on the fracture plane than those encountered under 2D load. The most likely case is that all the three stresses σ_n , τ_{nt} and τ_{n1} are acting together on the fracture plane. The substantial difference between all the possible combinations is the algebraic sign of σ_n . The mechanical difference lies in the fact that a tensile stress $\sigma_n > 0$ promotes IFF while compressive stress $\sigma_n < 0$ impedes it (see Sec. 4.2.1). Mathematically this fact is expressed by two different fracture conditions, one for positive and one for negative σ_n (see Sec. 4.2.3). It is also conceivable, that pure shear (τ_{n1} and/or τ_{nt}) acts on the fracture plane. According to this there is a complete scheme of conceivable stress combinations on the fracture plane (see Tab. 4.3).

Although in the 3D case the categorisation into Modes A, B and C seems no longer adequate, the differentiation between fractures with positive or negative σ_n on their fracture plane is still significant regarding the consequences of the fracture: While fractures with σ_n^t acting on their fracture plane are generally supposed to be tolerable if the load can be redistributed to neighbouring laminae, fracture planes with σ_n^c indicate the risk of an abrupt fatal disintegration (local splitting and delamination) of the laminate by their wedge effect [6, 39] if a compressive σ_2 is present. The considerations above are relevant

Mode A $\theta_{fp} = 0^\circ$	Mode B $\theta_{fp} = 0^\circ$	Mode C $\theta_{fp} \neq 0^\circ$
$\{\sigma_n^t \ 0 \ 0\}$	$\{\sigma_n^c \ 0 \ \tau_{n1}\}$	$\{\sigma_n^c \ \tau_{nt} \ \tau_{n1}\}$
$\{\sigma_n^t \ 0 \ \tau_{n1}\}$		$\{\sigma_n^c \ \tau_{nt} \ 0\}$
$\{0 \ 0 \ \tau_{n1}\}$		

Table 4.2: Possible 2D stress combinations leading to the different IFF fracture modes.

$\sigma_n < 0$	$\sigma_n = 0$	$\sigma_n > 0$
$\{\sigma_n^c \quad \tau_{nt} \quad \tau_{n1}\}$	$\{0 \quad \tau_{nt} \quad \tau_{n1}\}$	$\{\sigma_n^t \quad \tau_{nt} \quad \tau_{n1}\}$
$\{\sigma_n^c \quad \tau_{nt} \quad 0\}$	$\{0 \quad \tau_{nt} \quad 0\}^{**}$	$\{\sigma_n^t \quad \tau_{nt} \quad 0\}^{**}$
$\{\sigma_n^c \quad 0 \quad \tau_{n1}\}$	$\{0 \quad 0 \quad \tau_{n1}\}$	$\{\sigma_n^t \quad 0 \quad \tau_{n1}\}$
$\{\sigma_n^c \quad 0 \quad 0\}^*$		$\{\sigma_n^t \quad 0 \quad 0\}$

* A fracture plane on which σ_n^c acts exclusively is not conceivable because the fracture resistance of the action plane against compressive stress is $R_{\perp}^{A_c} = \infty$ (see Sec. 4.2.3).

** In UD-composites with common ratios between material strengths R_{\perp}^c and R_{\perp}^t these combinations do not appear.

Table 4.3: Possible 3D stress combinations on a fracture plane.

for the post-failure degradation analysis and are resumed in chapter 5.

4.3 Influences on the IFF beyond Mohr's hypothesis

In the context of this section it is important to stress that Puck's IFF criteria predict brittle *macroscopic* IFF failure by means of cracks through the entire thickness of the lamina. Pre-fracture micro-damage-induced constitutive nonlinearities (see Fig. 2.5) are not considered by Puck's failure theory itself but by the preceding nonlinear stress analysis (see Sec. 3.1.2). However the extended theory accounts for the influence of micro-damage on the load bearing capacity of the material.

It was previously stated that only stresses acting on the fracture plane ($\sigma_n, \tau_{n1}, \tau_{nt}$) are relevant for the fracture itself (see Sec. 4.2). In accordance with Mohr [85], neither the fibre-parallel stress σ_1 nor the levels of IFF stress exposures on planes other than the fracture plane have been included so far. Considering the gradual development of an IFF due to the progressive formation of micro cracks and for probabilistic reasons (see Sec. 2.1), there are states of stress where a pure Mohr approach is expected to be on the non-conservative side. Therefore the following two extensions of the IFF criteria have been developed by Puck beyond Mohr's hypothesis (see Secs. 4.3.1 and 4.3.2).

4.3.1 Influences of fibre-parallel stress σ_1

According to Mohr, the stress σ_1 does not have any influence on an IFF because that stress' action plane is perpendicular to any possible IFF fracture plane – thus $\sigma_n(\theta)$, $\tau_{n1}(\theta)$ and $\tau_{nt}(\theta)$ are independent from σ_1 . Experiments, however, have revealed a series of effects

which require the inclusion of a σ_1 -term to reduce the IFF strength somewhat [39]. The most essential effect is explained by the statistical scatter in the fibre strength. Macroscopically detected fibre fracture (FF) at $|\sigma_1| = R_{||}$ is the moment, when a very large number of elementary fibres breaks and the UD lamina loses most of its load-bearing capacity in fibre direction. Statistical laws state that some elementary fibres will already have been broken before the fibre fracture limit $R_{||}$ of the UD lamina has been reached – this is the case for both fibre fractures (tensile σ_1) and fibre kinking (compressive σ_1). The result of those *micro fibre fractures* is a local damage of the UD lamina in the form of a local fibre-matrix debonding and micro-fractures in the highly loaded neighbouring matrix material [10]. They weaken the overall fibre-matrix cohesion and thus reduce its resistance against IFF.

In order to include the weakening effect of σ_1 in the IFF analysis, the fracture resistances of the action planes are reduced by a weakening factor $\eta_{w1} = [0; 1]$. This factor can be used in the tensile and compressive range of σ_1 in the same way. For the sake of simplicity η_{w1} has the same value for all the three fracture resistances R_{\perp}^{At} , $R_{\perp\perp}^A$ and $R_{\perp\parallel}^A$. This assumption has the effect that the orientation of the fracture plane θ_{fp} is independent from η_{w1} since σ_1 is independent from θ [4]. That means the identification of the fracture plane will be carried out the same way whether including the σ_1 -influence or not.

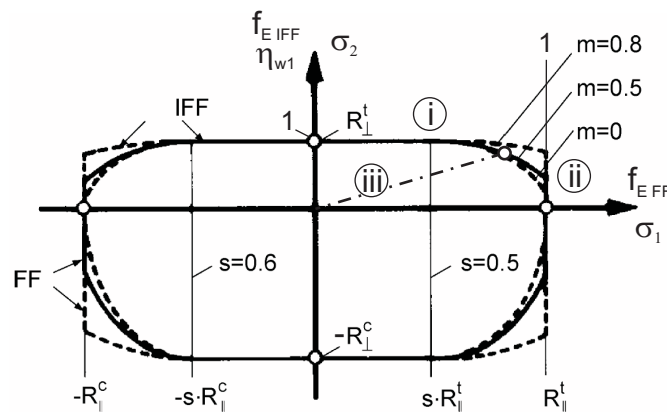


Figure 4.9: (σ_1, σ_2) -fracture curve including the σ_1 -influence on IFF.

Regarding the definition of η_{w1} , the considerations of Puck and Schürmann [6, 39] may be explained by studying the fracture curve of a simple (σ_2, σ_1) -load case (see Fig. 4.9) in the first quadrant. Gradually starting at a specific σ_1 -value (horizontal tangent, see Fig. 4.9, i) the weakening effect increases with increasing σ_1 but presumably leaves some IFF fracture resistance when reaching the fibre fracture limit (ii). Hence the weakening is described by a fracture curve in the form of a segment of an ellipse. The segment starts at $s \cdot R_{||}$ ($s = [0; 1]$) and ends at the FF-limit $|\sigma_1| = R_{||}$. Here, the bearable σ_2 reaches its

minimum $m \cdot R_{\perp}^t$ ($m = [0; 1]$). Both m and s can be chosen freely between their limits and may differ for compressive or tensile σ_1 . Without adequate experimental results the currently suggested values are $m = s = 0.5$ [88] but as soon as the authors get to know relevant data these parameters may be adjusted.

Aiming on the stress exposures $f_{E\ FF}$ and $f_{E\ IFF}$ being the central parameters in the η_{w1} -definition also, the (σ_2, σ_1) -fracture curve may be transferred into a $f_{E\ IFF}(\sigma_2)$ against $f_{E\ FF}(\sigma_1)$ curve by dividing σ_2 by R_{\perp}^t or $-R_{\perp}^c$ and σ_1 by R_{\parallel}^t or $-R_{\parallel}^c$, respectively. This operation results in solely positive values between $[0; 1]$ and now the former curves of quadrant 1 and 4 coincide in one curve valid for tensile σ_1 and the former curves of quadrant 2 and 3 coincide in another curve valid for compressive σ_1 – now both in the first quadrant. If compressive and tensile σ_1 are treated equally regarding s and m , both remaining curves are identical and for simplicity reasons this case is shown in figure 4.9.

Accepting the hypothesis above, that high σ_1 – hence high fibre fracture stress exposure $f_{E\ FF}$ (see Sec. 4.7) – weakens all the IFF fracture resistances of all the action planes in the same way, the considerations may be continued without distinction whether σ_2 or any other combination of applied stresses leads to the IFF. Thus the first quadrant of figure 4.9 simultaneously shows the generally bearable $f_{E\ IFF}$ against $f_{E\ FF}$. In order to stick to the general fracture condition $f_E = 1$, the bearable IFF stress exposure $f_{E\ IFF}$ is corrected by $(\eta_{w1})^{-1}$ which represents a reduction of the fracture resistances:

$$f_{E\ IFF_{w1}} = \frac{f_{E\ IFF}(\theta_{fp})}{\eta_{w1}} \quad (4.25)$$

Setting $f_{E\ IFF} = 1$ (fracture condition) in equations 4.21 and 4.22 and multiplying all the fracture resistances of the action planes by the same η_{w1} -value, it may be brought to the left hand side and accordingly the first quadrant of figure 4.9 also shows the value of η_{w1} against $f_{E\ FF}$. The weakening factor $\eta_{w1}(f_{E\ FF})$ is now defined by an elliptical function for $f_{E\ FF} = [s; 1]$:

$$\eta_{w1}(f_{E\ FF}) = \sqrt{1 - \frac{(f_{E\ FF} - s)^2}{a^2}} \quad \text{with} \quad a = \frac{1 - s}{\sqrt{1 - m^2}} \quad (4.26)$$

Now that we have defined the conditions on the fracture curve we address a general load case:

An η_{w1} -value is not only valid for a specific point on the fracture curve but it is applied to all the load cases whose proportional increase leads to that specific fracture (see Eq. 4.25). The set of these load cases forms a straight line in figure 4.9, iii with an equal ratio between $f_{E\ IFF}$ and $f_{E\ FF}$. Accordingly the correlation $\eta_{w1}(f_{E\ FF})$ has to be transferred

into $\eta_{w1} \left(\frac{f_{E\ IFF}}{f_{E\ FF}} \right)$. The relation between $\frac{f_{E\ IFF}}{f_{E\ FF}}$ and $f_{E\ FF}$ is given by the fact that $f_{E\ FF}$ is the abscissa value of the intersection between the line and the segment of the ellipse:

$$f_{E\ FF} = \frac{s + \sqrt{s^2 - (1 + a^2 c^2)(s^2 - a^2)}}{1 + a^2 c^2} \quad \text{with} \quad c = \frac{f_{E\ IFF}(\theta_{fp})}{f_{E\ FF}} \quad (4.27)$$

Equation 4.27 inserted into equation 4.26 the weakening factor is

$$\eta_{w1} \left(\frac{f_{E\ IFF}}{f_{E\ FF}} \right) = \frac{c \left(a \sqrt{c^2 (a^2 - s^2) + 1} + s \right)}{(ca)^2 + 1} \quad \text{for} \quad \frac{1}{s} \geq \frac{f_{E\ IFF}(\theta_{fp})}{f_{E\ FF}} \geq m. \quad (4.28)$$

Note that for $\frac{f_{E\ IFF}(\theta_{fp})}{f_{E\ FF}} > \frac{1}{s}$, there is no σ_1 -influence ($\eta_{w1}=1$) while for $\frac{f_{E\ IFF}(\theta_{fp})}{f_{E\ FF}} < m$ there is no IFF [4]^{sec p. 86}.

4.3.2 Influence of non-fracture plane stresses

Micromechanical studies show that an IFF does not happen suddenly without any advance notice (see Sec. 2.3.1). Once the standardised IFF stress exposure

$$f'_{E\ IFF}(\theta) = \frac{f_{E\ IFF}(\theta)}{f_{E\ IFF}(\theta_{fp})} \quad (4.29)$$

exceeds a threshold value of about $f'_{E\ IFF}(\theta) \approx 0.5$, instances of micro-damage to the fibre-matrix composite will occur which increase progressively with increasing stress exposure. In the example of a transverse/longitudinal shear stressing $\tau_{\perp\parallel}$, these are the familiar 45° micro cracks (hackles) [21] which are stopped at the fibres and cause tiny debondings. It is only when micro-fractures have exceeded a certain magnitude that the IFF will suddenly occur. Generally the micro-fractures resulting from one or more specific stressings have a weakening effect on the fracture resistances R^A of all fibre-parallel sections.

Additionally *every* real fibre-matrix composite contains flaws – in the form of curing cracks, flat air entrapments (voids) or local imperfections in the fibre-matrix bonding. Flaws of that kind do have a sense of direction. There is a high probability that a section with an orientation other than the theoretically defined θ_{fp} contains a flaw which triggers the fracture despite its somewhat lower $f_{E\ IFF}(\theta)$. This is a probabilistic effect. It adds uncertainty to the prediction of the fracture angle and causes the fracture stresses at IFF to be lower than those calculated following Mohr strictly.

In both examples there is a mixture of effects of micro-damage and of probabilistic effects – they cannot be treated separately. In the analysis both effects are treated by a

weakening factor η_{m+p} . Generalising, these examples lead to the following conclusion:

It is to be expected that the effects of micro-damage and probabilistic reducing the magnitude of IFF stresses will rise with the number of fibre-parallel sections which experience relatively high IFF stress exposures.

In the following the weakening effect of micro-damage and probabilistics on the load bearing capacity of the material is discussed by means of combined (σ_2, σ_3) -load cases with varying ratios. Figure 4.10a presents sections of the fracture curves – the dashed line is the fracture curve predicted by the IFF fracture criterion described above (see Sec. 4.2) whereas the bold line represents the fracture curve including micro-damage and probabilistic effects as experimentally observed. Figures 4.10b - d show the standardised stress exposure curves for the three load ratios discussed in detail:

- b Solely applied σ_2 ($\sigma_3 = 0$) or cases with a small additional amount of σ_3 lead to only few highly stressed action planes in a small interval around the fracture angle $\theta_{pf} = 0^\circ$. Only few of the contained flaws are sensitive against the applied load and develop into correspondingly oriented micro-cracks (see insert). These few micro-defects have only a limited weakening effect on the load bearing capacity of the material (see Fig. 4.10a, i). The associated weakening factor η_{m+p} is only slightly below 1.
- c Load cases with a higher ratio between σ_3 and σ_2 lead to considerably more action planes where the threshold for micro-damage (here $f'_{E\ IFFthr} = 0.5$ [88]) has been exceeded. More flaws are activated and develop to micro-defects with a larger variety of orientations (see insert) but their weakening effect is considered to be orientation-independent. The associated weakening factor η_{m+p} is noticeably below 1 and the fracture curve is accordingly corrected to lower bearable stresses (see Fig. 4.10a, ii).
- d Load cases with a σ_3/σ_2 -ratio approaching 1 are close to the extreme case where all the sections are experiencing the same stress exposure, i.e. $f'_{E\ IFF}(\theta) = 1 = \text{constant}$ for $\sigma_3 = \sigma_2$. Having only tensile load components applied, in case d the normal stress σ_n is nearly equally high on all action planes and all kinds of contained flaws are activated (see insert). The resulting micro-defects significantly weaken the load bearing capacity of the material which is represented by an associated $\eta_{m+p} \approx 0.7$ (see Fig. 4.10a, iii).

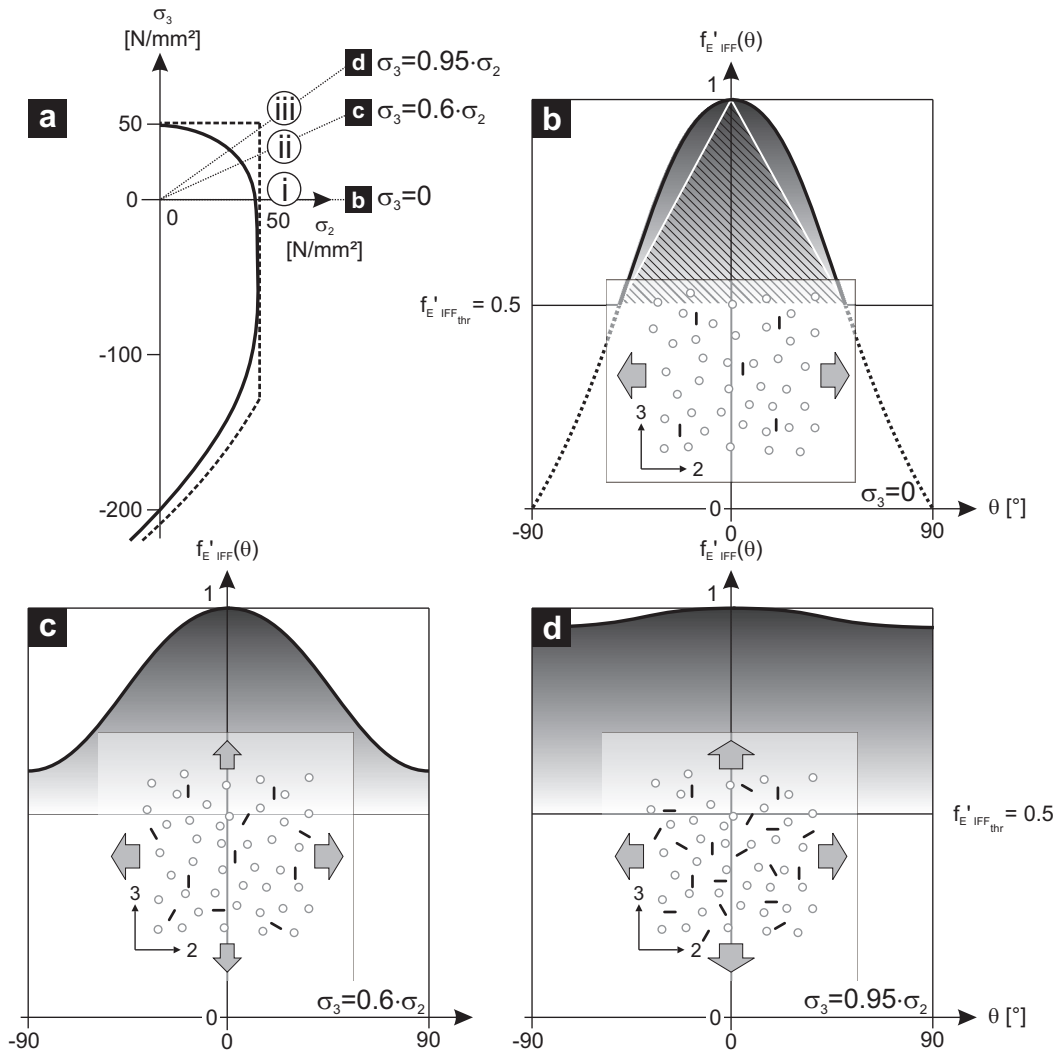


Figure 4.10: For a (σ_2, σ_3) -stress combination: (a) Fracture curves before (thin lines) and after η_{m+p} -correction (bold lines) and (b) standardised stress exposure curves $f'_{E\ IFF}(\theta)$. The hatched triangle in (b) represents S_{ref} .

The three load cases above illustrate the hypothesis, that the weakening effect of micro-damage and probabilistic on the load bearing capacity is related to the fraction of highly loaded action planes. Regarding the analytical treatment however, neither micromechanical failure analysis nor probabilistic methods can be included in an efficient component design process. Therefore the following calculation method has been developed by Puck which is applicable in engineering practice – it is a phenomenological though physically founded approach. The η_{m+p} -determination is based on the following assumptions:

- The IFF fracture plane appears at the angle θ_{fp} for which - according to Mohr's hypothesis – the maximum stress exposure $[f_{E\ IFF}(\theta)]_{max} = f_{E\ IFF}(\theta_{fp})$ has been

calculated (see Eqs. 4.21 and 4.22).

- The IFF fracture stresses are obtained by correcting the fracture stresses $\{\sigma\}_{fr}^{\text{Mohr}}$ calculated from $f_{E\text{ IFF}}(\theta_{fp})$ to lower stresses $\{\sigma\}_{m+p}$ using the correction factor $\eta_{m+p} = [0; 1]$ (see Eq. 4.30). Correspondingly, the IFF stress exposures calculated by Mohr $f_{E\text{ IFF}}(\theta_{fp})$ are corrected to higher values $f_{E\text{ IFF}_{m+p}}$ by dividing them by η_{m+p} (see Eq. 4.31).

$$\{\sigma\}_{m+p} = \{\sigma\}_{fr}^{\text{Mohr}} \cdot \eta_{m+p} = \frac{\{\sigma\}}{f_{E\text{ IFF}}(\theta_{fp})} \cdot \eta_{m+p} = \frac{\{\sigma\}}{f_{E\text{ IFF}_{m+p}}} \quad (4.30)$$

$$f_{E\text{ IFF}_{m+p}} = \frac{f_{E\text{ IFF}}(\theta_{fp})}{\eta_{m+p}} \quad \text{or} \quad = \frac{f_{E\text{ IFF}_{w1}}}{\eta_{m+p}}, \text{ respectively} \quad (4.31)$$

The integrated amount S of standardised stress exposure on all the relevant fibre-parallel sections represents the area below the respective $f'_{E\text{ IFF}}(\theta)$ -curve (see Fig. 4.10b) and is calculated as follows:

$$S = \int_{\text{all planes}^*} (f'_{E\text{ IFF}}(\theta) - f'_{E\text{ IFF}_{thr}}) d\theta \approx \sum_{0^\circ}^{179^\circ*} (f'_{E\text{ IFF}}(\theta) - f'_{E\text{ IFF}_{thr}}) \cdot \Delta\theta \quad (4.32)$$

* only including planes where $f'_{E\text{ IFF}}(\theta) \geq f'_{E\text{ IFF}_{thr}}$

The summing formula as presented above is valid for angular increments of $\Delta\theta = 1^\circ$. The integration or summing with a zero line shifted by $f'_{E\text{ IFF}_{thr}}$ results in a considerably higher weight of high $f'_{E\text{ IFF}}(\theta)$ -values than of low ones.

Puck has described the dependence of η_{m+p} on the integrated standardised stress exposure S by

$$\eta_{m+p} = 1 - \Delta_{max} \frac{S - S_{ref}}{S_{max} - S_{ref}} \quad (4.33)$$

with $S_{max} = 90^\circ$ and $S_{ref} = 30^\circ$ [88].

The reference value S_{ref} achieves a reasonable sensitivity on η_{m+p} against the differences in the S -values of different states of stress. S_{ref} represents large parts of that area below the standardised stress exposure curve which is already contained below a uniaxial load case curve (see Fig. 4.10b, hatched triangle) and hence contained below *every* standardised stress exposure. The value $\Delta_{max} = [0.15; 0.25]$ calibrates the η_{m+p} -correction.

Note that $\{\sigma\}_{fr}^{\text{Mohr}}$ and $f_{E\text{ IFF}}(\theta_{fp})$ (Eqs. 4.30 and 4.31) have to be calculated by a corrected set of material parameters. The reason is that the experimentally determined

strengths R_{\perp}^t , R_{\perp}^c and $R_{\perp\parallel}$ (the anchor points of the IFF criteria) ab initio include micro-damage and probabilistic effects. Thus the analytical procedure of the η_{m+p} -corrections should not degrade these values a second time – the experimentally measured basic material strengths have just to be met by an analysis *including* η_{m+p} .

Correcting the material strengths suggests the correction of the inclination parameters $p_{\perp\parallel}^{t,c}$ and $p_{\perp\perp}^{t,c}$, too. This matter is discussed in detail in [4] ^{see p. 94ff} but up to now the experimental data is limited to (σ_2, τ_{21}) -fracture curves which prove the following correction for $p_{\perp\parallel}^c$:

$$\frac{p_{\perp\parallel}^c \text{ cor}}{p_{\perp\parallel}^c} = 1 + 0.6 \cdot \frac{\Delta_{max}}{p_{\perp\parallel}^c} \quad (4.34)$$

$$\text{for } 0.15 \leq \Delta_{max} \leq 0.25 \text{ and } 0.25 \leq p_{\perp\parallel}^c \leq 0.35$$

The remaining inclination parameters $p_{\perp\parallel}^t$ and $p_{\perp\perp}^{t,c}$ stay unmodified for the time being.

The corrected strengths $R_{\perp \text{ cor}}^t$, $R_{\perp \text{ cor}}^c$ and $R_{\perp\parallel \text{ cor}}$ on which a fracture analysis including the η_{m+p} -corrections has to be based are derived by

$$R_{\text{cor}} = \frac{R}{\eta_{m+p}} \quad (4.35)$$

The η_{m+p} -values in the denominator have to be calculated from the respective load cases – uniaxial tension σ_{\perp}^t , uniaxial compression σ_{\perp}^c and pure inplane shear $\tau_{\perp\parallel}$ – by equations 4.32 and 4.33. The fact that the calculation of the $f'_{E \text{ IFF}}(\theta)$ -values should already be based on corrected strengths reveals a circular reference. In general this prohibits a closed-form solution but the problem may easily be solved using contemporary numerical software.

Regarding the pure inplane shear case $\tau_{\perp\parallel}$, such a procedure can be omitted due to the fact that $\tau_{\perp\parallel}(\theta) = \cos(\theta) \cdot \tau_{21}$ is the only stress component on any action plane. Using the *standardised* stress exposure in equation 4.32, the values $R_{\perp\parallel}$ or $R_{\perp\parallel \text{ cor}}$ are of no importance and $S_{\perp\parallel} = 39, 24^\circ$ exclusively results from the integration of the cosine shape of $f'_{E \text{ IFF}}(\theta)$ independent from the material. The result is the value $R_{\perp\parallel \text{ cor}}$ which exactly meets the fracture condition $f_{E \text{ IFF}_{m+p}} = 1$ for an applied inplane shear of $\tau_{21} = R_{\perp\parallel}$.

The uniaxial compression case may be simplified accordingly: Using equation 4.6 and assuming an unmodified $p_{\perp\perp}^c$, the compressive strength R_{\perp}^c remains the only material parameter and vanishes after the the standardisation (Eq. 4.29). Hence the value S_{\perp}^c depends on $p_{\perp\perp}^c$ only and is about 36° for the suggested values of $p_{\perp\perp}^c$ (see Tab. 4.1). The resulting $R_{\perp \text{ cor}}^c$ leads to $f_{E \text{ IFF}_{m+p}} = 1$ for an applied $\sigma_2 = -R_{\perp}^c$. Equation 4.6 provides the associated $R_{\perp\perp \text{ cor}}^A$.

Only in the case of a uniaxial tension there are more than one mutually independent material parameters relevant in equation 4.21 and the shape of $f'_{E\ IFF}(\theta)$ depends on both, $R_{\perp\perp\ cor}^A$ and $R_{\perp\ cor}^t$ (assuming an unmodified $p_{\perp\perp}^t$). However, using the $R_{\perp\perp\ cor}^A$ defined in the step above, an $R_{\perp\ cor}^t$ can be found which leads to $f_{E\ IFF_{m+p}} = 1$ for an applied $\sigma_2 = R_{\perp}^t$. The η_{m+p} -influence for this load case is expected to be rather small and may be neglected if no adequate numerical software is at hand. In general it is highly advisable to use the η_{m+p} -corrections. Even if based on uncorrected material parameters the IFF prediction including η_{m+p} will be more accurate than any analysis neglecting the influence of micro-damage and probabilistics.

4.4 Puck's IFF criteria and the Mohr' circle

It has been stated that Puck's Theory for IFF is based on Coulomb's and Mohr's fracture criterion (see Sec. 4.2). In the following section the relation between Puck's action plane-related IFF criterion and Mohr's perception of stresses is outlined.

The Mohr's circle of stresses is a graphical approach to derive the stress components (σ^A, τ^A) acting on an arbitrary section A due to applied plane stress $(\sigma_x, \sigma_y, \tau_{xy})$ (see Fig. 4.11a). Figure 4.11c defines the relevant orientations and includes the principal stresses associated with the applied load. It is these principal stresses, between which the Mohr's circle is spanned (c) but it may also be constructed by the following definition of its centre and radius:

$$\sigma_M = \frac{1}{2}(\sigma_x + \sigma_y) \quad (4.36)$$

$$r = \sqrt{\left(\frac{\sigma_x - \sigma_y}{2}\right)^2 + \tau_{xy}^2} \quad (4.37)$$

Neglecting the 1-direction, the situation described above is equivalent to a lamina subjected to the fibre-perpendicular stress components $(\sigma_2, \sigma_3, \tau_{23})$ (b) and thus the Mohr's circle also provides the possible combinations (σ_n, τ_{nt}) of all the relevant action planes in a lamina (see Fig. 4.5). Transferred to the lamina the abscissa has the meaning of an σ_n -axis and the ordinate of an τ_{nt} -axis. Interpreted in that sense, the Mohr's circle associated with a particular state of stress in a lamina may be combined with the illustration of the Master Fracture Body (see Sec. 4.2.3). The Mohr's circle lies in the σ_n - τ_{nt} -plane of the MFB and serves as the basis for the additional shear components $\tau_{n1}(\theta)$ following equation 4.3. They are plotted as a vertical vector starting from the respective position on the Mohr's circle. The result is a closed curve in the $(\sigma_n, \tau_{nt}, \tau_{n1})$ -space which represents the set of possible stress combinations acting on all the action planes (see Fig. 4.12). As

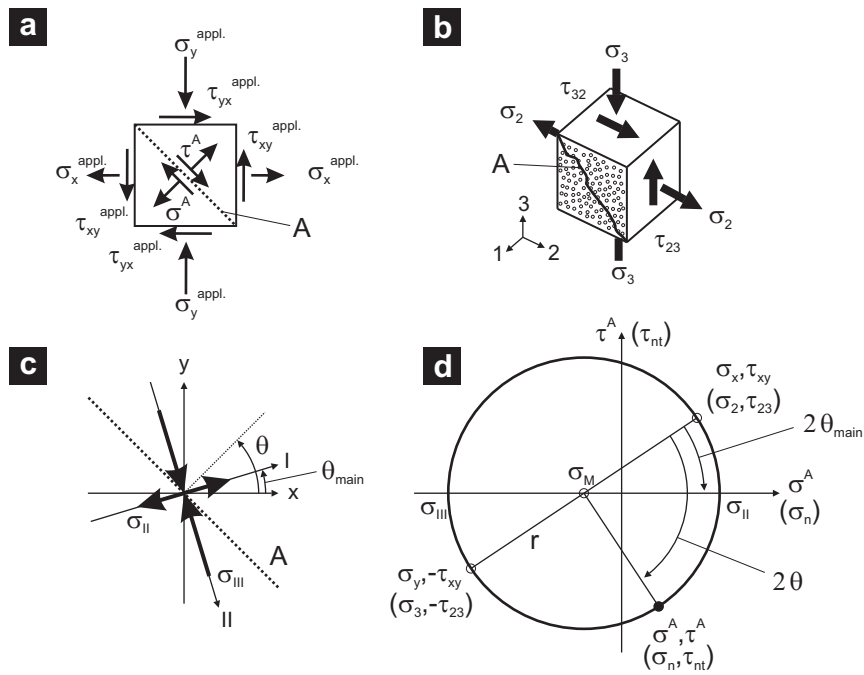


Figure 4.11: Plane stress state applied to a shell (a), fibre-perpendicular stress components applied to a lamina (b), principal stresses (σ_I, σ_{II}) associated with the applied load (c), Mohr's circle giving the stress combination (σ^A, τ^A) acting on an arbitrary plane A.

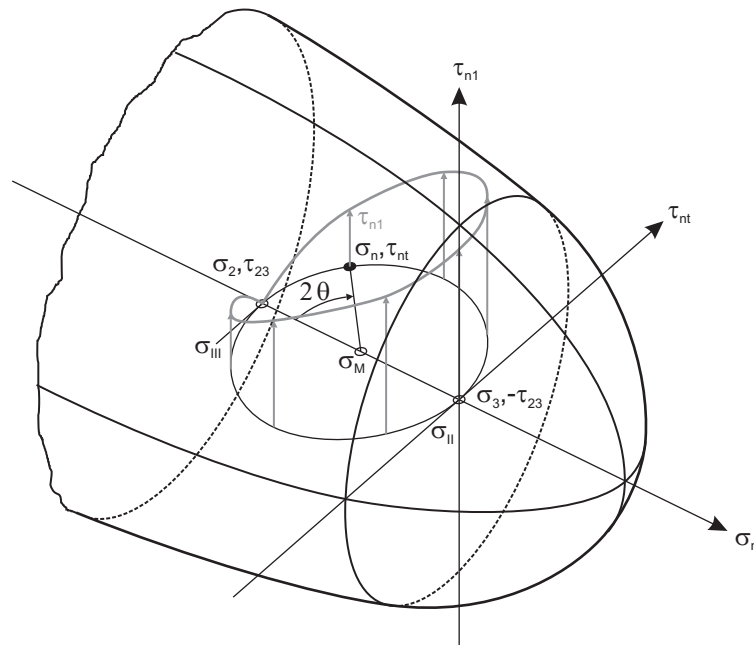


Figure 4.12: MFB (black) with the set of possible stress combinations (grey) acting on an action plane of a lamina due to applied compressive σ_2^c together with positive τ_{13} .

long as the complete curve lies within the MFB, the IFF criterion is not fulfilled and no inter-fibre fracture occurs. Increasing the load, the orientation of the fracture plane θ_{fp} is defined by the first point of the curve which touches the MFB. In the present example this happens at two points at the same time – at about $\theta_{fp} = 90^\circ \pm 22.5^\circ$.

The Mohr's circle within the MFB also visualises why a lamina subjected to a pure compressive σ_2^c does not break at the action plane with the largest shear stress $\tau_{nt_{max}} = \tau_{nt}(45^\circ)$. Figure 4.13 shows the Mohr's circle of a – at the beginning – small compressive σ_2^c (grey) which is increased until the circle touches the master-fracture body at $\theta_{fp} = 54^\circ$ (black). Comparing the 45° and 54° action planes, it becomes evident that the decrease of

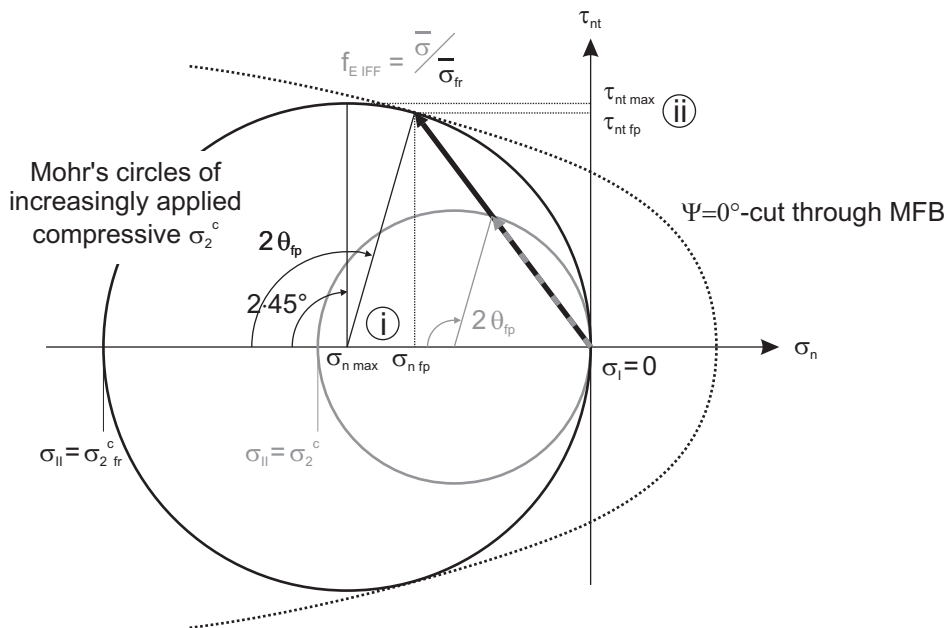


Figure 4.13: Mohr's circles (grey and black) of an increasingly applied compressive σ_2^c touching the MFB at $\theta_{fp} = 54^\circ$. The stress exposure value f_{EIFF} associated with the grey stress state is related to the stress state at fracture.

fracture impeding compressive σ_n (see Sec. 4.2) is larger (i) than the decrease of fracture promoting τ_{nt} (ii). Accordingly the fracture occurs on a fracture plane $\theta_{fp} > 45^\circ$. This example proves why the relation between Puck's IFF criterion and the Mohr's circle is regarded to be helpful in the process of understanding specific results of Puck's inter-fibre failure prediction although the subject is not essential in terms of application.

4.5 Confined laminae – the In-Situ Effect

When confined into a laminate, the lamina's IFF strengths are observed to be higher than measured in isolated UD laminae [90]. The lay-up configuration apparently obstructs the development of Mode A and B cracks (see Sec. 4.2.4). While the effect itself is indisputable, there is only little information on its quantity. Therefore in all the laminate test cases (cases 8 to 12) the measured basic strengths are multiplied with the following roughly estimated factors:

- Inplane transverse tensile strength $R_{\perp 2}^t$: 1.35
- Inplane transverse/longitudinal shear strength $R_{\perp\parallel 21}$: 1.175

The transverse compressive strength $R_{\perp 2}^c$ and the through-thickness strengths including shear ($R_{\perp 3}^{t/c}$ and $R_{\perp\parallel 31}$) are assumed to be unaffected. While the present implementation accounts for different values for $R_{\perp 2}^t$ and $R_{\perp 3}^t$ (see Sec. 7.2.2) it enforces $R_{\perp\parallel 21} = R_{\perp\parallel 31}$. Furthermore, the present implementation does not yet distinguish between embedded and outer plies, although it is known that the in-situ effect on outer plies is smaller if not negligible. Taking into account the in-situ effect by increasing the strengths of materials is another case where the given nonlinear stress-strain relations are exceeded as they end at the original strengths. Thus the affected curves have been scaled in a self-similar way according to section 3.1.2.

4.6 Application of Puck's IFF criterion to special cases

4.6.1 Application to isotropic material

The fundamental difference between fracture of a UD-composite and an isotropic pure matrix material is that in the latter case the fracture may occur in a plane at *any* orientation (θ, φ) (see Fig. 4.14). In a UD-composite fracture may only occur in planes parallel to the fibres and thus *one* angle θ unambiguously defines possible fracture planes (see Fig. 4.5).

Therefore in the isotropic case, the stresses acting on an action plane are $\sigma_n(\theta, \varphi)$ and $\tau_{n\psi}(\theta, \varphi)$. Once these stresses are calculated from the applied stresses [91], the search for the plane with the largest stress exposure may be performed using a slightly modified formulation of the usual f_E now depending on (θ, φ) :

In an isotropic material there are no different fracture resistances of the action plane against the two shear stresses τ_{n1} and τ_{nt} and accordingly $R_{\perp\perp}^A$ and $R_{\perp\parallel}^A$ can be replaced

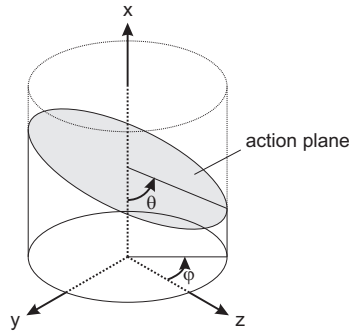


Figure 4.14: Definition of an arbitrary action plane.

by $R^{A\tau}$. That means that in the isotropic case just *one* fracture resistance of the action plane against shear has to be derived from the measured strengths of the material. The value for the isotropic fracture resistance against shear can be easily derived in the style of equation 4.6 using the compressive strength of the material R^c :

$$R^{A\tau} = \frac{R^c}{2(1 + p^c)} \quad (4.38)$$

This approach is consistent with the fact that the transverse-transverse direction of a UD lamina is its isotropic direction. Accordingly the proposed values of $p_{\perp\perp}^{t,c}$ [88] are used as benchmark to define the only set of inclination parameters left $p_{\perp\perp}^{t,c} = p_{\perp\parallel}^{t,c} = p^{t,c}$. If the isotropic material behaves *intrinsically brittle* (see Sec. 4.2.2) the considerations which led to the fracture resistance of the action plane against tension (see Eq. 4.4) are still valid and $R^{At} = R^t$. Otherwise R^{At} is a parameter of the fracture criteria whose definition demands more effort (see Sec. 7.2.1).

The interpolation for the inclination parameters in equation 4.23 is now obsolete and with equation 4.1 the definitions of the stress exposure $f_E(\theta, \varphi)$ (see Eqs. 4.21 and 4.22) become:

$$f_E(\theta, \varphi) = \sqrt{\left[\left(\frac{1}{R^{At}} - \frac{p^t}{R^{A\tau}} \right) \sigma_n(\theta, \varphi) \right]^2 + \left(\frac{\tau_{n\psi}(\theta, \varphi)}{R^{A\tau}} \right)^2} + \frac{p^t}{R^{A\tau}} \sigma_n(\theta, \varphi) \quad (4.39)$$

for $\sigma_n \geq 0$ and

$$f_E(\theta, \varphi) = \sqrt{\left(\frac{\tau_{n\psi}(\theta, \varphi)}{R^{A\tau}} \right)^2 + \left(\frac{p^c}{R^{A\tau}} \sigma_n(\theta, \varphi) \right)^2} + \frac{p^c}{R^{A\tau}} \sigma_n(\theta, \varphi) \quad (4.40)$$

for $\sigma_n < 0$

For the sake of simplicity we will assume in the following $p^c = p^t = p$.

The procedure above leads to a rotationally symmetric MFB (see Fig. 4.8a) with identical longitudinal sections for any angle ψ . This representation equals the reduction of the MFB to a Master Fracture Curve (see Fig. 4.8c) depending only on σ_n and $\tau_{n\psi}$ as it was stated for isotropic materials in the very beginning (see Sec. 4.2). It goes without saying that in isotropic material neither the x_1 -direction does have the usual exceptional position nor the FF criterion is of any significance.

The modified Puck's IFF criterion for isotropic material has been applied to the test case 1 of the WWFE-II (see Sec. 7.2.1)

4.6.2 Application to not intrinsically brittle materials

While intrinsically brittle behaviour (see Sec. 4.2.2) may be assumed for most FRCs, a pure matrix material as given in test case 1 of the WWFE-II (see Sec. 7.2.1) may require further consideration. For MY750 the given shear strength $R^\tau = 54$ MPa is considerably lower than the given tensile strength $R^t = 80$ MPa (see App. B.2). Applied shear stress leads to a maximum tensile stress σ_n^t of equal magnitude on a section inclined by 45° . So if the given material was intrinsically brittle, then R^τ would be close or equal to R^t and this section would be the fracture plane. As this is obviously not the case here, fracture is probably driven by a mixed-mode stressing ($\sigma_n, \tau_{n\psi}$) on the fracture plane. Having detected this behaviour for an applied pure shear stress, there is no reason to expect exclusively σ_n^t -driven fractures due to an applied uniaxial tensile stress – a mixed-mode fracture on a section inclined against the action plane of the applied uniaxial tension will probably occur. Thus equation 4.4 is *no longer valid* and there are now two unknowns, mutually dependent model parameters to determine: p and R^{At} .

As the calibration of the model demands the determination of *two* parameters, we use those two given states of stress leading to fracture ($\sigma^t = R^t$ and $\tau = R^\tau$) which have not yet been incorporated into any other relation ($\sigma^c = -R^c$ is already used in equation 4.38). For both cases it is possible to determine the set of value pairs (R^{At}, p) where the model exactly predicts the given failure stresses for uniaxial tension and pure shear (see Fig. 4.15). The use of an analytical tool is the most efficient way to derive the presented chart [92]. Based on the parameters met by both curves (see Fig. 4.15), the results of test case 1 are summarised in figure 7.1.

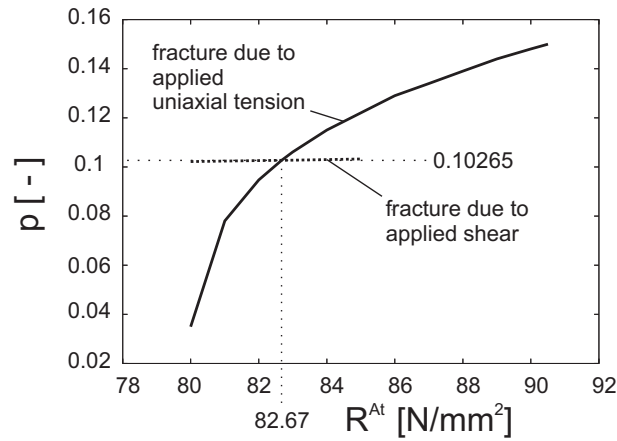


Figure 4.15: Determination of the model parameters R^{At} and p in the case of not intrinsically brittle, isotropic material.

4.7 Puck's fibre fracture criterion

Puck's Theory clearly distinguishes between the two fracture types of a UD-lamina: Inter-fibre fracture (IFF) and fibre fracture (FF). In an elementary approach those two cases are treated with mutually independent criteria, where the FF criterion represents two simple stress limits for the tension and compression mode (see Fig. 4.16).

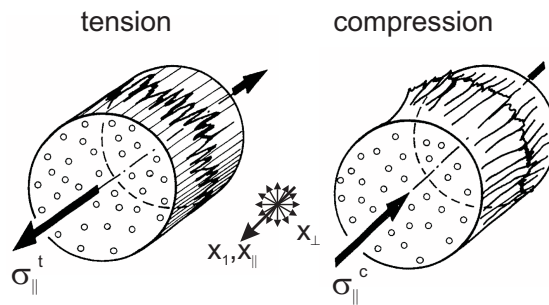


Figure 4.16: Fibre failure modes of a UD-composite, from [39].

By definition the lamina is treated as a homogenised orthotropic continuum, thus the stress exposure $f_{E\,FF}$ with regard to fibre fracture is defined as a ratio between homogenised stress σ_1 in the lamina (*not* in the fibre) parallel to the fibre direction and the tension or compression stress at fracture of the lamina in fibre direction R_{\parallel}^t and $-R_{\parallel}^c$ respectively (see Eq. 4.41). Fibre fracture is predicted for any of the two values by $f_{E\,FF} = 1$. Please note that all strength parameters are defined as positive values.

$$f_{E\ FF} = \begin{cases} \frac{\sigma_1}{R_{\parallel}^t} & \text{for } \sigma_1 > 0 \\ \frac{\sigma_1}{(-R_{\parallel}^c)} & \text{for } \sigma_1 < 0 \end{cases} \quad (4.41)$$

While these maximum stress criteria have been generally approved by extensive experimental work [25] there are findings which suggest more sophisticated fibre fracture criteria [5, 6]. Although this is an ongoing matter [4] ^{sec p. 16ff}, there are applicable formulations covering the influence of transverse – particularly compressive – stress [23] and shear [26] whereas the former does have a significantly larger impact on FF. Analysing 3D states of stress it is therefore highly recommended to account for the transverse effect in the following way:

The fundamental hypothesis for UD-laminae is [5, 6, 39]:

The maximum sustainable longitudinal stresses σ_{1f} acting in the fibres are the same whether the FF occurs under combined $(\sigma_1, \sigma_2, \sigma_3)$ or uniaxial (exclusively σ_1) stresses.

In contrast the homogenised longitudinal stresses in the UD-lamina at FF do differ whether combined or uniaxial stress is applied because the two cases lead to different longitudinal stresses σ_{1f} in the fibre. The reason is that transverse stresses (σ_2 and/or σ_3) – due to a Poisson's effect – do influence the strain in the fibre direction. The effect is locally enlarged due to the inhomogeneously distributed stress in the matrix: Close to the fibre, the transverse stress is higher than the homogenised value on the lamina-level. Puck accounts for this stress magnification by the use of a magnification factor m_{σ_f} and proposes the values 1.3 for GFRC and 1.1 for CFRC [25, 39].

The starting point for the corresponding analysis is the strain ϵ_{1f} in the fibres due to the combined stresses $(\sigma_1, \sigma_2, \sigma_3)$:

$$\epsilon_{1f} = \frac{\sigma_{1f}}{E_{\parallel f}} - \frac{\nu_{\parallel\perp f}}{E_{\perp f}} \cdot m_{\sigma_f} \cdot (\sigma_2 + \sigma_3) \quad (4.42)$$

With

$$\frac{\nu_{\parallel\perp f}}{E_{\perp f}} = \frac{\nu_{\perp\parallel f}}{E_{\parallel f}} \quad \text{and} \quad \epsilon_{1f} = \epsilon_1 \quad (4.43)$$

the longitudinal stress in the fibres σ_{1f} is

$$\sigma_{1f} = E_{\parallel f} \cdot \epsilon_1 + \nu_{\perp\parallel f} \cdot m_{\sigma_f} \cdot (\sigma_2 + \sigma_3) \quad (4.44)$$

From equation 4.44 a new fracture condition can be derived. First ϵ_1 is replaced by the elastic law of the UD-lamina

$$\epsilon_1 = \frac{\sigma_1}{E_{\parallel}} - \frac{\nu_{\perp\parallel}}{E_{\parallel}} \cdot (\sigma_2 + \sigma_3) \quad (4.45)$$

then the fibre stress σ_{1f} by the fracture resistance of the fibre $R_{\parallel f}$

$$R_{\parallel f} = E_{\parallel f} \cdot \epsilon_{FFf} \quad \text{and} \quad R_{\parallel} = E_{\parallel} \cdot \epsilon_{FF} \xrightarrow{\text{with } \epsilon_{FFf} = \epsilon_{FF}} R_{\parallel f} = \frac{E_{\parallel f}}{E_{\parallel}} \cdot R_{\parallel} . \quad (4.46)$$

The resulting FF condition for UD-lamina is:

$$\frac{1}{\pm R_{\parallel}^{t,c}} \left[\sigma_1 - \left(\nu_{\perp\parallel} - \nu_{\perp\parallel f} \cdot m_{\sigma_f} \frac{E_{\parallel}}{E_{\parallel f}} \right) (\sigma_2 + \sigma_3) \right] = 1 \quad (4.47)$$

with $\begin{cases} R_{\parallel}^t & \text{for } [\dots] \geq 0 \\ -R_{\parallel}^c & \text{for } [\dots] < 0 \end{cases}$

The fracture function is homogeneous of grade 1 and thus can directly be understood as a formulation for the stress exposure $f_{E FF}$ of UD-lamina with regard to fibre fracture:

$$f_{E FF} = \frac{1}{\pm R_{\parallel}^{t,c}} \left[\sigma_1 - \left(\nu_{\perp\parallel} - \nu_{\perp\parallel f} \cdot m_{\sigma_f} \frac{E_{\parallel}}{E_{\parallel f}} \right) (\sigma_2 + \sigma_3) \right] \quad (4.48)$$

with $\begin{cases} R_{\parallel}^t & \text{for } [\dots] \geq 0 \\ -R_{\parallel}^c & \text{for } [\dots] < 0 \end{cases}$

Please note that $\nu_{\perp\parallel}$ and $\nu_{\perp\parallel f}$ are the major Poisson's ratios of the UD-lamina and the fibres, respectively. The first index denotes the direction of the lateral strain caused by the stress acting in the direction of the second index.

Puck has found that in the case of plane $(\sigma_1, \sigma_2, \tau_{21})$ -stress, the results of equations 4.41 and 4.48 differ by only a few percent. However, the influence of transverse stresses on FF can become important in the region of combined compressive σ_2^c and σ_3^c of similar magnitude, where $|\sigma_2|$ and $|\sigma_3|$ can exceed the transverse compressive strength R_{\perp}^c by a factor of up to 4 [23] (see Sec. 7.2.2).

5 Post-failure degradation analysis

It has been stated earlier (see Sec. 2.2) that fibre fracture in one or more laminae is currently defined as the limit of application of the laminate. Consequently this chapter deals with the successive damage evolution process *beyond inter-fibre fracture*.

In the context of post-failure analysis it is important to stress that Puck's fracture criteria predict layer-wise macroscopic failure. The stress exposure $f_{E\ IFF} = 1$ denotes the state of stress in a lamina where the first macroscopic crack through the entire thickness of the respective lamina occurs (see Sec. 2.3). In the case of a lamina confined within a laminate, reaching a lamina's fracture condition is not equivalent with the disintegration of the whole material and the state of stress is labelled as *initial failure stress* of a laminate. In such a confined lamina a further increased applied load starts a successive damage evolution process in the form of a growing macroscopic crack density $\delta = t/d$ (see Fig. 5.1). This goes along with the reduction of the lamina's load carrying capacity and the process is called *degradation*. The maximum bearable stress of a laminate is not reached before

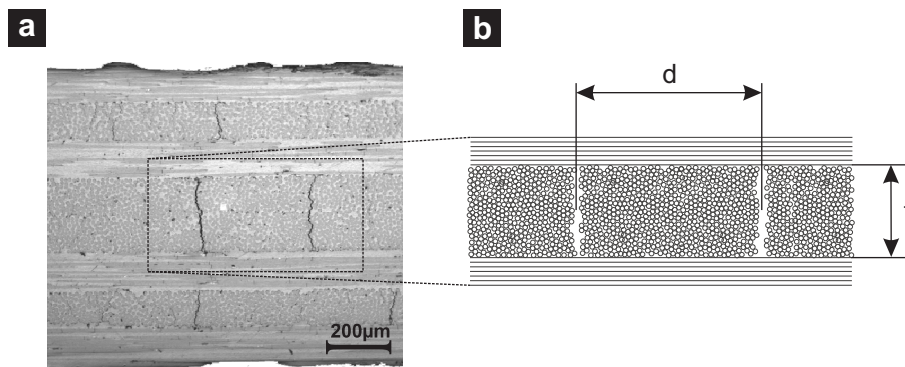


Figure 5.1: Macroscopic cracks in a glass fibre reinforced $0^\circ/90^\circ$ laminate loaded in y -direction (a) and the definition of the crack density in a degrading lamina (b).

the strongest lamina reaches its failure condition. The related state of stress is understood as *final failure stress* of a laminate.

5.1 Stability of the damage evolution in a laminate

Within the laminate, the load which caused the lamina's IFF may or may not be redistributed to neighbouring laminae depending on the load case and the laminate's stacking

sequence. If a redistribution is possible, there will always be an equilibrium between the further increased applied load and the decreasing load share of the degrading lamina together with the increasing load share of the neighbouring ones. This is the definition of a *stable damage evolution* in a laminate. If no load redistribution is possible the abrupt damage evolution due to an infinitesimally increased load will only be retarded by micromechanical supporting effects which are not covered by the present model. The result is the *unstable damage evolution* in a laminate. Inplane load cases are generally expected to produce stable damage evolutions. Exceptions are stacking sequences where all the laminae are equally loaded and hence no load redistribution is possible. However there is no chance to redistribute any through-thickness loads and/or shear to neighbouring laminae. Thus any 3D load cases are generally expected to produce unstable damage evolutions resulting in rapid final laminate failure after the occurrence of the first IFF.

5.2 Smearred crack representation

The smeared crack approach does not consider cracks as discrete, local discontinuities but considers only their consequences in a continuum mechanical sense. The topological description of the material stays the same before and after the occurrence of cracks – in the present case as an orthotropic continuum. Its constitutive behaviour after the occurrence of cracks is homogenised over the sections of sound material between the cracks and the cracks themselves. In the present case inter-fibre fractures lower the amount of load which is introduced and hence carried by the respective lamina. The load has to be transmitted between the sound section – i.e. over the cracks – via the neighbouring laminae (see Fig. 5.2a). A laminate incorporating a damaged lamina will – under the same load – deform stronger than the same laminate in a completely undamaged state. Accordingly the consequence of the cracks in a continuum mechanical sense is a reduced stiffness of the damaged lamina. The degradation process of a lamina due to an increasing macroscopic crack density is hence reproduced in a smeared crack representation by the reduction of the stiffness (see Eq. 5.1) in the way that both representations exhibit the same constitutive behaviour. In the present example (see Fig. 5.2a), this means the same elongation $\Delta l/l_0$ for a given load F .

$$\text{reduced stiffness} = \eta \cdot \text{original stiffness} \quad (5.1)$$

Now η is the governing parameter for the degradation process in the smeared crack representation. During the degradation process it goes down from the value 1 (no damage) to $\eta_R =]1; 0]$ (residual stiffness fraction at the saturated crack density). The reduction of

the stiffnesses is then

$$\text{reduction} = 1 - \eta \quad (5.2)$$

and starts from 0 (no damage) and increases up to $1 - \eta_R$.

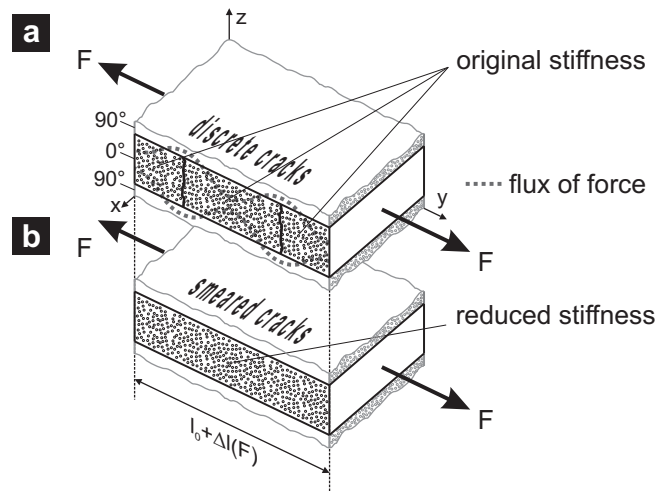


Figure 5.2: Discrete crack (a) and smeared crack representation (b) of a confined degrading lamina.

There are numerous approaches to correlate the density, form, size and position of cracks with their effects on the stiffness [93], but the following degradation rules are exclusively defined in the smeared crack representation of the degrading lamina. Hence it is important for the development and validation¹ to keep in mind that the degradation process is a growth of crack density in reality, but neither the actual value of the crack density δ nor possible correlations between the discrete and smeared crack representation do play a role in this work.

5.3 Existing degradation procedures

It is obvious, that the amount of load beyond the IFF, the thereby generated crack density and the according degradation parameter η of the smeared crack representation are to be correlated to define a valid material behaviour for a post-failure degradation analysis. Keeping strictly inside the smeared crack representation, the detour via the crack density may be omitted and the correlation between the amount of load beyond the IFF and the degradation parameter η or the resulting reduced stiffnesses is the remaining task of any degradation rule.

¹Does the model meet the reality?

5.3.1 Excessive IFF stress exposure

Early experiments with laminates loaded inplane (σ_y and/or τ_{xy}) beyond IFF [39] led to an empirical correlation between the applied load beyond the IFF and the degradation parameter η via the IFF stress exposure persistently calculated with original stiffnesses (see Eq. 5.3). Calculating $f_{E\ IFF}$ with the unchanged original stiffnesses results in values $f_{E\ IFF} > 1$ for load cases beyond an IFF.

$$\eta(f_{E\ IFF}) = \frac{1 - \eta_R}{1 + a(f_{E\ IFF} - 1)^\zeta} + \eta_R \quad \text{for } f_{E\ IFF} > 1 \quad (5.3)$$

The definition (Eq. 5.3) results in $\eta = 1$ for the onset of damage ($f_{E\ IFF} = 1$) and converges against the residual stiffness fraction η_R at the saturated crack density for $f_{E\ IFF} \rightarrow \infty$. Loading a laminate inplane, the laminae are subjected to transverse stress σ_2 and inplane shear stress τ_{12} only. Hence only the transverse Young's modulus E_2 and the inplane shear modulus G_{12} are available for degradation (see Eq. 5.4). It is obvious, that IFFs continue to transmit pressure $\sigma_n < 0$ over the crack edges hence there is no reduction of the respective stiffness in these cases. In the early development stages also the Poisson's ratios were degraded but later experiments strongly suggested keeping them constant [94]. Accordingly no Poisson's ratio degradation is specified throughout the present work.

$$E_2^{red} = \begin{cases} \eta \cdot E_2^{orig} & \text{for tensile } \sigma_n \text{ on the fracture plane} \\ E_2^{orig} & \text{for compressive } \sigma_n \text{ on the fracture plane} \end{cases} \quad (5.4)$$

$$G_{12}^{red} = \eta \cdot G_{12}^{orig}$$

The mentioned original stiffnesses (index *orig*) which are used to calculate the exceeded IFF stress exposure are the secant moduli at the IFF limit, thus the last valid secant moduli in the case of a nonlinear constitutive material model (see Sec. 3.1.2).

Further experiments [95, 96] have revealed that reasonable parameters for equation 5.3 are $a = [0.95; 5.5]$ and $\zeta = [1.17; 1.5]$ depending on the material. These studies also suggest to reduce G_{12} less than E_2 . Using the excessive IFF stress exposure approach this is implemented in equation 5.3 by different residual stiffness fractions $\eta_{R_E} = 0.03$ and $\eta_{R_G} = 0.25$ for GFRC or $\eta_{R_G} = 0.6$ for CFRC [88]. The suggested values are equivalent with the reduction of G_{12} by only $k = 77\%$ for CFRC and $k = 41\%$ for GFRC of the reduction of E_2 :

$$E_2^{red} = \begin{cases} E_2^{orig} \cdot (1 - \text{reduction}) & \text{for tensile } \sigma_n \text{ on the fracture plane} \\ E_2^{orig} & \text{for compressive } \sigma_n \text{ on the fracture plane} \end{cases} \quad (5.5)$$

$$G_{12}^{red} = G_{12}^{orig} \cdot (1 - k \cdot \text{reduction})$$

It has been stated in earlier works that the approach has proven its applicability on a wide range of materials and stacking sequences [4, 94]. However aiming on a completely 3D failure and post-failure analysis, this approach is judged as strictly limited to inplane load cases without the potential of being extended to 3D load cases. The approach completely neglects that a stable damage evolution process requires and is governed by a load redistribution process. In the case of loads or stacking sequences leading to an unstable damage evolution process or even for an isolated single lamina, the excessive IFF stress exposure approach predicts an unrealistic, smooth degradation process of the damaging laminae. The application of this method is restricted to the analysis of doubtlessly stable damage evolution processes under inplane load.

Validity check

Puck's Theory is a stress-based, layer-wise fracture criterion, it defines the maximum bearable *stress* state in a lamina. Increasing the applied load beyond IFF there is no reason why the laminate should be able to bear more stress, in fact it partly gets rid of its load by a redistribution in the process of the reduction of stiffnesses and the associated increase of strain. A degradation procedure which plausibly predicts this process enables to associate any given state of strain in a lamina (beyond IFF) with the transmitted load by the lamina or the state of stress in the smeared crack representation of the lamina, respectively. However the procedure may *not* define a state of strain for an arbitrary high amount of stress, because the stress-based fracture criterion defines a stress threshold, beyond which the states of stress are just not bearable.

Applying the excessive IFF stress exposure approach to any given state of strain beyond IFF, the original stiffnesses provide a state of stress based on which the IFF stress exposure takes a value of $f_{E\ IFF} > 1$. Equation 5.3 leads to a value of $\eta =]1; \eta_R]$ and equation 5.5 provides the reduced stiffnesses of the degrading lamina. The application of these stiffnesses to the given state of strain leads to the associated state of stress in the smeared crack representation of the degrading lamina. The excessive IFF stress exposure approach also permits to assign a state of strain to any given state of stress beyond IFF. At a given state of stress beyond IFF, the IFF stress exposure takes a value of $f_{E\ IFF} > 1$, equation 5.3 leads to a value of $\eta =]1; \eta_R]$ and equation 5.5 offers the reduced stiffnesses. Applying these stiffnesses to the given state of stress leads to the associated state of strain in the smeared crack representation of the degrading lamina. This result is completely unphysical and does not qualify the presented approach for a general application.

5.3.2 Constant IFF stress exposure

The constant IFF stress exposure approach overcomes the purely empirical nature of the approach above and is based on physical and mechanical considerations [5, 6]. The approach conserves the meaning of the value $f_{E\ IFF} = 1$ as a fracture criterion and is in accordance with degradation procedures based on different failure criteria which also postulate the failure criterion to be the degradation governing measure [97]. There is no conceivable situation in which a *sound* lamina experiences an IFF stress exposure above 1. When the stress exposure of a lamina reaches this value an IFF occurs and therewith the lamina gets rid of parts of its load by a redistribution or all of its load by separation, respectively. In reverse the density of cracks emerging due to an increasing load beyond the IFF permanently adjusts to that value at which the IFF stress exposure threshold of $f_{E\ IFF} = 1$ is not exceeded. This means for the degradation process of a lamina, that – at a given state of strain beyond IFF – the degradation parameter η takes exactly that value, for which the the resulting stresses generate an IFF stress exposure of 1. There is no longer an analytical degradation rule like equation 5.3 but the amount of degradation is defined by the threshold

$$f_{E\ IFF} = 1 = \text{constant} . \quad (5.6)$$

For inplane load cases, the impact of the degradation on the respective stiffnesses defined in equation 5.5 stays valid but the residual stiffnesses are no longer accounted for by residual stiffness fractions η_R . Now the impact of the degradation process on the respective stiffness is stopped when it has reached its experimentally determined residual stiffness value. The degradation process in the respective lamina is completed when – after a stable damage evolution process – a valid solution for η can no longer be found. This is the case after all the relevant stiffnesses have already been degraded down to their residual stiffness values.

The approach meets the requirements of the validity check above (see Sec. 5.3.1). For any given state of strain beyond the IFF the original stiffnesses result in $f_{E\ IFF} > 1$ but there will generally be a value of η which reduces the stiffnesses and hence the stresses down to the state where $f_{E\ IFF} = 1$. For any given state of stress beyond the IFF there will be no value of η within its domain of definition $[1; 0]$ which is able to generate $f_{E\ IFF} = 1$. As a result the approach does not provide a valid solution for unstable damage evolution where the stresses in the laminae inevitably rise with an increasingly applied load beyond IFF. Accordingly the approach is capable of identifying unstable damage evolution processes. The approach has proven its capability and reliability in the WWFE-I inplane load cases [5, 6] and it is implemented in the material subroutines in the present work (see Ch. 6). In the course of the application there were however identified two problems of the method:

Degradation locking in the case of fibre-perpendicular compression

Using equation 5.5 for the definition of the impact of the degradation on the respective stiffnesses results in no valid solution for η in the case of fibre-perpendicular compression although compression in the y-direction might result in a stable damage evolution process up to a certain point. Experimental experience however suggests, that inclined IFFs due to inplane compression in the respective lamina (Modus C fractures, see Sec. 4.2.4) define the limit of use of the laminate (see Sec. 2.3). The amount of load beyond the IFF, which can be transmitted over the crack edges before the wedge effect leads to a sudden disintegration of the laminate, is currently unpredictable. Accordingly such IFFs are classified as non-tolerable fractures and no post-failure degradation analysis is started after such fractures. There are currently no experimental results concerning the damage evolution in a laminate subjected to compression in the z-direction. This kind of applied load is expected to result in a crushing of the damaging lamina which is a mechanism far beyond the capabilities of a continuum based smeared crack representation. Within the present work aiming on macroscopic and physical (in contrast to empirical) material descriptions such post-failure behaviour is classified as currently unpredictable.

Lack of adjustability to experimental results

Although the extremely limited availability of experimental degradation process data, the lack of adjustability of the constant IFF stress exposure approach is identified as a drawback. This becomes even more evident if the following theoretical aspect is considered: The applied threshold for the occurrence of further inter-fibre fractures during the degradation process $f_{E\ IFF} = 1$ is defined in the smeared crack representation of the damaging lamina, but the actual crack presumably emerges in the centre of a sound section of the lamina between two discrete cracks (see Fig. 5.2). Predicting fractures in the sound sections of the discrete crack representation with a criterion based on the smeared crack representation implies identical states of stress in both of them. Comprehending the derivation of the reduced stiffnesses of the smeared crack representation (see Sec. 5.6.1) identifies the approach above to be based on a reasonable but simplifying assumption. Without further experimental or numerical investigations $f_{E\ IFF} = 1 = \text{constant}$ is an acceptable degradation approach, but the enhancement described below (see Sec. 5.4) prepares the degradation rule for future findings.

5.4 Variable IFF stress exposure

The degradation rule described above (see Sec. 5.3.2) becomes adjustable to experimental findings if the threshold IFF stress exposure $f_{E\ IFF}$, at which new inter-fibre fractures emerge, is not constantly 1 but depends on the progress in the degradation process [98]. As the central degradation parameter is η , a linear dependence of $f_{E\ IFF}^{red}(\eta)$ is a straightforward ansatz. Now the degradation process has not only an impact on the stiffnesses according to equation 5.5 but also on the bearable stress exposure of the lamina:

$$f_{E\ IFF}^{red} = f_{E\ IFF}^{orig} \cdot (1 - l \cdot \text{reduction}) = 1 - l \cdot \text{reduction} \quad (5.7)$$

Latest experiments suggest the bearable IFF stress exposure to decline in the course of the degradation process. This finding is in accordance with theoretical aspects arising from the smeared crack representation (see Secs. 5.2 and 5.6.1, particular Eq. 5.13). However it has to be assured that the involved stiffnesses decline faster than the bearable stress exposure – otherwise no valid solution for η can be found. Without further experiments the range for the impact factor l is theoretically limited to $]0; k[$ for inplane load cases but more detailed information is currently not available. The question whether there is a residual bearable IFF stress exposure or not is currently unanswered. Hence the variable IFF stress exposure approach is not implemented in the material subroutines in the present work (see Ch. 6).

5.5 3D degradation procedure

The existing degradation procedures have been developed, validated and calibrated for inplane load cases. The aim of providing a comprehensive failure prediction for UD fibre-reinforced laminates with complex geometries and under 3D load (see Ch. 1) requires the development of a 3D post-failure degradation analysis even if it has been stated, that through-thickness load and/or shear will in the majority of cases lead to unstable damage evolution processes (see Sec. 5.1). The desired output of a 3D degradation analysis will either be

- the reliable information that an unstable damage evolution process starts when exceeding the IFF criterion,
- or the 3D constitutive behaviour of a degrading lamina at any state of a stable damage evolution process.

If only the stable damage evolution process is to be analysed it is sufficient to define those reduced stiffnesses, which influence the load redistribution process. If the structure fulfils multiple purposes or is subjected to cyclic load (see Sec. 2.4) it is furthermore important to know how the damaged structure behaves under a general load case which is different from the one which produced the damage. This analysis task requires the full 3D constitutive behaviour of the damaging lamina at any state during its degradation process.

The previous sections have outlined that a degradation procedure consists of two definitions:

- The definition, how far a degradation process progresses due to an applied load beyond IFF (see Eqs. 5.3, 5.6 or 5.7):

The application of the excessive IFF stress exposure approach disqualifies for the 3D case due to its disability to identify unstable damage evolution. The variable IFF stress exposure approach is not even experimentally confirmed for inplane cases, hence the constant IFF stress exposure approach is chosen to be the governing rule for the 3D degradation procedure.

- The definition of the impact of the degradation process on the involved measures (see Eqs. 5.4, 5.5 or 5.7):

In the 3D case there are significantly more stiffnesses available for a degradation beyond IFF – E_2 , E_3 , G_{12} , G_{13} and G_{23} . The impact of the degradation process on the respective stiffness is depending on the orientation of the IFF fracture plane θ_{fp} . Existing considerations on these dependencies [76] have turned out to be incomplete but are the basis for the described development of the approach.

For the development of a fracture angle-dependent degradation rule the relevant question is, which fracture plane orientation degrades which stiffness to which amount. The investigation is expected to be more efficient if the question is changed to:

Which are the two fracture plane orientations which have the most direct and the least impact on the load bearing capacity of a lamina against the respective types of load?

The results are regarded to be transferable to the impact of the fracture plane orientation on the degradation of the associated stiffnesses one-to-one. It has been stated earlier that tension and compression are affected unequally by the degradation hence positive and negative loads are treated separately. Regarding transverse tension (see Fig. 5.3) a fracture plane orientation of $\theta_{fp} = 0^\circ$ is expected to have the most direct impact on the load bearing capacity whereas a fracture at $\theta_{fp} = 90^\circ$ has no influence. In the case of through-thickness tension it is vice versa and in the compressive cases no impact of any fracture plane orientation on the respective load bearing capacity is determinable.

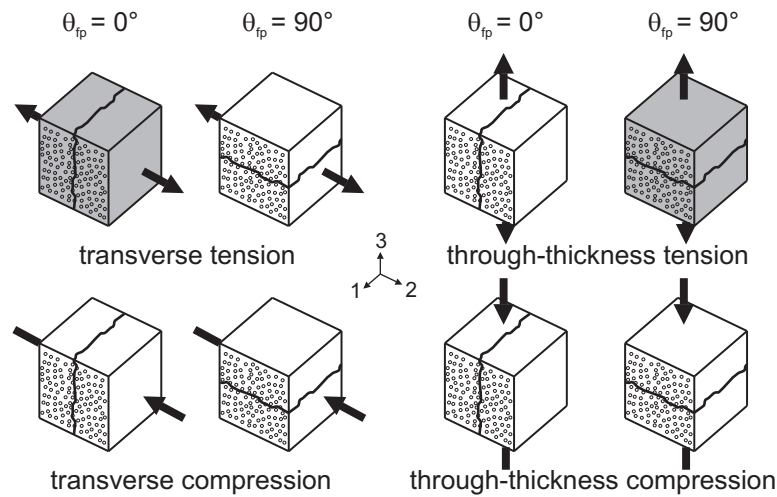


Figure 5.3: Basic fibre-perpendicular loads on a UD lamina: Fracture plane orientations having the most direct (grey) and no impact (white) on the respective load bearing capacity.

Regarding inplane shear (see Fig. 5.3) for both the positive and negative load a fracture plane orientation of $\theta_{fp} = 0^\circ$ exerts the strongest influence on the load bearing capacity whereas none is expected for $\theta_{fp} = 90^\circ$, for transverse shear it is vice versa. Among the

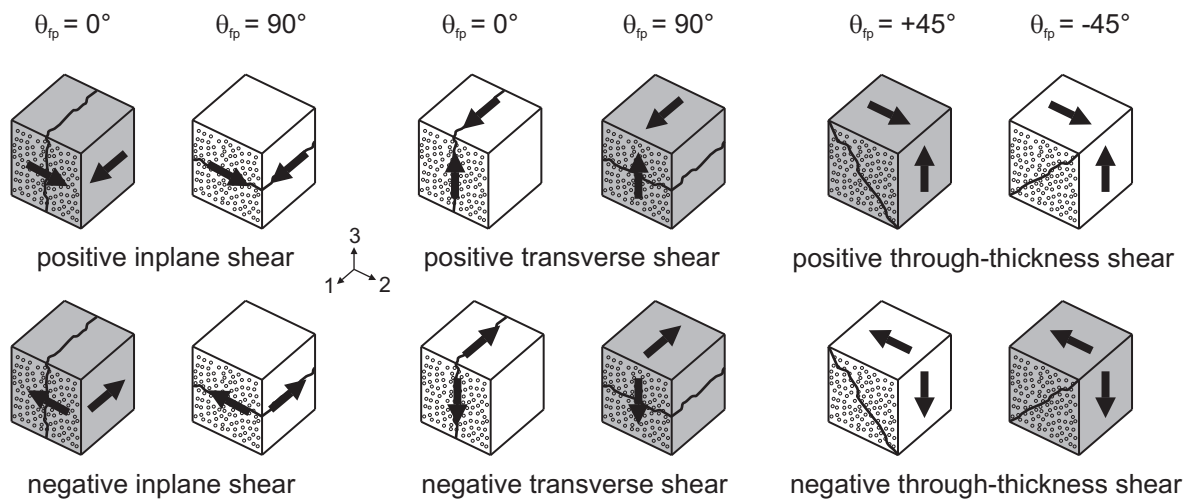


Figure 5.4: Basic shear loads on a UD lamina: Fracture plane orientations having the most direct (grey) and no impact (white) on the respective load bearing capacity.

shear load cases only the through-thickness case shows directionality and for the positive load the $\theta_{fp} = +45^\circ$ fracture plane and for the negative load the $\theta_{fp} = -45^\circ$ fracture plane is expected to have the greatest impact because the applied load creates pure tension on these action planes. The action planes $\theta_{fp} = -45^\circ$ in the case of positive and $\theta_{fp} = +45^\circ$ in the case of negative through-thickness shear transmit compression exclusively, hence

there is no impact assumed on the respective load bearing capacity.

Transferred to stiffnesses the definition of the lower extremum is eased from *no* impact to *the least* impact which results in a range for the *orientation impact degradation measure* n from 1 (the most direct impact) down to $n_{min} = [1; 0]$ (the least impact). Without further knowledge about the impact of IFFs between the identified extrema it seems reasonable to use the trigonometric function $n = F[\cos(\theta_{fp})]$ to describe the fracture orientation-dependent impact of the degradation on the respective stiffnesses. The requirement for a domain of values $n = [1; n_{min}]$, a periodicity of 180° and the abscissa adjustment by θ_{md} leads to

$$n = \left[\frac{1 - n_{min}}{2} \cdot \cos[2(\theta - \theta_{md})] \right] + \frac{1}{2} + \frac{1}{2}n_{min} \quad (5.8)$$

where θ_{md} defines the orientation where $n(\theta_{fp}) = 1$ is required, hence the orientation of the **most direct** impact. As long as no experimental results are available, a common value of n_{min} for all the stiffnesses close to 0 seems reasonable, the specific values of θ_{md} following figures 5.3 and 5.4 are summarised in table 5.1.

θ_{md}	E_2	E_3	G_{12}	G_{13}	G_{23}
n_i	0°	90°			
n_{ij}^+			0°	90°	$+45^\circ$
n_{ij}^-			0°	90°	-45°

Table 5.1: θ_{md} controlling the impact of degradation on the respective stiffnesses depending on the fracture plane orientation θ_{fp} .

The orientation impact measure $n(\theta_{fp})$ weights the reduction of the respective stiffnesses:

$$E_i^{red} = \begin{cases} E_i^{orig} \cdot (1 - n_i \cdot \text{reduction}) & \text{for tensile load in the } i\text{-direction} \\ E_i^{orig} & \text{for compressive load in the } i\text{-direction} \end{cases}$$

$$G_{ij}^{red} = \begin{cases} G_{ij}^{orig} \cdot (1 - n_{ij}^+ \cdot k \cdot \text{reduction}) & \text{for positive } ij\text{-shear load} \\ G_{ij}^{orig} \cdot (1 - n_{ij}^- \cdot k \cdot \text{reduction}) & \text{for negative } ij\text{-shear load} \end{cases} \quad (5.9)$$

Please note that existing degradation rules (see Sec. 5.3.1) and literature [4] present the normal stress σ_n transmitted over the crack edges as the relevant measure for the differentiation between the two degradation cases in equation 5.9. Recent RVE studies (see Sec. 5.6), however, suggest that this is exclusively valid and adequate for the definition of the material behaviour regarding that specific *inplane* load case which produced the IFF

and its further proportional increase. The RVE results have revealed, that the lamina's stiffness against through-thickness tensile σ_3^t is influenced by a 45° IFF even if the lamina is subjected to a larger transverse compressive σ_2^c at the same time and thus compressive σ_n is transmitted over the crack edges. Until further experimental or numerical experience has been gained, σ_n is no longer recommended to be used as the relevant parameter to distinguish between the two degradation cases. Regarding 3D load cases and aiming on a general material description of a damaging lamina valid for any load case, the relevant measure is expected to be orthotropic and the preliminary suggestion is included in equation 5.9). Regarding the influence of the degradation process on the shear stiffnesses the normal stress σ_n is no relevant parameter anyway. Without experimental experience equation 5.9 is based on the consciously simplifying and distorting assumption of tangentially frictionless crack edges which have the same effect on the shear load transmission whether they are open or closed.

Please note that for the analysis of the degradation process it is sufficient to calculate the reduced stiffnesses according to the actual load case. If the constitutive behaviour of the damaged material due to an arbitrary load is to be analysed afterwards, it is necessary to provide both sets of stiffnesses calculated for positive and negative load. The functions $n(\theta_{fp})$ are to be regarded as a rough estimation which mainly aims on a numerically sound post-failure degradation analysis. The actual influence of different IFF orientations has been studied by means of a discrete representation of cracks within Representative Volume Elements (RVE, see Sec. 3.5) in the following Section (see Sec. 5.6).

5.6 RVE-studies on a discrete cracks

The presented degradation rules including the trigonometric impact interpolation (see Eq. 5.8) are not experimentally validated and widespread analytical and numerical investigations have been started. While latest investigations at the RWTH Aachen University are approaching the problem by calibrating FEA smeared crack representations to experimental results [94] the own investigations presented below are approaching the actual mechanisms in a model representation. Virtual material tests by means of Finite Element Analysis are run on Representative Volume Elements (RVEs, see Sec. 3.5) containing discrete IFFs in varying orientations. The ongoing studies address the following questions:

- What is the homogenised constitutive behaviour of a degrading lamina depending on the fracture plane orientation?

- What is the homogenised constitutive behaviour of a degrading lamina depending on the crack density?
- What is the homogenised constitutive behaviour at a saturated crack density (residual stiffness)?
- Are the proposed ratios between E and G degradation [88, 95, 96] valid in 3D space?
- Is the resulting homogenised constitutive behaviour still met by an orthotropic material model?
- How far is the smeared crack representation acceptable in the degradation process?
- Is there an effective residual stiffness in the case of an unstable damage evolution process?

The degradation of a lamina is only conceivable if it is confined between neighbouring laminae. Virtual material test of a laminate containing a lamina with discrete cracks between two undamaged laminae with known constitutive behaviour allow to conclude on the homogenised constitutive behaviour of the damaging lamina. Within virtual material test, the influence of different types of failure can be studied separately (see Sec. 2.2). In the first studies the influence of a single inter-fibre fracture on the homogenised stiffness has been investigated without the effects of micro-delamination at interlaminar interfaces (see Sec. 2.2.3 and Fig. 2.3d, ii) or friction between closed crack edges. The investigated RVE represents a $90^\circ/0^\circ/90^\circ$ laminate made of the CFRC IM7 8551-7 (see App. C). Its middle lamina contains an IFF with orientations of $\theta_{fp} = 0^\circ, 15^\circ, 30^\circ, 45^\circ$ and 54° (see Fig. 5.5). The chosen dimensions of the cubical RVE represent a crack density of $\delta = 1/3$.

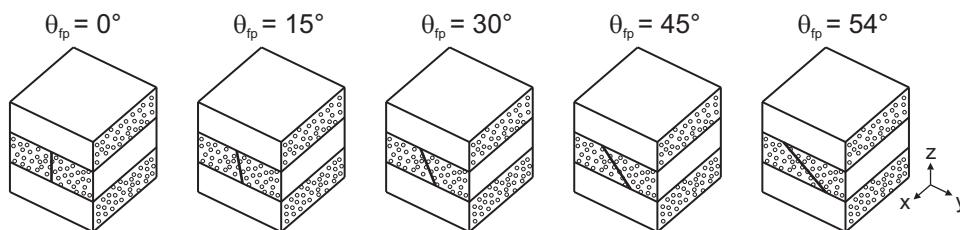


Figure 5.5: RVEs of a $90^\circ/0^\circ/90^\circ$ laminate containing the investigated fracture plane orientations.

5.6.1 Derivation of the equivalent stiffness of a damaging lamina

The homogenised constitutive behaviour of the smeared crack representation (see Sec. 5.2) of the damaging lamina is defined by the fact, that the same load applied to the laminate containing the discrete crack representation and containing the smeared crack representation results in the same global deformation of the laminate and accordingly in the same global deformation of the damaging lamina. The task is comparable to the determination of the *equivalent stiffness* of a structure (see Fig. 5.6a). Considering a structure

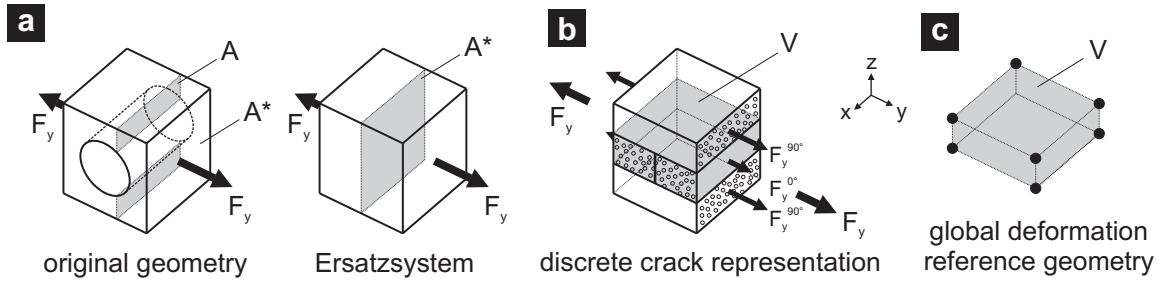


Figure 5.6: (a) Equivalent system for the derivation of the equivalent stiffness of a structure made of a single homogeneous material, (b) load distribution in a damaging laminate and (c) exterior vertices of the damaging lamina for the determination of the global strains (see Fig. 5.8).

– here an RVE – made of a single, homogeneous material, it is sufficient to relate the force F_y to the elongation Δl_y to determine the equivalent stiffness E_y^{subst} . The force F is introduced into the RVE via the front surface A^* , but has to be transferred through the entire RVE via all the x - z -sections A hence

$$F_y = \int \sigma_y dA = \text{constant} \quad \text{for every section } A. \quad (5.10)$$

In the homogenised equivalent system there is a constant σ_y^{subst} over a constant x - z -section A^* hence

$$F_y = \sigma_y^{subst} \cdot A^*. \quad (5.11)$$

From equations 5.10 and 5.11 it becomes obvious, that σ_y^{subst} equals

$$\sigma_y^{subst} = \frac{\int \sigma_y dA}{A^*} \quad (5.12)$$

and σ_y^{subst} is most efficiently determined from the stress analysis of the original geometry as the mean value of σ_y over the front surface A^* .

Considering a laminate, the applied force F_y is only partly transmitted by the damaging lamina ($F_y^{0^\circ}$) for which the equivalent stiffness is to be determined and partly by the

neighbouring laminae ($F_y^{90^\circ}$). The relation between both fractions changes for different x-z-sections in the discrete crack representation – for the section at which the IFF is located, there is certainly $F_y^{0^\circ} = 0$ while $F_y^{90^\circ} = 1/2 \cdot F_y$ (see Fig. 5.2a). The relevant $F_y^{0^\circ}$ of the damaging lamina is no longer constant (no validity of Eq. 5.10) but changes with the y-position. Accordingly the σ_y^{subst} in the smeared crack representation of the damaging lamina is no longer only a mean value over a single x-z-section but over all the x-z-sections of the damaging lamina. These considerations are transferable to all types of load and the resulting stresses (see Eq. 5.13).

$$\begin{aligned}\sigma_i^{subst} &= \frac{\int \sigma_i dV}{V} \\ \tau_{ij}^{subst} &= \frac{\int \tau_{ij} dV}{V}\end{aligned}\quad (5.13)$$

The resulting stresses are now ready to be related to the corresponding global deformation to determine a constitutive behaviour of the smeared crack representation of the damaging lamina. The global strains are derived from the relative motion of the exterior vertices of the damaging lamina and related to its overall dimensions (see Fig. 5.6c). The inclined fracture planes are destroying the symmetry planes which allow to reduce the generally anisotropic material model to an orthotropic or even transversely isotropic description of the sound lamina (see Sec. 3.1.2 and [99]^{see p. 173ff}). The generally anisotropic material model in Voigt notation is

$$\begin{bmatrix} \sigma_1 \\ \sigma_2 \\ \sigma_3 \\ \tau_{12} \\ \tau_{13} \\ \tau_{23} \end{bmatrix} = \underline{E} \cdot \begin{bmatrix} \epsilon_1 \\ \epsilon_2 \\ \epsilon_3 \\ \gamma_{12} \\ \gamma_{13} \\ \gamma_{23} \end{bmatrix} \quad \text{with } \underline{E}^{-1} = \underline{S} = \begin{bmatrix} C_{11} & C_{12} & C_{13} & C_{14} & C_{15} & C_{16} \\ C_{21} & C_{22} & C_{23} & C_{24} & C_{25} & C_{26} \\ C_{31} & C_{32} & C_{33} & C_{34} & C_{35} & C_{36} \\ C_{41} & C_{42} & C_{43} & C_{44} & C_{45} & C_{46} \\ C_{51} & C_{52} & C_{53} & C_{54} & C_{55} & C_{56} \\ C_{61} & C_{62} & C_{63} & C_{64} & C_{65} & C_{66} \end{bmatrix}. \quad (5.14)$$

Applying an individual load to the laminate makes a single virtual material test and the discrete crack RVE offers six equivalent stresses $[\sigma_1 \ \sigma_2 \ \sigma_3 \ \tau_{12} \ \tau_{13} \ \tau_{23}]$ related to six global strains $[\epsilon_1 \ \epsilon_2 \ \epsilon_3 \ \gamma_{12} \ \gamma_{13} \ \gamma_{23}]$ of the damaging lamina. Running a set of six virtual material tests with mutually independent load cases – for example pure σ_x , σ_y , σ_z , τ_{xy} , τ_{xz} and τ_{yz} one after the other – determines the 36 parameters of \underline{S} for a single fracture plane orientation at a single crack density.

Comparison between stresses in the smeared crack and the discrete crack representation

From equation 5.13 it is evident that the equivalent stresses are mean values over sound

sections of the damaging lamina and sections of discrete cracks (see Fig. 5.2). The stresses close to a discrete crack are apparently lower than those in the sound sections of the lamina and occasionally go down to zero in the actual crack section for certain load cases. Accordingly the maximum stresses in the centre of a sound lamina area where the subsequent IFF is likely to occur are higher than the equivalent stresses calculated for the smeared crack representation. The discrepancy between both states of stress grows with the number of crack sections included in the mean values, hence with a growing crack density or with the progress of damage evolution in general. The problem can be tackled by reducing the maximum bearable stress exposure $f_{E\ IFF}$ in the smeared crack representation to predict subsequent IFFs in the higher stressed sound areas of the actual discrete crack representation (see Sec. 5.4).

5.6.2 Results of the RVE virtual material tests

Up to now it has not been possible to derive the general anisotropic material behaviour of a damaging lamina depending on the fracture plane orientation and the crack density, but first results have revealed the relations presented below.

Coupling between shear and normal deformation

The results confirm the perception that the homogenised material behaviour of a damaging lamina should no longer be orthotropic. Starting from an orthotropic behaviour at $\theta_{fp} = 0^\circ$, with rising angles the compliance matrix \underline{S} shows an increasing unbalance and growing values at the coupling positions of the matrix which are 0 for orthotropic behaviour (see Sec. 3.1.1). The results confirm the impression that inclined fracture planes result in a behaviour where shear deformations produce normal *and* shear stresses or vice versa. Figure 5.7a exemplary shows a through-thickness tension load case (σ_z^t) leading to significant γ_{23} in the damaging lamina and hence γ_{yz} in the complete laminate.

Sensitivity against the algebraic sign of load

It has been stated that a compliance matrix is determined by the set of six mutually independent virtual material tests, namely pure σ_x , σ_y , σ_z , τ_{xy} , τ_{xz} and τ_{yz} one after the other. It has been found that different combinations of positive and negative loads within a single set result in different compliance matrices, hence there have been run four combinations at each fracture plane orientation; tensile loads or compressive loads each with positive and negative shear loads.

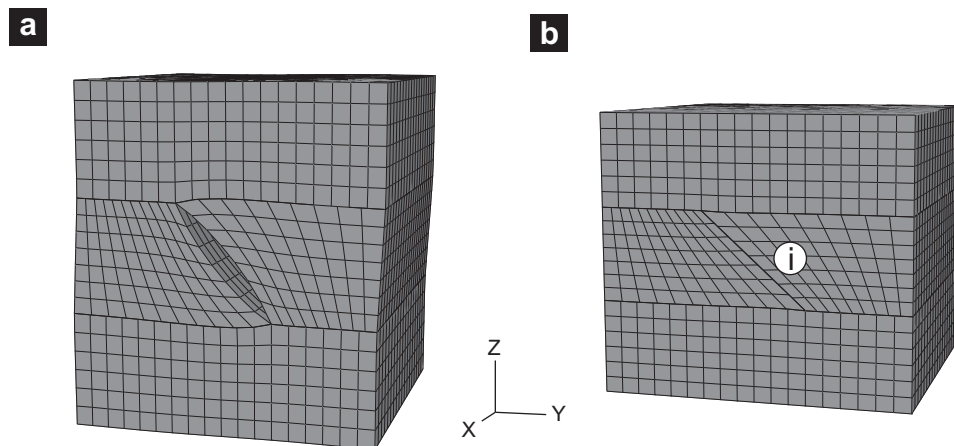


Figure 5.7: FEA results: Pure through-thickness tension σ_z^t on an $\theta_{fp} = 45^\circ$ RVE leads to a γ_{23} deformation component (a), the stiffness against pure through-thickness compression σ_z^c is weakened by the crack due to the relative tangential motion of the crack edges (b).

The difference of the resulting compliance matrices \underline{S} proves the sensitivity of the material behaviour against the algebraic sign of load in general (see Sec. 5.3.1). The considerations of section 5.5 regarding the different behaviour against positive or negative through-thickness shear can be studied visually by means of the respective RVE results (see Fig. 5.8). Particularly the results containing closed crack edges are promising regarding future investigations including friction.

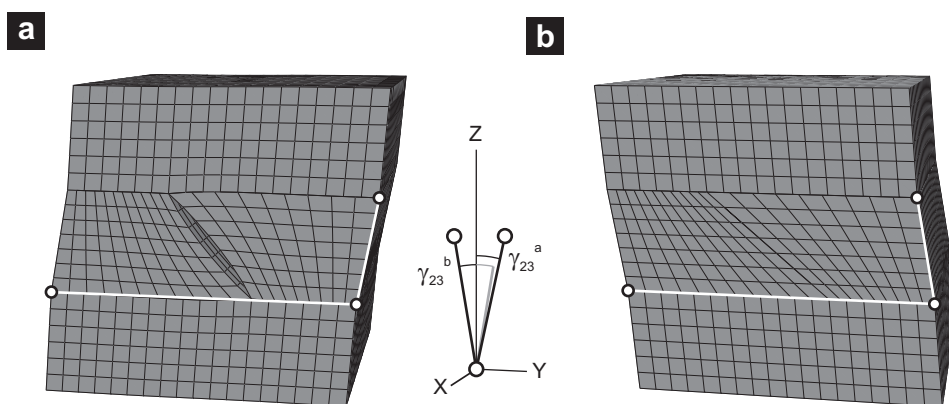


Figure 5.8: FEA results: Positive through-thickness shear τ_{yz}^p on an $\theta_{fp} = 45^\circ$ RVE (a) leads to a larger absolute value of global γ_{23} (see Fig. 5.6c) than negative τ_{yz}^n (b).

Results concerning the orthotropic material model

Neglecting the coupling positions of the resulting compliance matrices \underline{S} which have to be 0 in an orthotropic compliance matrix (see Sec. 3.1.1) and averaging the unbalanced positions, the results of the discrete crack RVE are transferable to the impact of degradation on the common material parameters of an orthotropic material model E_2 , E_3 , G_{12} , G_{13} and G_{23} (see Sec. 5.5). By means of these parameters related to the fracture plane orientation (see Fig. 5.9) the analytical thoughts summarised in section 5.5 are reviewed in the following.

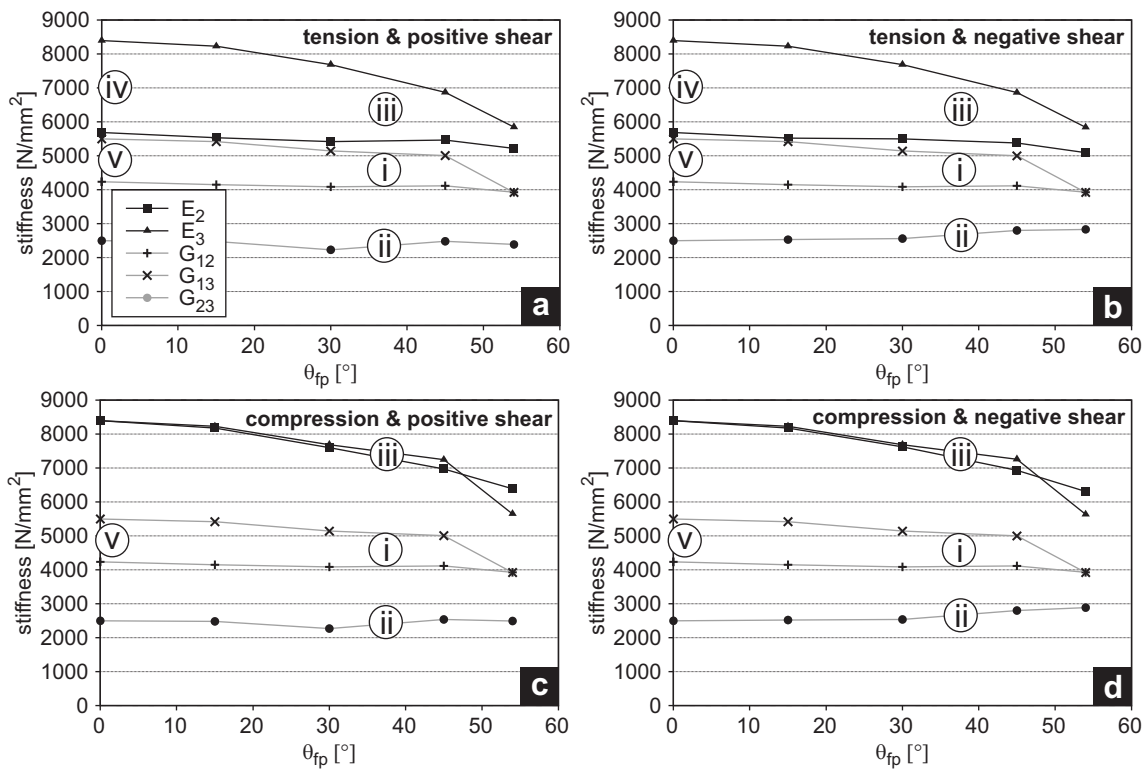


Figure 5.9: Orthotropic stiffnesses derived from the compliance matrices of different virtual material test sets: (a) tensile loads and positive shear loads, (b) tensile loads and negative shear loads, (c) compressive loads and positive shear loads and (d) compressive loads and negative shear loads.

Looking at the reduced stiffnesses resulting from the four load sets (see Fig. 5.9a-d), the orientation-dependent behaviour of G_{12} and G_{13} is equal in all the four cases (i). Hence their insensitivity against the algebraic sign of the shear load assumed in section 5.5 is confirmed by the RVE results. G_{23} behaves equally in both combinations comprising positive shear (a and c) and in both combinations comprising negative shear (b and d) hence it does behave sensitive against the algebraic sign of through-thickness shear load

(see Fig. 5.9, ii). The same is the case for E_2 and E_3 which behave in the tensile (a and b) load sets different from the compressive (c and d) ones (see Fig. 5.9, iii). The results furthermore confirm that 0° IFFs have a large impact on E_2^t whereas E_3^t is basically unaffected (iv). Accordingly these IFFs have the expected impact on G_{12} whereas G_{13} is unaffected (v).

Figure 5.10 compares the orientation-dependent slope of the RVE results with the stiffnesses resulting from equation 5.9. The degradation measure η has been adjusted to the $E_2^t(0^\circ)$ so that the crack density of the RVE $\delta = 1/3$ corresponds to a degradation progress measure of $\eta = 0.678$. The shear impact degradation measure k has subsequently been adjusted to meet the $G_{12}(0^\circ)$ resulting in $k = 0,755$. This value is close to 0.77 proposed for CFRC in section 5.3.1.

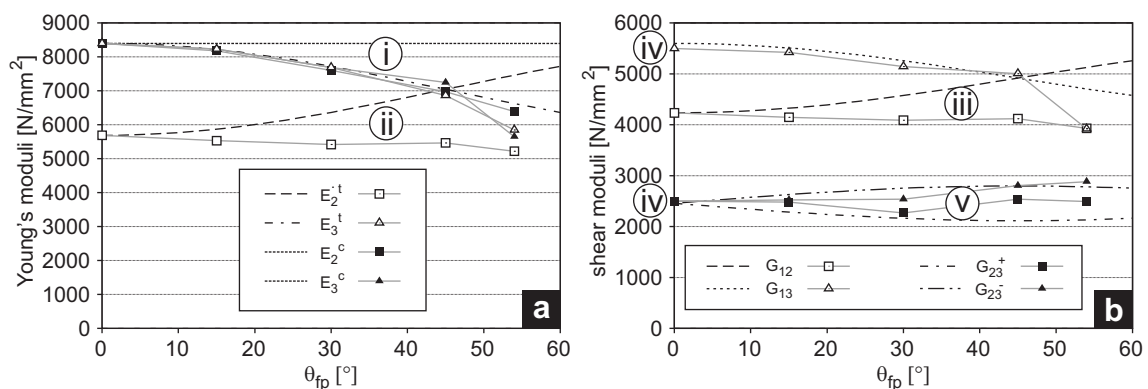


Figure 5.10: Comparison between the orthotropically reduced results of the RVE and the prediction of the 3D degradation procedure (see Sec. 5.5): (a) Young's Moduli and (b) shear moduli.

The most obvious difference between the degradation rule and the RVE results is the orientation-dependent behaviour of the compressive Young's moduli (see Fig. 5.10a, i). While E_2^c and E_3^c are unaffected by 0° IFFs, the assumption that the compressive Young's moduli E_2^c and E_3^c are generally unaffected by IFFs can be identified as strongly simplifying by means of the RVE results at higher θ values. The reason is that the closed crack edges do transmit the compressive σ_n furthermore, but the tangential load component arising with a growing θ_{fp} leads to a tangential motion of the crack edges (see Fig. 5.7b, i). This goes along with the reduction of the effective transverse compressive stiffness E_2^c and the through-thickness compressive stiffness E_3^c . The amount of this tangential motion depends on the pressure on the crack edges and the friction between them. The presented RVE results are based on a frictionless behaviour, accordingly the effect of IFFs in the compressive stiffnesses is strongly overestimated here and as far as no experimental results are available, it is furthermore suggested to keep E_2^c and E_3^c constant

during a degradation analysis.

In the case of E_3^t and G_{13} the RVE results and the degradation rule prediction correspond well. The orientation dependence of E_2^t is however strongly overestimated by the prediction in the examined range of $\theta_{fp} = [0^\circ; 54^\circ]$ (see Fig. 5.10a, ii). A virtual material test with an RVE containing a 90° crack proves that the slope of $E_2^t(\theta_{fp})$ rises to its undamaged value there but the complete slope of the curve is currently unknown. In contrast to through-thickness loads, inplane loads are not partly transmitted by sound areas (whose size depends on the fracture orientation) but the whole load has to be transmitted over the crack by the neighbouring laminae no matter what the fracture plane orientation is (see Fig. 5.2a). Being $\theta_{fp} = 90^\circ$ the only exception from this, such a slope is not sufficiently predictable by equation 5.8 and further inquiries are necessary. The same is the case for the slope of the stiffness against the second inplane load G_{12} (see Fig. 5.10b, iii). Currently it cannot be decided whether it is more accurate to run a post-failure analysis with a θ_{fp} -independent E_2^t and G_{12} which neglects the exceptional position of 90° cracks or to use equation 5.8.

Looking at the shear moduli at $\theta_{fp} = 0^\circ$, the common k value which is adjusted to $G_{12}^t(0^\circ)$ results in good predictions for $G_{23}(0^\circ)$ and G_{13} in general (see Fig. 5.10b, iv). This suggests to keep the proposed ratios between the degradation of Young's and shear moduli (see Sec. 5.3.1) unchanged for the 3D post failure degradation analysis. Although the slopes of G_{23} generally differ between RVE and prediction (v), the different character of G_{23}^+ and G_{23}^- is met by equation 5.9 and it can reasonably be used until further experimental results become available.

Regarding the fibre-parallel 1-direction the RVE results prove that E_1 , ν_{12} and ν_{13} are unaffected by any IFF orientation but ν_{23} changes with different θ_{fp} and even leaves the common range $[0; 0.5]$ for homogeneous materials. This is judged to be reasonable due to the fact that here a continuum-based material model is used to describe the general behaviour of a non-continuous structure. Without reasonable analytical thoughts (see Sec. 5.5) however, there is currently no description of $\nu_{23}(\theta_{fp})$ suggested.

In summary the comparison between RVE virtual material test results and the 3D degradation rule (see Sec. 5.5) document the general applicability of the presented rules. In that context it is important to have in mind that the RVE itself contains significant simplifications like the lack of friction between the crack edges. Furthermore the influence of the constitutive behaviour of the two neighbouring laminae is completely unknown at this time just as the influence of micro-delamination (see Sec. 2.2.3 and Fig. 2.3d, ii). Generally the reduction of the compliance matrices to an orthotropic material model is as arguable as the representation of the constitutive behaviour of a damaging lamina by

such a continuum-based model itself. Accordingly the presented comparison is not recommended as the basis of any parameter fitting.

Studies on residual stiffnesses

After having reached the saturated crack density, a confined lamina is still transmitting load (see Sec. 2.3). This fact is included in the smeared crack representation by residual stiffnesses which are constantly assigned to the damaged lamina after the degradation process has reached the saturated level (see Sec. 5.3.2). Numerous experiments suggest that the assumption of the saturated crack density at $\delta = 1$ is a reasonable guess for a majority of UD fibre reinforced $0^\circ/90^\circ$ laminates under inplane tensile load independent from their lamina thickness [100–102]. Although newer investigations revealed a significant dependence on load types and laminate stacking sequences [30, 103], the presented discrete crack RVE has geometrically been adjusted to represent a $\delta = 1$ crack density of 0° IFFs. Using the materials given in the WWFE-II (see Ch. 7) the results of the virtual material tests with an applied tensile σ_y^t provide first information about the significance of the numerical approach for the determination of residual stiffnesses (see Tab. 5.2).

Material	IM7	T300	A-S	S2-glass	E-glass
	8851-7	PR-319	Epoxy1	Epoxy2	MY750
	CFRC			GFRC	
$\eta_R^{E_2^t}$	0.31	0.31	0.29	0.26	0.22
$\eta_R^{G_{12}^t}$	0.67	0.77	0.69	0.83	0.83

Table 5.2: Results of a 0° RVE representing the crack density $\delta = 1$: Residual stiffness fraction η_R .

It has been found, that in the present RVE geometry the maximum stresses in the damaged lamina is below the IFF fracture criterion, thus the analysed crack density $\delta = 1$ represents a state of damage beyond the saturated crack density which will never be reached in reality. Hence the resulting residual stiffness fraction values (see Tab. 5.2) are generally suspected to be underestimated.

Keeping in mind that neither this RVE analysis includes micro-defects or micro-delamination (see Sec. 2.2.3) nor it is known how close the actual saturated crack density is to the assumed value $\delta = 1$, it is less surprising that the values above do not correlate well with those determined experimentally (see Sec. 5.3.1 and [88]). The results do confirm the finding, that the residual shear modulus fraction is higher than the residual

Young's Modulus fraction. The numerical $\eta_R^{E_2^t}$ however is ten times larger than the experimental value 0.03 from [88] which itself is the lowest value compared with numerous other sources [100–103]. Looking at CFRC the $\eta_R^{G_{12}}$ values correspond well with the experimentally determined value of 0.6 but the lower experimental value for GFRC is not numerically confirmed. Using the same RVE geometry only differing by the material's constitutive behaviour does not explain the experimentally determined difference between CFRC and GFRC residual stiffnesses. As a result these two groups of materials are either expected to differ due to a different evolution of those damage types which are not included in the RVE or due to different saturated crack densities. Furthermore the influence of the constitutive behaviour of the neighbouring laminae is currently unknown and a subject of further investigations.

5.7 Application-oriented summary

The current post-failure degradation implementation developed in this work (see Ch. 6) includes the constant IFF stress exposure approach $f_{E\ IFF} = 1 = \text{constant}$ (see Sec. 5.3.2) to govern the degradation progress represented by the degradation progress measure η . The degradation's impact on the different orthotropic stiffnesses of the damaging lamina depends on the orientation of the IFF fracture plane and is implemented by the developed 3D degradation procedure (see Sec. 5.5). The reduced stiffnesses of the damaging lamina result from the orientation impact measure n applied to the respective original stiffnesses (see Eq. 5.9) whereas $n(\theta_{fp})$ (see Eq. 5.8 and Tab. 5.1) preliminary follows the results of basic considerations (see Figs. 5.3 and 5.4). Their comparison with virtual material tests (see Sec. 5.6) revealed an acceptable level of agreement which qualifies the developed 3D degradation routine for a general application for the time being. The residual stiffness fraction values are currently taken from [88].

The implemented approach reliably results in an orthotropic lamina behaviour not only valid for the load which led to the respective state of damage but for an arbitrary load case with arbitrary combinations of positive and negative stress components. The approach gives reasonable results for both stable and unstable degradation processes (see Sec. 5.1) and identifies fibre-perpendicular compressive load cases leading to the hazardous wedge effect or an unpredictable crushing by a degradation locking (see Sec. 5.3.2).

6 Implementation of Puck's Theory in ABAQUS

The implementation of Puck's fracture criteria and post-failure degradation rules completes the prediction capabilities of commercial FE packages regarding UD FRCs. The available codes provide a large variety of element definitions for the representation of laminates and laminate structures (see Sec. 3.3). The inter-laminar behaviour between the respective laminae (delamination, see Sec. 2.2.4) is satisfactorily representable by the provided interface elements which predict the separation onset and evolution. With the implementation of Puck's Theory and its enhancements an FE analysis covers all macroscopic and mesoscopic aspects of damage and damage evolution in UD FRCs (see Sec. 2.1). Puck's Theory meets FEA on the level of the material description. Whereas the pure failure analysis (see Ch. 4) may be accomplished in form of a post-processing of the stress results, the presented failure and post-failure analysis (see Ch. 5) requires the presented implementation within a subroutine for user-defined material behaviour *UMAT* [8].

6.1 Implicit and explicit FEA

The difference between an implicit or explicit FEA does not play a central role regarding the FE-representation of laminates and laminate structures (see Sec. 3.3) whereas it comes into play when a user-defined material is to be implemented. Puck's Theory has been developed and verified for nonrecurring, uninterrupted, slow loading processes with applied combinations of proportionally increasing stress or strain components [4]. Accordingly Puck's Theory predicts material behaviour in the *quasi-static* domain where time and thus velocity or inertia do neither play a role nor are considered in the respective material models and the related analyses (in contrast to the *dynamic* domain). In the context of nonlinear FEA the mentioned situation is generally related to an *implicit* solution of the equation systems. Accordingly the following section describes the generation of a material user subroutine in the case of an implicit FEA in detail. However Puck's Theory is expected to be transferable to dynamic situations in which generally an *explicit* solution approach is recommended. The difference between the *implicit* and *explicit* solution strategy for differential equations is fundamental not only in terms of mathematical approaches [104] but the appropriate choice is up to the user and significantly influences the accuracy and the computational costs of an FEA. Note that explicit and implicit approaches are not exclusively attributed to dynamic or quasi-static situations respectively.

Thus the integration steps are commonly referred to as *time increments* whereas its meaning is tacitly reduced to *load increments* in the case of quasi-static analyses.

Both processes involve a numerical time integration scheme to solve for the unknown displacement solution at the end of the respective time step. This solution is the basis for the calculation of the resulting strains and stresses. Explicit integration schemes (e.g. the Central Difference method [105]) assume a linear change in displacement over each time step. They calculate the displacements at the end of the time step based on the state variables – which include the material description in the case of damage analysis – at the beginning of the time step. The updated state variables are then the basis for the calculation of the subsequent time step. The procedure corresponds to a linear extrapolation based on the material's tangent moduli (see Fig. 3.1) and – in dynamic situations – the velocity and acceleration at the beginning of the time step.

Implicit integration schemes (e.g. the Newmark Forward Differencing method [106]) assume a constant average load increase and – in dynamic situations – constant acceleration over each time step. The governing equation is evaluated *at the end of the time step* based on the actual state variables. The major difference between implicit and explicit algorithms is that the implicit solution method requires a matrix inversion of the structural stiffness matrix, the explicit solution does not. However, unlike the implicit solution scheme, which is unconditionally stable for large time steps, the explicit scheme is only stable if the size of the time step is smaller than the critical time step size for the structure being simulated. The undamped critical time step size is $2/\omega_{max}$ (where ω_{max} is the largest natural circular frequency), which is usually a very small value. This very small time step size requirement for stability thereby makes explicit solutions recommendable for short transient situations. But, even though the number of time steps in an explicit solution may be orders of magnitude greater than that of an implicit solution, it may be more efficient than an implicit solution since no matrix inversion is required. Neither an implicit nor explicit solution is the clear winner in all cases.

Regarding the implementation of a degrading material behaviour the difference between the explicit and implicit approach lies in the requirements for the material user subroutine. Whereas the explicit approach eventually relies on the definition of the material's constitutive behaviour in terms of tangent moduli, there is no corresponding requirement in the case of an the implicit approach. ABAQUS finds an acceptable implicit solution by guessing a displacement field for the end of the respective time step (called *attempt* within ABAQUS). Based on the actual constitutive behaviour associated with that guess the solver evaluates whether the equilibrium equations are fulfilled within specified tolerances or not. If this is not the case the guess will be corrected. Both, the original guess

and the corrections are based on the material's *Jacobian Matrix* calculated at the end of the past time increment or attempt. This matrix defines the change of the resulting stress component increments depending on a change of each individual strain component increments $\partial\Delta\bar{\sigma}/\partial\Delta\bar{\epsilon}$. It effectively includes information corresponding to the tangent stiffnesses which means that in both cases their definition is inevitable. In the case of an explicit approach the quality of the tangent stiffnesses definition directly determines the accuracy of the results whereas in the implicit case it only influences the quality of the guesses, i.e. it influences the process of solution convergence but not the solution itself.

6.2 User-defined material behaviour subroutine

The presented User-defined material behaviour subroutine (UMAT) is written for implicit FEAs (see Sec. 6.1) and includes all the presented parts of Puck's Theory for the fibre fracture and inter-fibre fracture prediction (see Ch. 4), of the 3D degradation rule (see Ch. 5) and the nonlinear material behaviour (see Ch. 3) unless otherwise stated in the respective sections.

The task of the UMAT is to provide

- the particular state of stress for an input state of strain.
- the relevant parameters and state variables of Puck's failure theory.
- the Jacobian matrix $\partial\Delta\sigma/\partial\Delta\epsilon$ for all stress/strain components.

The subroutine is provided with the strain at the beginning of the load increment $\bar{\epsilon}^{begin\ incr.}$, the guessed strain increment for the current load increment $\Delta\bar{\epsilon}^{incr.}$ and the degradation progress $\eta^{begin\ incr.}$ by the main program and follows a straight forward structure to determine the associated stresses and failure or degradation parameters (see Fig. 6.1). If the respective load increment is part of the failure analysis period $\eta = 1$ (see Fig. 2.5), the stiffnesses are derived from given nonlinear stress strain relations (see Sec. 3.1.2). If the respective increment is part of the post-failure period $\eta < 1$, the reduced stiffnesses are derived from the stiffness reduction process according to equation 5.9. The resulting stresses are calculated based on the orthotropic material law (see Eq. 3.3). From these stresses, the fibre fracture stress exposure $f_{E\ FF}$ is derived (see Eq. 4.48) and a FF-flag is switched on if appropriate. Then the IFF stress exposure $f_{E\ IFF}$ (see Eq. 4.24) is addressed by the calculation of numerous $f_{E\ IFF}(\theta)$, currently for 180 different values of θ (see Eqs. 4.21 and 4.22). The calculated $f_{E\ FF}$ is then used to determine the

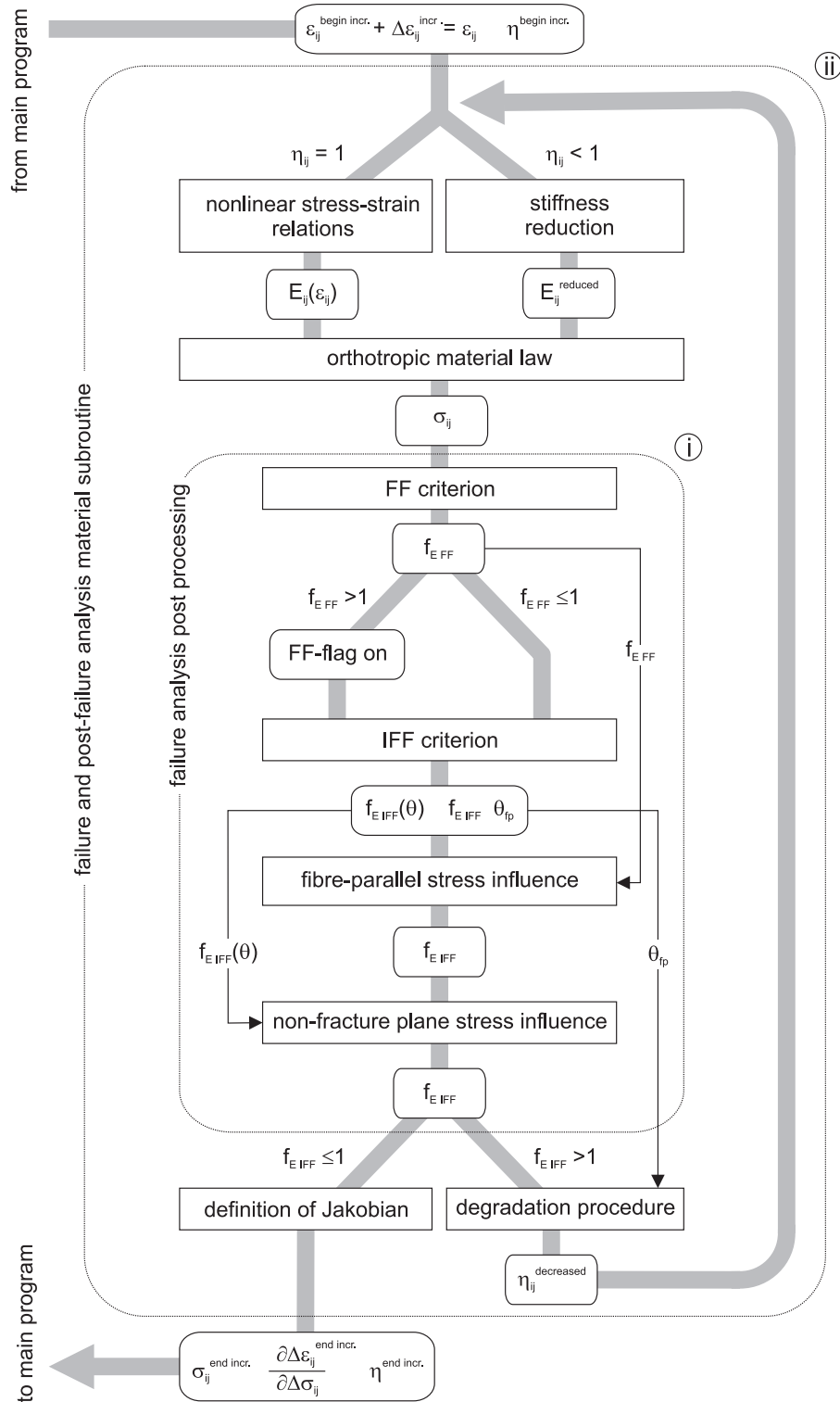


Figure 6.1: Structure of the material subroutine for failure and post-failure degradation analysis including the sequence of main procedures (boxed) and the propagation of resulting measures (encircled).

weakening effect η_{w1} due to the fibre-parallel stress (see Sec. 4.3.1). The calculated stress exposures of all action planes $f_{E\ IFF}(\theta)$ are used to determine the weakening effect η_{m+p} due to non-fracture plane stresses (see Sec. 4.3.2). The result is in both cases an increased $f_{E\ IFF}$. If its value is ≤ 1 at the end, the task of the subroutine is completed and the Jacobian matrix is determined by a difference quotient approach. In the case of $f_{E\ IFF} > 0$ the degradation progress measure η is decreased by a predefined increment or ratio and the orientation impact degradation measures n_{ij} are calculated from θ_{fp} (see Eq. 5.8). The overall impact of the degradation on the respective stiffnesses is represented by stiffness-specific η_{ij} values and the degradation loop is started. The degradation measure η which fulfils the $f_{E\ IFF} = 1$ requirement is determined iteratively.

Figure 6.1 reveals that the failure analysis part of the subroutine (i) may be separated to act as a pure post-processing for conventionally derived FEA stress results or even for existing stress fields. Hence the application of Puck's failure criteria requires a relatively small adaption of common analysis procedures without the need for further theoretical studies of FE solution approaches, material definition requirements and the associated syntax of the respective software. The computational cost for the determination of the stress exposure values is definitely small compared to the knowledge gain regarding the analysed laminate or laminate structure. On the other hand, the implementation of Puck's Theory including degradation (see Fig. 6.1, ii) is a procedure which resides deeper inside the FEA. Numerical matters like load increment size, determination algorithm for the Jacobian, the degradation progress increments and numerical damping parameters have to be adjusted carefully to ensure accurate results and acceptable computational effort [107].

The presented subroutine contains two iterative parameter-determinations which is generally inefficient and complicates the application of Puck's Theory within an explicit FEA context. There the small time increments require the material subroutine to run extremely often and iterative procedures are serious disadvantages. Accordingly there are current attempts to express the $f_{E\ IFF}(\theta_{fp})$ in a closed analytical form as already possible in the case of inplane load [4]. The same is aimed for the determination of the degradation progress measure η and – in the ultimate consequence – also for the Jacobian matrix [108].

7 World Wide Failure Exercise II

After the World Wide Failure Exercise which addressed inplane failure and post failure prediction of UD FRPCs [2], a second World-Wide Failure Exercise (WWFE-II) was launched by Kaddour and Hinton [69], to assess the capability and maturity of current 3D failure criteria. In the exercise, the originators of composite failure theories were invited to take part by agreeing to provide two papers (Part A and Part B) describing their model and its correlation with test data. The organisers provided a set of 12 test cases (see App. B.3) to challenge the current failure criteria, a set of material parameters (see App. B.2) and a set of guidelines (see App. B.1). The author, after a personal consultation with Puck, has accepted to participate as the exercise was seen to provide an opportunity to illustrate the usefulness of Puck's Theory and to validate its applicability to problems involving 3D stresses [109]. The results presented below (see Sec. 7.2) are blind predictions based on the provided information. The generation of these results involves the preparation of Puck's failure (see Ch. 4) and post failure approaches for an unrestricted three-dimensional use (see Ch. 5), the implementation into a powerful FE stress analysis environment (see Ch. 6) and the identification and solution of particular problems arising from the individual load cases. This includes the considerations about 3D degradation presented below before the actual test case results are discussed in section 7.2.

7.1 Degradation aspects of the WWFE-II

In order to ensure the unlimited 3D applicability of the developed approaches and analysis tools, the whole work aims on general three-dimensional load cases, particular in terms of post-failure degradation (see Ch. 5). However load redistribution from weaker to stronger laminae is excluded in cases where any load has to be transmitted in through-thickness direction of the laminate (σ_z , τ_{xz} and τ_{yz} namely) or where all the laminae are experiencing equal stress exposures. In these cases a lamina can not dispose of any load reducing its stiffness. From the numerical point of view the smallest further increase of the applied load leads to an immediate increase of the crack density up to infinity. This process is called *unstable degradation* (see Sec. 5.1). Neglecting damping or statistical effects, in these cases the curves of initial and final failure stress coincide.

After reaching the final failure stress there are laminate and load configurations which

allow a further deformation of the material at constant or declining applied loads before it completely disintegrates. As Puck's Theory is stress based on the one hand and the definition of a *complete disintegration* is arguable on the other hand, there is no final failure *strain* information provided in these cases.

A special case occurs for damage due to compressive σ_2 and/or σ_3 in a lamina because the resulting cracks are still capable of transmitting compressive forces in the respective directions. In these cases the lamina does transmit increasing applied stresses after exceeding the IFF fracture criterion up to a point where the laminate starts breaking due to the wedge effect or starts crushing due to through-thickness compression (see Sec. 5.3.2). Both effects are ruled by mechanisms on a microscopic level far below the capabilities of a smeared crack representation and a continuum-based constitutive model. The ongoing effort of covering such damage evolutions by granular media-based simulations [110] has not reached a level of applicability to classify the processes as a predictable – hence tolerable – damage evolution. As long as this is not the case the limits of application are considered to be reached when the stress exposure in one or more laminae reaches $f_E = 1$.

Regarding the WWFE-II none of the test cases meets the above mentioned requirements for a reliably stable post-failure degradation. Where the test cases ask for failure stresses (see test cases 8, 10 and 11, Secs. 7.2.3 and 7.2.3) the initial and final failure curve following the above definition coincide. Only a few load cases of test case 8 are considered to reach a final fibre failure after an initial inter-fibre failure. In test case 9 (see Sec. 7.2.3) all laminae are experiencing an equal stress exposure and in test case 12 (see Sec. 7.2.3) the applied pressure σ_z leads to damage resulting from compressive σ_3 in the lamina.

7.2 Results of the WWFE-II test cases

The developed user-defined material subroutine (see Ch. 6) is employed to predict the response of 12 test cases provided by the organisers of the WWFE-II. These test cases cover pure, isotropic polymer material (see Sec. 7.2.1), unidirectional laminae (see Sec. 7.2.2) and multidirectional laminates (see Sec. 7.2.3) made from glass/epoxy and carbon/epoxy. The cases include full three-dimensional loadings including superposed shear. The details of material properties, lay-ups and loadings as well as guidelines are described in [69] and appendix B. The following presentation of the results is not only intended to prove the applicability and versatility of Puck's Theory and its implementation but it provides useful examples for the understanding of the complex lamina and laminate behaviour and the functionality of Puck's Theory in particular. For this purpose every test case setup is

visualised within the presented fracture curve and demonstrative aspects of the results are interpreted.

The following results of the test cases have been obtained by applying the given stress ratios in the sense of nominal values (see Sec. 3.6.1). This means that the applied forces leading to the stresses are related to the undeformed geometry and are kept constant in value and direction during the deformation while the area of application and/or the direction of the material's orthotropic axis will change. This results in differences between the applied nominal stress value and the true state of stress in the deformed material (see Sec. 3.6). Note that this is an assumption, not a requirement arising from the application of FEA. Using FEA, the user is free to choose whether the load direction follows the material rotation or not, whether the applied stresses are meant to be related to the undeformed or deformed geometry or else, to neglect all those effects and run a geometrically linear analysis.

Regarding the presented fracture angles θ_{fp} it is important to note that in all the load cases the loads are applied symmetrically against the orthotropic axis of the failing lamina. In these cases the action planes at θ and $180^\circ - \theta$ analytically experience the same stress exposures $f_{E\ IFF}$. Which of the two orientations is reported as θ_{fp} depends on numerical inaccuracies.

The analyses have been run using the following of the given material parameters [69]: The orthotropic constitutive behaviour of every single UD lamina is characterised by its homogenised Young's moduli E_1, E_2 and E_3 , its shear moduli G_{12}, G_{13} and G_{23} and the three Poisson's ratios ν_{12}, ν_{13} and ν_{23} . The transverse and through-thickness moduli E_2 and E_3 (in the compressive domain) and the inplane and transverse shear moduli G_{12} and G_{13} are derived as secant moduli from the given nonlinear stress-strain-curves. Thermal expansion is considered orthotropically by α_1, α_2 and α_3 . The necessary input for the actual failure analysis is limited to few UD lamina strengths – the longitudinal tensile and compressive strengths R_{\parallel}^t and R_{\parallel}^c , the transverse tensile and compressive strength R_{\perp}^t and R_{\perp}^c (if different from through-thickness direction then $R_{\perp 2}^t, R_{\perp 2}^c, R_{\perp 3}^t, R_{\perp 3}^c$) and the inplane shear strength $R_{\perp \parallel}$. Applying the advanced FF criterion (see Sec. 4.7) the fibres' longitudinal Young's modulus $E_{\perp f}$ and Poisson's ratio $\nu_{\perp \parallel f}$ are needed additionally. The rest of the parameters follow the default values [4, 88] and therefore are not considered as input parameters.

7.2.1 Homogeneous isotropic matrix test case

Test case 1

In test case 1 isotropic matrix material is subjected to varying combinations of $\sigma_y = \sigma_z$ and σ_x . For this particular test case, an isotropic adaption of Puck's IFF criterion has been developed (see Sec. 4.6.1). Additionally the given material has been identified as not behaving intrinsically brittle which requires an elaborated parameter identification procedure (see Sec. 4.6.2). In figure 7.1 there's only one angle θ_{fp} denoted defining the orientation of the fracture plane while the second one φ_{fp} is arbitrary. The prediction of the second angle in space is impossible since the applied stressing is rotationally symmetric around the x -axis and thus all sections rotated around that axis experience the same stress exposure. In the case of $\sigma_x = \sigma_y = \sigma_z$ (see Fig. 7.1, ii) both angles θ_{fp} and φ_{fp} are arbitrary.

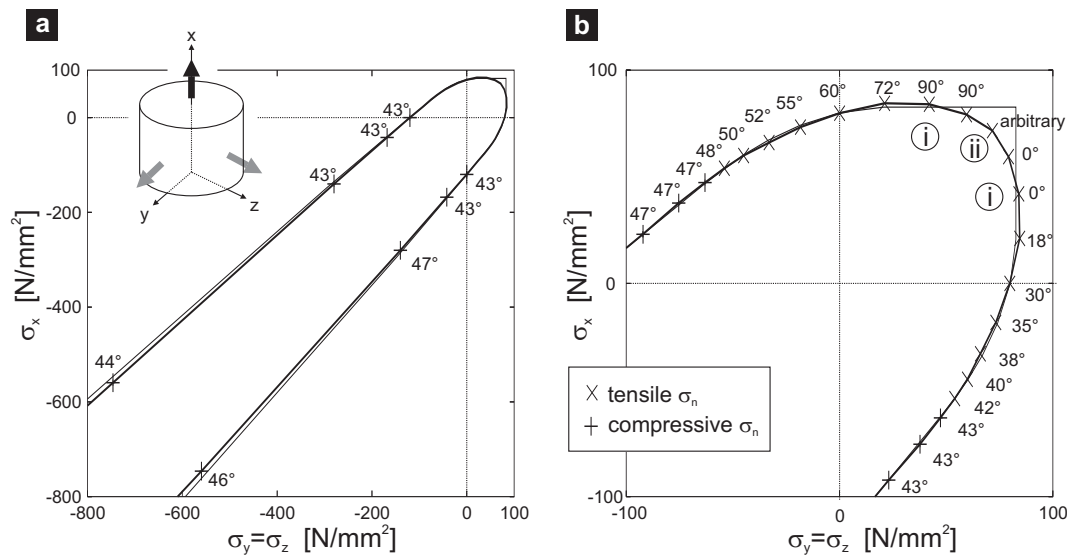


Figure 7.1: Results of test case 1 (a) and close-up (b) indicating the orientation of the fracture plane θ_{fp} and the normal stress on the fracture plane σ_n , results before (thin) and after η_{m+p} -correction (bold lines).

Looking at the results without η_{m+p} -correction (thin lines) note that the tensile cut-off in the first quadrant takes place at slightly higher stresses $82.67 \text{ MPa} = R^{At}$ than the given tensile strength $R^t = 80 \text{ MPa}$ (see Fig. 7.1b, i). Apparently there do exist tensile fractures which occur in the section of maximum tensile stress $\sigma_n^t = R^{At}$ although we have stated that we are dealing with a not intrinsically brittle material here. The reason for this is the proximity of these stressings to the hydrostatic situation towards which the shear stresses $\tau_{n\psi}$ on arbitrary sections tend to zero.

Including the η_{m+p} -correction (see Sec. 4.3.2), the analysis has to be based on the corrected values R_{cor}^t , R_{cor}^c and p_{cor} . As the fracture due to applied pure compression is independent from R_{cor}^t and – in the present case – not very sensitive against the variation of p , this case is used to calibrate the R_{cor}^c -value first. Then the values for R_{cor}^t and p_{cor} are calibrated according to the method described above (see Fig. 4.15). The corrected values are $R_{\text{cor}}^t = 95.5$ MPa, $R_{\text{cor}}^c = 123.71$ MPa and $p_{\text{cor}} = 0.073$. The resulting fracture curve does no longer exhibit the completely unphysical sharp edge in the first quadrant (see Fig. 4.10 and Sec. 4.3.2). Note that the η_{m+p} -correction may lead to slightly higher failure stresses in some cases.

7.2.2 Lamina test cases

Test case 2

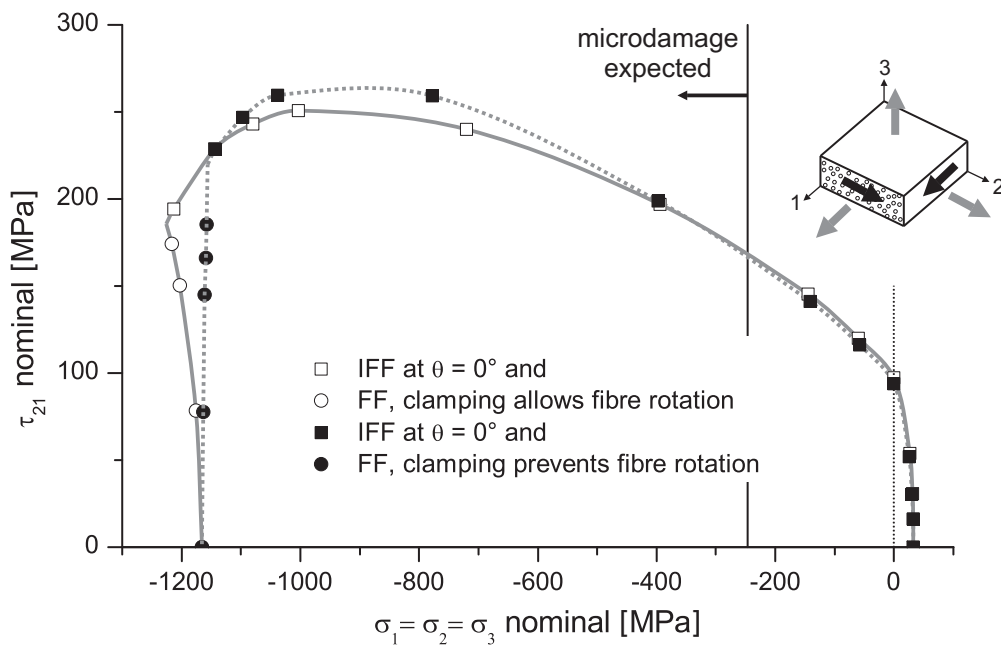


Figure 7.2: Results of test case 2 for two different clamping situations: The fibre-perpendicular side clamped allows fibre rotation, the fibre-parallel clamping prevents fibre rotation.

The result of test case 2 (see Fig. 7.2) is the fracture curve of a UD carbon/epoxy lamina for varied ratios of the applied shear stress τ_{21} and normal stresses $\sigma_1 = \sigma_2 = \sigma_3$. Continuing through test cases 3 and 4 these cases address the effect of hydrostatic pressure on the mechanical properties of a lamina [111]. In the tensile regime the applied state of stress leads to transverse fractures due to tensile σ_n on the respective fracture plane.

These fractures are promoted by additional τ_{n1} due to the applied τ_{21} . In the compressive regime the equal amount of σ_2 and σ_3 excludes fractures due to τ_{nt} on any action plane (see Eq. 4.3). At the same time the bearable τ_{n1} rises with increasing compressive stress σ_n^c on the fracture plane resulting in a high amount of bearable τ_{21} if it is combined with high $\sigma_2 = \sigma_3$ -values. For a decreasing ratio between τ_{21} and compressive $\sigma_1 = \sigma_2 = \sigma_3$ the failure mode eventually changes to fibre fracture due to compressive σ_1 . Using the extended FF criterion (see Sec. 4.7), the lamina bears more compressive σ_1 than the given longitudinal compressive strength $R_{||}^c = 950$ MPa. The according true FF stress is -1463 MPa, which is reached at the plotted nominal value of -1165 MPa.

Although having stated that a compressive $\sigma_2 = \sigma_3$ does not lead to an IFF according to the application of Puck's Theory, which predicts – by definition – macroscopic fracture, there are experimental findings that micro-damage starts at $\sigma_2 = \sigma_3 \approx -2R_{\perp}^c$. This conclusion has been drawn from acoustic emission studies [23], but the prediction of these micro-defects merging to a macroscopic crack [110] is still a challenging task and far beyond engineering application. Hence the corresponding thresholds are included (see Secs. 7.2.2 and 7.2.2) for information only but there is the possibility that micro-defects merge to macroscopic IFF before the predicted failures at high hydrostatic pressures may occur.

The high amount of bearable τ_{21} leads to a considerable change in fibre direction if permitted by the applied boundary conditions. For the nominal hydrostatic pressure of -600 MPa the γ_{21} -results of test case 4 (see Fig. 7.4) provide the magnitude of the fibres' rotation. Rotations of that magnitude increase the discrepancy between applied nominal stresses and the true stresses which the failure analysis is based on. Therefore the plot shows the results for two different boundary conditions where either the (x_1, x_3) - or the (x_2, x_3) -plane of the material is fixed in space. Regarding the FF, the bearable σ_1 slightly increases with rotated fibres because now σ_1 is only partly acting in the fibre's longitudinal direction.

Note that in the present case of a geometrically nonlinear analysis the constitutive behaviour influences the stress results as they are derived from the deformed geometry (see Sec. 3.6). As the bearable shear stresses are considerably above those bearable under a pure τ_{21} -loading, the given nonlinear $\tau_{21}(\gamma_{21})$ -relation is exceeded. In such cases we have proposed the use of a self-similarly scaled stress-strain relation (see Sec. 3.1.2). However in the present case of rather small nonlinearities in the given $\tau_{21}(\gamma_{21})$ -relation the effort of a separate iteration for every point on the fracture curve seems not rewarding, hence we decided to step back to a linear $\tau_{21}(\gamma_{21})$ -relation for test case 2 and 3.

Test case 3

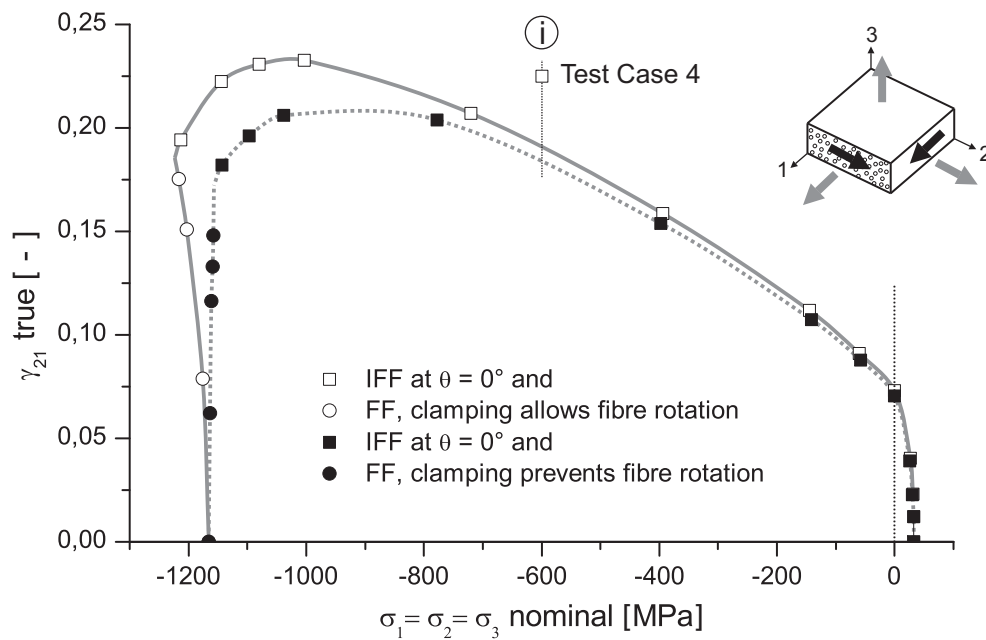


Figure 7.3: Results of test case 3 for the two different clamping situations.

The result of test case 3 shows the γ_{21} -values of the fractures predicted for test case 2 in both clamping cases (see Fig. 7.3). The shown strain values are expected to be slightly lower than if calculated following the iterative approach for nonlinear stress-strain relations (see Secs. 3.1.2 and 7.2.2). This fact can also be discovered by comparing the failure strains of test case 3 and 4 (see Fig. 7.3, i).

Test case 4

The result of test case 4 (see Fig. reffig:Case4) is a $\tau_{21}(\gamma_{21})$ -curve after the application of a $\sigma_1 = \sigma_2 = \sigma_3 = -600$ MPa pre-load on the same lamina as used in case 2 and 3. As stated above, the compressive $\sigma_2 = \sigma_3$ does not lead to any τ_{nt} on either of the action planes but leads to a constant compressive $\sigma_n = \sigma_2 = \sigma_3$ for any action plane orientation θ .

As compressive σ_n adds a portion to the intrinsic fracture resistance of the action plane against shear – here $R_{v_{\perp\parallel}}^A$ is of importance only – the applied preload can be represented by adding an induced fracture resistance $\sigma_n \cdot p_{\perp\parallel}^c$ to $R_{v_{\perp\parallel}}^A$ if analytically calculated. However, in FEA it is no problem to include a load history and thus the existing routine needs no modification. Both approaches result in a bearable shear of $\tau_{21} = 252$ MPa. In contrast to

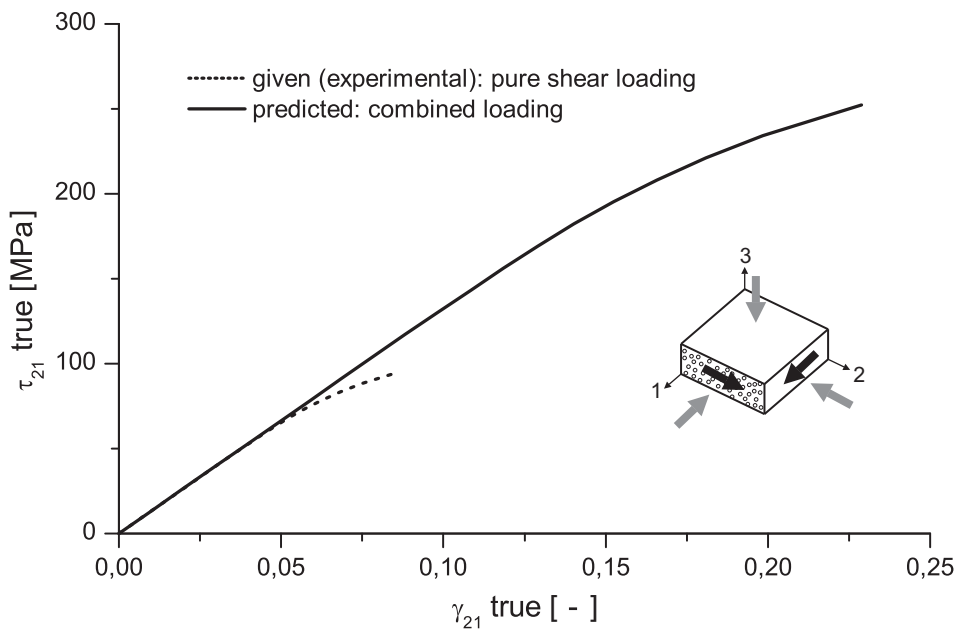


Figure 7.4: Results of test case 4, the clamping allows fibre rotation.

test case 3 we applied the iterative scaling of the $\tau_{21}(\gamma_{21})$ -relation for this particular load case (see Sec. 3.1.2) and figure 7.4 shows the predicted *nonlinear* behaviour.

Test case 5

The results of test case 5 form a fracture curve of a glass/epoxy lamina for varied combinations of σ_2 and $\sigma_3 = \sigma_1$ (see Fig. 7.5). It is dominated by IFFs, fibre fractures only occur close to the axis of hydrostatic pressure. The fact that the IFF part of the curve has no discontinuities is due to the application of η_{m+p} (see Sec. 4.3.2 and Fig. 4.10). The result figure includes a comparison between the simple FF criterion where only σ_1 is decisive and the improved criterion (see Sec. 4.7). In the latter case the additional stresses in the fibre due to the different Poisson's ratios in the matrix and the fibre are considered, thus the fibre fracture shows a dependence on the applied transverse stresses. The dependence visible in the case of the simple FF criterion is due to geometric nonlinearities only (see Sec. 3.6). The threshold for micro-damage is included for information only (see Sec. 7.2.2) but points out the possibility that micro-defects merge to macroscopic IFF before the predicted FF may occur.

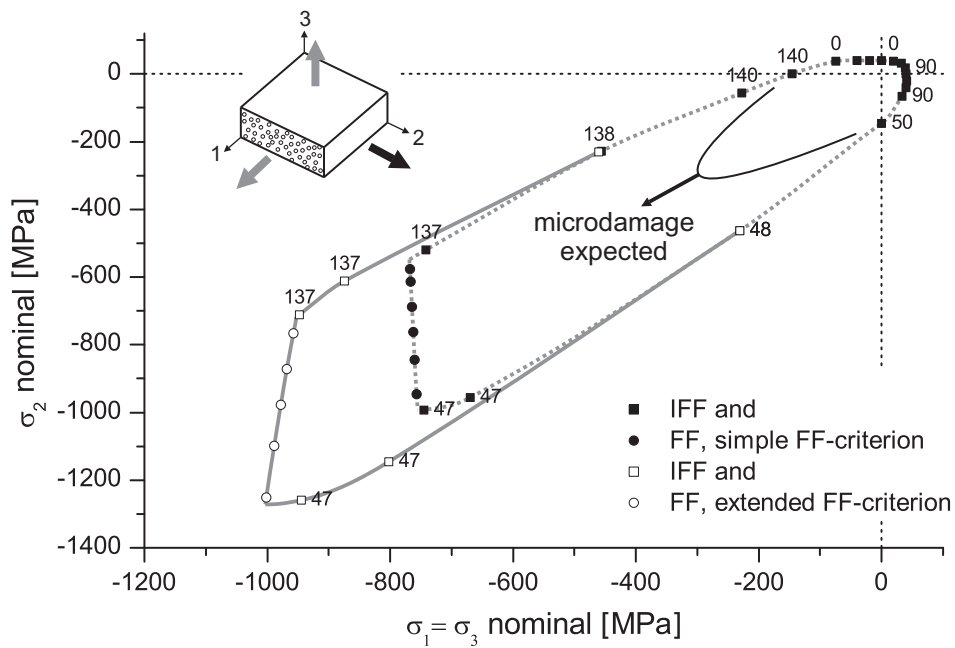


Figure 7.5: Results of test case 5 indicating the fracture angle θ_{fp} [deg]: Comparison between simple and extended fibre fracture criterion.

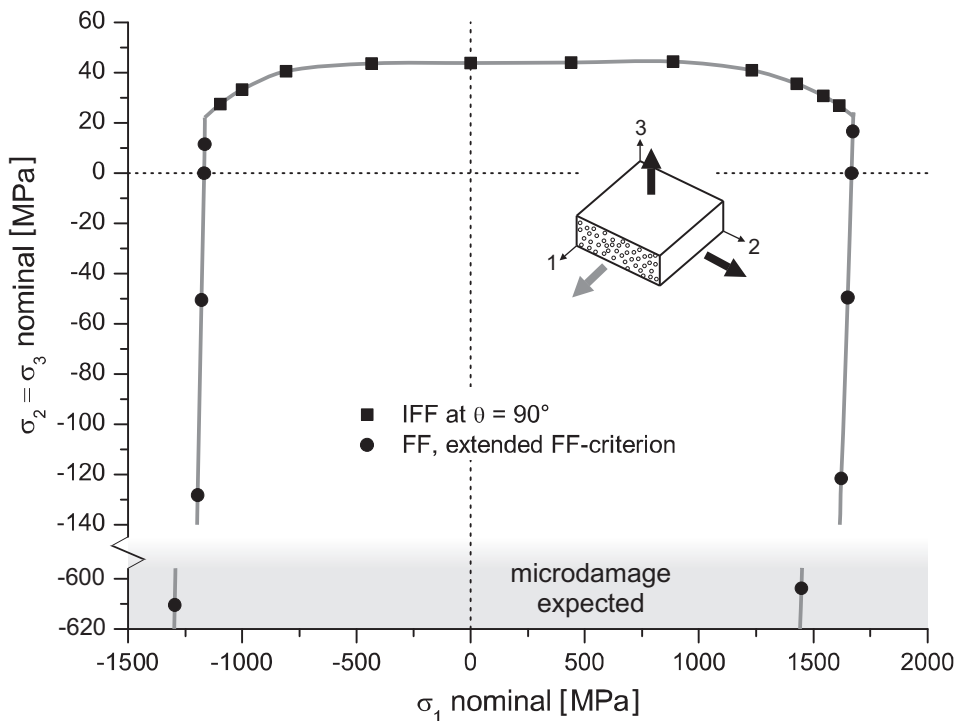


Figure 7.6: Results of test case 6: GFRC.

Test cases 6 and 7

The results of test cases 6 and 7 are the fracture curves of a glass/epoxy and carbon/epoxy lamina for varied combinations of σ_1 and $\sigma_2 = \sigma_3$ (see Figs. 7.6 and 7.7). These curves

– the predicted FF is reached experimentally depends on how fast the growing micro-defects merge to a macroscopic IFF beyond $\sigma_1 = \sigma_2 = \sigma_3 = -2R_{\perp}^c$ [110]. This process is expected to be highly dependent on the experimental setup.

Regarding the fibre fractures please note that the lines are not vertical – the reason is the extended FF-criterion with its dependence on transverse stresses. The comparison between the fibre fractures of test case 6 and 7 reveals a stronger dependence in the case of glass fibre reinforced composites (see Fig. 7.6). This is the result of a larger magnification factor $m_{\sigma f}$ for GFRC (1.3) than for CFRC (1.1, see Sec. 4.7).

Regarding the fracture angle θ please note that in test case 6 there is a predicted value of $\theta = 90^\circ$ although there is $\sigma_2 = \sigma_3$ both in nominal and in true stresses. This is the result of the given through-thickness tensile strength which is lower than the transverse tensile strength. The implemented routine is capable of differentiating between the two given strengths $R_{\perp 2}^t$ and $R_{\perp 3}^t$ and calculates the valid tensile strength $R_{\perp}^t(\theta)$ depending on the orientation of the respective action plane. This means that the calculation of the stress exposure $f_E(\theta)$ on a plane oriented at $\theta = 0^\circ$ is automatically based on $R_{\perp}^t(\theta) = R_{\perp 2}^t$ while that on a plane at $\theta = 90^\circ$ is dealt with on the basis of $R_{\perp}^t(\theta) = R_{\perp 3}^t$. The definition of $R_{\perp}^t(\theta)$ for an arbitrary orientation is done by an elliptical interpolation (see Eq. 7.1). In test case 7 both strengths have the same value and the fracture angle becomes a random value.

$$R_{\perp}^t(\theta) = \frac{R_{\perp 3}^t}{\sqrt{1 - a^2 \cdot \cos^2 \theta}} \quad \text{with} \quad a = \frac{\sqrt{R_{\perp 2}^t{}^2 - R_{\perp 3}^t{}^2}}{R_{\perp 2}^t} \quad (7.1)$$

7.2.3 Laminate test cases

Test case 8

This test case deals with a symmetric ± 35 glass/epoxy laminate where the ratio between $\sigma_x = \sigma_z$ and σ_y is varied (see Fig. 7.8). The influence of residual stresses due to thermal expansion is insignificant for most sections of the curve excluding those in the positive σ_y -regime (see Fig. 7.9). Here the tensile residual stresses in 2-direction lower the load carrying capacity of the laminate against the applied tensile load σ_y while the load carrying capacity against σ_z stays unaffected.

The location of the first ply failure is arbitrary since all the laminae are experiencing the same state of stress. While tensile σ_z excludes that any post failure degradation process results in a higher bearable load (see Fig. 7.8, 1st and 2nd quadrant), for any other load

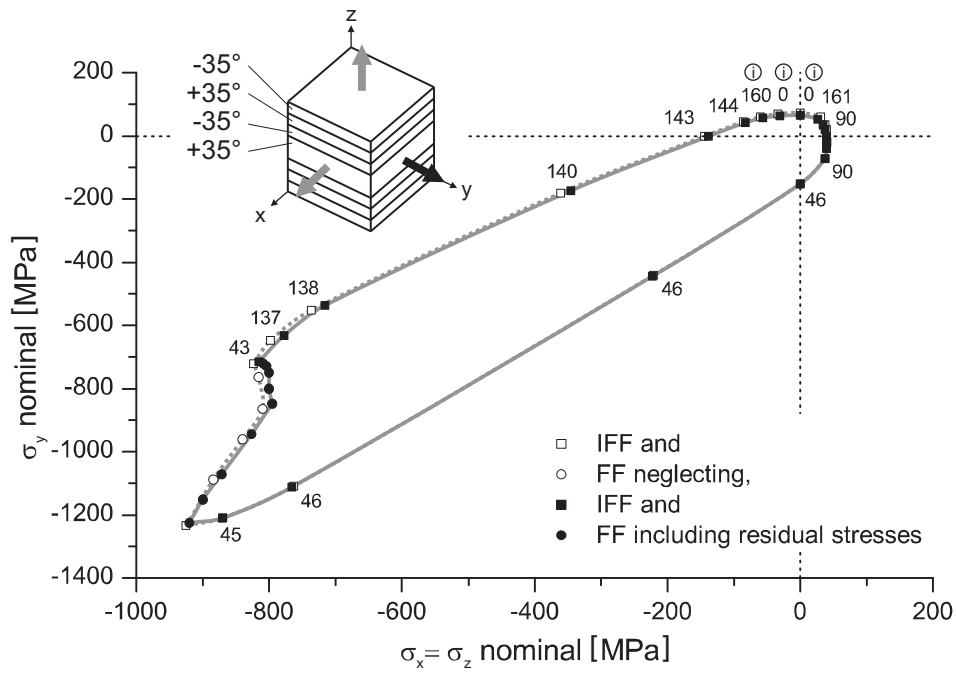


Figure 7.8: Results of test case 8 indicating the orientation of the fracture plane θ_{fp} [°] in an arbitrary lamina.

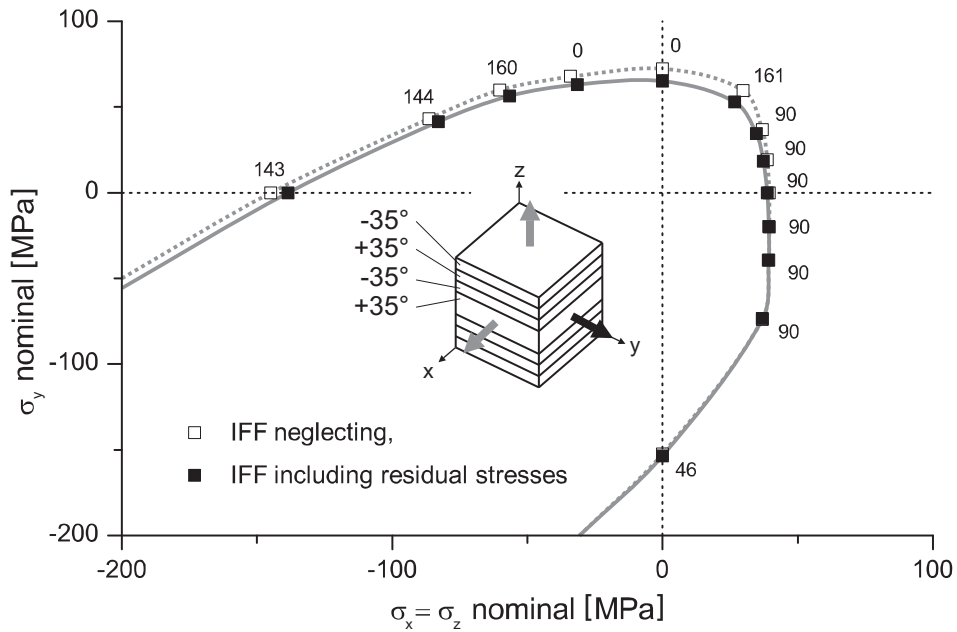


Figure 7.9: Zoom of the results of test case 8 indicating the orientation of the fracture plane θ_{fp} [°] in an arbitrary lamina.

case no load redistribution among the laminae is possible either. Where tensile σ_y leads to tensile σ_n on the IFF plane (see Fig. 7.8, i), an unstable degradation process is expected to begin where the remaining load carrying capacity results from known mutually sup-

porting effects of the successively disintegrating laminae [6]. This process is not covered by our continuum-based smeared damage representation. In the remaining load cases (mainly 3rd quadrant) we assume that the inclined IFFs are transmitting compressive σ_n like before the fracture. Such fractures are *generally* classified as non-tolerable IFFs due to their wedge effect (see Secs. 4.2.4 and 5). Without being able to predict the quantity of the resulting forces in thickness direction that promote local splitting or delamination, it is evident that these are absorbed to a certain extent by the present compressive σ_z . Therefore figure 7.10 provides a final fibre-failure curve assuming that no splitting or delamination occurs during the degradation process. During the degradation process the relevant inplane shear moduli rapidly reduce to a defined residual value of 25% of the initial value [4, 88].

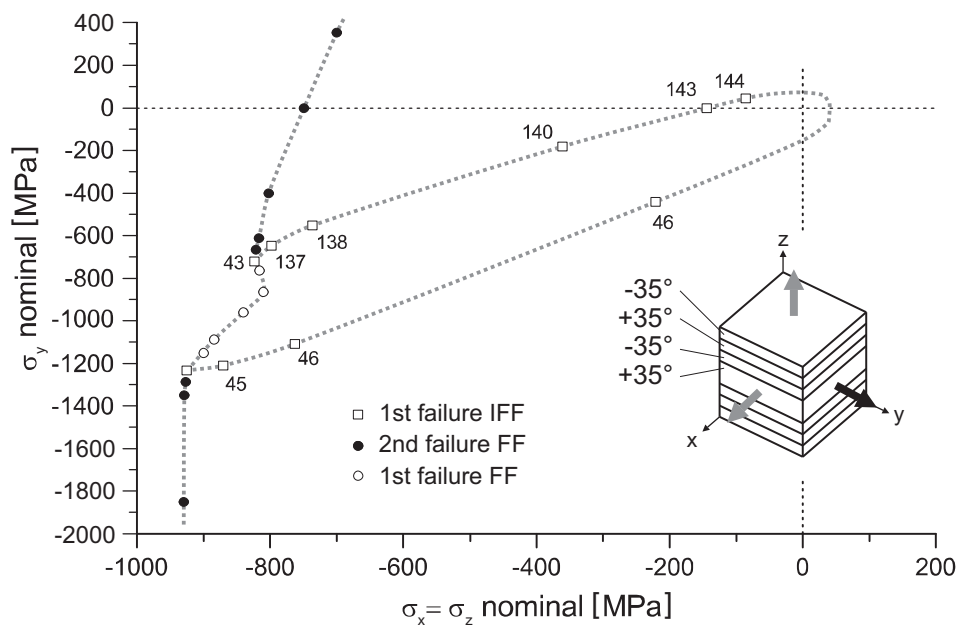


Figure 7.10: Test case 8: Initial inter-fibre failure and final fibre failure for those load cases that result in compressive σ_n (residual stresses neglected).

Test case 9

The results show the deformation of the above lamina while increasingly loaded until $\sigma_x = \sigma_y = \sigma_z = -100$ MPa (see Fig. 7.11). Keeping this level for σ_x and σ_z , the compressive σ_y is further increased until fracture. The nominal fracture stress corresponds to the according load case in test case 8 (see Fig. 7.8). It is judged unlikely that the small amount of compressive σ_z absorbs the wedge effect (see Sec. 5.3.2) hence no degradation process is started after inter-fibre failure.

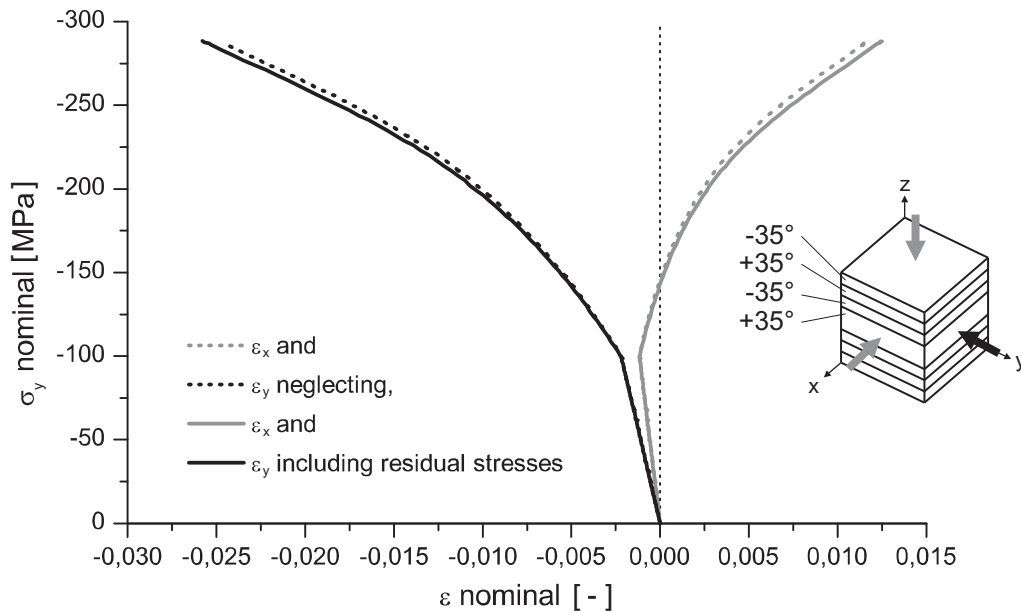


Figure 7.11: Results of test case 9.

Test cases 10 and 11

The two test cases deal with symmetric $0/90/\pm 45$ (case 10) and $0/90$ (case 11) carbon/epoxy laminates loaded with a varied ratio between σ_z and τ_{yz} (see Fig. 7.12). The fracture curves of both cases are identical, because it is the 0° -ply which fails in both cases while experiencing identical states of stress. It is remarkable that the influence of residual stresses increases from no influence under pure tensile σ_z -loading to its maximum under pure compressive loading – always keeping in mind that there is no residual stress in the material's through-thickness direction! The residual stresses in the material's 2-direction do not influence the stresses on the fracture plane due to tensile σ_z at $\theta_{fp} = 90^\circ$. However they do influence the stresses on a fracture plane at $\theta_{fp} = 41^\circ$ or 139° as it arises from pure compressive σ_z . In this case, the tensile residual stresses in 2-direction lower the compressive stress σ_n on the fracture plane and consequently lower its fracture resistance against τ_{nt} (see Sec. 4.2.3).

Test case 12

The results show the *deformation* of the test case 11 laminate under compressive σ_z (see Fig. 7.13). The result is based on the scaled $\sigma_3(\epsilon_3)$ -relation presented in section 3.1.2. While the deformation in z-direction enters the nonlinear regime after half the nominal fracture stress applied, $\epsilon_x = \epsilon_y$ stays in the linear regime until fracture. The fracture

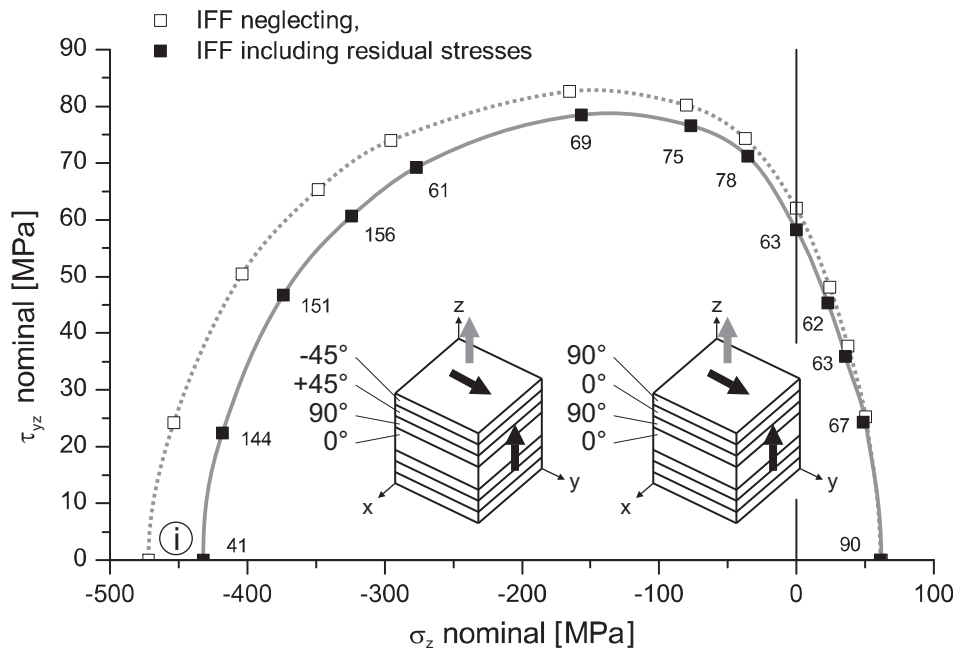


Figure 7.12: Results of test cases 10 and 11.

stresses correspond to figure 7.12, i.

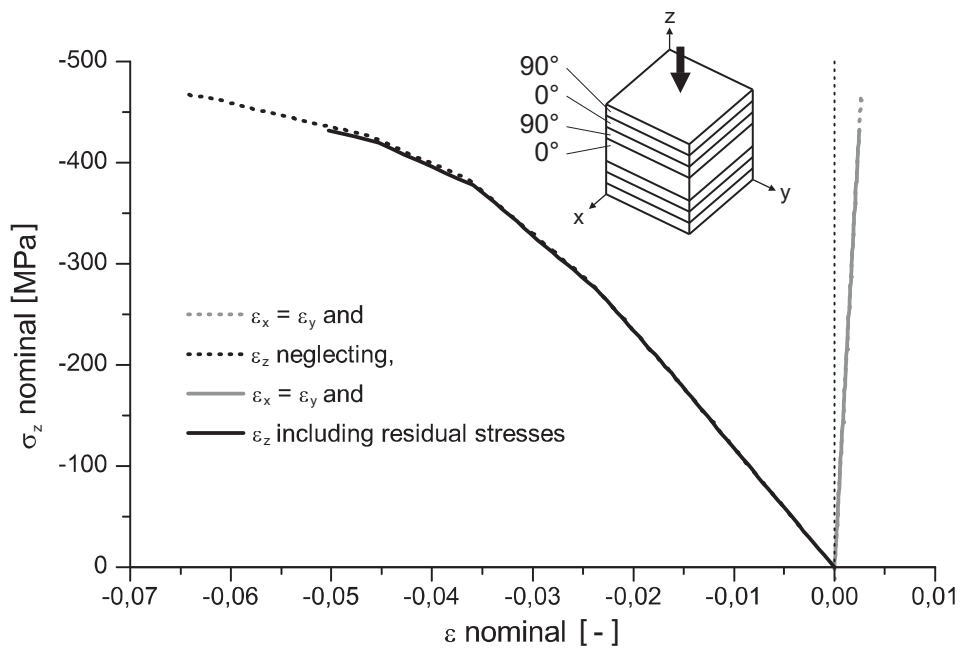


Figure 7.13: Results of test case 12.

8 Conclusion and Outlook

The 3D work-over and verification of Puck's Theory, the development of a three-dimensional degradation rule and the implementation and application within a commercial FEA package have gained significant knowledge in the field of 3D fracture analysis, FEA and RVE application to UD fibre/polymer laminae, laminates and laminate structures regarding the following aspects:

1. Stress analysis

- In terms of 3D stress analysis of laminates and laminate structures the use of numerical FEA has turned out to be efficient and reliable enough to keep up with any conceivable spatial extension to existing analytical methods (see Ch. 3). The modelling of stacking sequences and laminate structures is convenient, efficient and transparent in contemporary commercial FEA packages.
- An appropriate nonlinear constitutive model for UD FRCs is commonly not included in commercial packages, particularly in the case of interactions between transverse and shear deformation (see Sec. 3.1.3). The potential three-dimensional adaptation of an existing 2D approach covering these interactions has been rejected. Its range of validity has turned out to be too narrow to cover the stronger interactions in the case of 3D load and its stress-based character is inconvenient for the FEA implementation. A self-similar scaling of the uniaxially determined stress-strain relations has been developed instead and successfully applied to the test cases.
- The quality of stress analyses accomplished by the different approaches provided by commercial FEA packages has been evaluated. An analytical solution by Pagano which has been reconstructed and applied to a multi-layered laminate plate, serves as reference (see Sec. 3.4). The comparison points out, that solid continuum elements provide fully three-dimensional stress results exclusively. Despite their extraordinary high computational cost, they have been chosen as the basis of any detailed three-dimensional failure analysis of laminae and laminates.
- For the determination of general laminate behaviour the Representative Volume Element (RVE) approach provides homogenised laminate results without any undesired boundary effects (see Sec. 3.5). Applying periodic boundary conditions, the

results represent the material behaviour of the entire laminate independent from its lateral extensions.

- The ability of contemporary FEA packages to perform geometrically nonlinear analysis is particularly valuable in the present case. When running a geometrically nonlinear FE analysis the incremental load is applied to the deformed geometry. Regarding UD composites this means that fibre rotations are considered in all the results automatically (see Secs. 3.6 and 7.2.2).
- Regarding thermal residual stresses, the combination of Puck's Theory and FEA offers a complete decoupling of the failure analysis from that topic. The cooling down process of the laminate is represented in a separate analysis step before the outer load is applied. The following failure analysis needs no modification, whether thermal stresses are considered or not (see Sec. 3.7).

2. Puck's failure theory

- The physical and fracture mechanical basis and the spacial character of Puck's fibre- and inter-fibre fracture criteria have been thoroughly approved by the present work. Where adaptations of the previously published relations have been made they are to be attributed to the commonly inplane focussing of the model's application, never to two-dimensional restrictions of the actual theory (see Ch. 4).
- It has become evident that an applied 3D stress state may result in a significantly larger number of highly loaded action planes than a two-dimensional problem will ever be able to. Accordingly Puck's η_{m+p} -extension to Mohr's fracture hypothesis gains superior importance (see Sec. 4.3.2). It accounts for the stress exposures on all the action planes by adding a portion to the stress exposure of the fracture plane.
- Despite the decided differentiation between fibre and inter-fibre fracture, Puck's Theory accounts for mutual influences between fibre-parallel and fibre-perpendicular load. The η_{w1} -extension accounts for the influence of fibre-parallel stresses on inter-fibre fractures. Thus a σ_1 -loading close to the longitudinal strength of a lamina significantly lowers its IFF resistance (see Sec. 4.3.1). The extended fibre fracture criterion accounts for the influence of transverse and through-thickness stresses on the fibre fracture. Both, the Poisson's effects and the local stress concentration around the fibres, are included (see Sec. 4.7).

- Originally developed for intrinsically brittle UD FRPC laminae, Puck's Theory turned out to be extraordinary versatile. It has successfully been adapted to isotropic, pure matrix material which does not behave intrinsically brittle in the present case (see Secs. 4.6 and 7.2.1).
- In the 3D context it is emphasised that Puck's Theory is capable of differentiating between given strengths in the transverse and through-thickness direction. Within the WWFE-II the routine accounts for the two given strengths $R_{\perp 2}^t$ and $R_{\perp 3}^t$ and calculates the valid tensile strength $R_{\perp}^t(\theta)$ depending on the orientation of the respective action plane (see Sec. 7.2.2).

3. Three-dimensional post failure degradation analysis

- Existing degradation processes have turned out to be insufficient for the application within fully three-dimensional post-failure degradation analyses (see Ch. 5). Having several Young's moduli and shear stiffnesses available for degradation, the appropriate 3D procedure has to be related to the fracture plane orientation.
- The degradation of a lamina confined within a laminate is a process based on load redistribution among neighbouring laminae. The requirements for such a stable degradation have been identified. The ability of potential degradation approaches to differ between stable and unstable damage evolution has been judged to be the main attribute (see Sec. 5.1).
- Based on analytical thoughts the angle-dependent impact of the degradation on the different stiffnesses has been characterised (see Sec. 5.5). The approach is based on the constant stress exposure hypothesis (see Sec. 5.3.2) and relates the reduction of the relevant stiffnesses to the current fracture plane orientation.
- The developed approach has been validated by means of virtual material test. RVEs of laminates containing discrete cracks were loaded in several directions to determine the homogenised material behaviour in the sense of a smeared crack representation (see Sec. 5.6). The results have proven the basic applicability of the developed analytical relations until the general material behaviour depending on the fracture plane orientation and the crack density will have been determined.
- The RVE-results have revealed, that an orthotropic material is insufficient to describe the constitutive behaviour of a successively damaging lamina. Couplings

between shear and normal deformations have been identified as well as a sensitivity against the algebraic sign of load (see Sec. 5.6.2).

4. Implementation into FEA

- The implementation and application of Puck's action plane-related fibre and inter-fibre fracture criteria in the frame of the commercial FE-package ABAQUS turned out to be straightforward (see Ch. 6). Being a stress-based and three-dimensional theory ab initio, the calculation of the stress exposures including the corrections η_{w1} and η_{m+p} may be carried out within a simple post processing routine. This fact qualifies Puck's criteria for the application to conventionally derived or even already existing FE analysis results for a large group of application-orientated users.
- Only if advanced problems like coupled nonlinearities or degradation processes are to be included, more demanding extensions to the standard FE analysis are necessary in form of a user defined material model.
- The present implementation takes into account nonlinear constitutive behaviour for shear, transverse, and through-thickness compression. However, being subject to combined compressive σ_2 and σ_3 , the material bears much higher loadings than the uniaxial experiments provide stress-strain relations for. As the interval of validity of existing formulations has been exceeded by far, a self-similar scaling approach has been developed (see Sec. 3.1.3).
- Regarding explicit FE analysis for dynamic situations, the currently iterative determination of the IFF stress exposure and the degradation measure has been identified as a drawback.

5. Application

- Implementing Puck's Theory into FEA has resulted in a consistent method for the analysis of all 12 test cases (see Ch. 7). An *identical* user-defined material subroutine has been applied to isotropic, lamina and laminate material and qualified for the application on the specimen or structural level.
- Although being an action plane-related fracture criterion, it requires less experimentally determined parameters than competing approaches. Puck's Theory includes

- many additional parameters for adjustment purposes whose recommended values are profoundly based on existing experimental data.
- Puck's Theory predicts open IFF fracture curves in cases of equal compressive σ_2 and σ_3 (see test cases 1, 6 and 7, Secs. 7.2.1 and 7.2.2). Going along with the intuitive imagination that such a combination will not be able to produce any macroscopic IFF, this load combination clearly exceeds the capability of a macroscopic model. It is known, when the micro-damage starts yet the speed at which these nuclei merge to a macroscopic failure is expected to be strongly dependent on the experimental setup and its prediction within a continuum-based model is highly questionable. In the hydrostatic pressure case the fracture curves are closed by predicted fibre fractures (see test case 5, Sec. 7.2.2).
 - The three-dimensional load cases of the WWFE-II rarely enabled a stable degradation process to start (see Sec. 7.1). The determination of the complete three-dimensional constitutive behaviour of a damaging lamina is judged to be rather important in the case of changing applied loads than for the analysis of a damage evolution process due to 3D load.

The identified future issues are as widespread as the FEA failure analysis of UD FRCs itself and concern various numerical and experimental fields. Regarding the pre-fracture constitutive behaviour, the development of a sophisticated material model including three-dimensionally interacting nonlinearities is an outstanding problem. Due to the expected growing complexity of the material description the more efficient FE representation of structures which are thin compared to their lateral extension becomes inevitable. In this context the further negligence of through-thickness quantities is not acceptable for a detailed failure analysis. The determination of the fracture angle-dependent homogenised behaviour of a damaging lamina is an issue to both, the experimental and numerical field. RVEs containing the discrete crack representation of a damaging laminate will be of great value if their required periodicity is expanded from displacement to stress boundary conditions. The general applicability of Puck's Theory to complex geometries and load histories will rise after closed solutions for the stress exposure and the degradation measure have been derived as available for inplane load cases.

In summary Puck's Theory turned out to be an promising failure and post failure prediction approach in terms of three-dimensional application. It's modular structure allows the used-friendly implementation within FEA despite the fact that it is stress-based and the degradation procedures rely on secant moduli. The presented results emphatically suggest the use of Puck's Theory within FEA. The present work reveals an extraordinary positive

ratio between additional effort and additional knowledge about the failure and post failure processes within the analysed lamina.

Appendix

A Derivation of the Pagano analytical solution

This appendix presents a condensed derivation of the Pagano analytical solution following [36, 67] and [112]. The regarded laminate is loaded and supported following equation 3.11 and figure 3.5. It consists of several lamina (index i) which are stacked together in the positive z -direction. Each lamina extends in through-thickness direction from z_i^{bottom} to z_i^{top} , the whole laminate from $z = -t/2$ to $+t/2$. All the laminae behave orthotropic but may be of different material and/or may be individually oriented. This results in an individual constitutive behaviour for each lamina following equation 3.3 with individual stiffness matrices \underline{E}_i , here in the Pagano notation:

$$\begin{bmatrix} \sigma_x \\ \sigma_y \\ \sigma_z \\ \tau_{yz} \\ \tau_{xz} \\ \tau_{xy} \end{bmatrix} = \begin{bmatrix} C_{11i} & C_{12i} & C_{13i} & 0 & 0 & 0 \\ C_{12i} & C_{22i} & C_{23i} & 0 & 0 & 0 \\ C_{13i} & C_{23i} & D_{33i} & 0 & 0 & 0 \\ 0 & 0 & 0 & C_{44i} & 0 & 0 \\ 0 & 0 & 0 & 0 & C_{55i} & 0 \\ 0 & 0 & 0 & 0 & 0 & c_{66i} \end{bmatrix} \cdot \begin{bmatrix} \epsilon_x \\ \epsilon_y \\ \epsilon_z \\ \gamma_{yz} \\ \gamma_{xz} \\ \gamma_{xy} \end{bmatrix} \quad (\text{A.1})$$

Though the relation above is lamina-related as equation 3.3, it is formed in the common, i.e. global laminate coordinate system (see Sec. 2.1), thus *here* equation 3.4 is not applicable without an appropriate transformation in the case of arbitrary lamina orientations β_i . Note that Pagano [67] uses a different order of the components in the Voight notation. The following derivation is **strictly layer-wise** thus the layer-defining **index i** is **omitted until further notice**.

The kinematic relations are

$$\begin{aligned} \epsilon_x &= \frac{\partial u_x}{\partial x} = u_{x,x} \quad ; \quad \epsilon_y = \frac{\partial u_y}{\partial y} = u_{y,y} \quad ; \quad \epsilon_z = \frac{\partial u_z}{\partial z} = u_{z,z} \\ \gamma_{yz} &= \frac{\partial u_y}{\partial z} + \frac{\partial u_z}{\partial y} = u_{y,z} + u_{z,y} \quad ; \quad \gamma_{xz} = \frac{\partial u_x}{\partial z} + \frac{\partial u_z}{\partial x} = u_{x,z} + u_{z,x} \\ \gamma_{xy} &= \frac{\partial u_x}{\partial y} + \frac{\partial u_y}{\partial x} = u_{x,y} + u_{y,x} . \end{aligned} \quad (\text{A.2})$$

Equation A.2 put into equation A.1 allows to form the derivations requested in the equilibrium equation 3.10 and the result is a linearly coupled partial differential equations

system (see Eq. A.3). The queried displacement field $\bar{u}(x, y, z)$ is a solution of the equations system, which currently depends on the stiffness matrix \underline{E} of the respective lamina only.

$$\begin{aligned} C_{11} \cdot u_{x,xx} + C_{66} \cdot u_{x,yy} + C_{55} \cdot u_{x,zz} + (C_{12} + C_{66}) \cdot u_{y,xy} + (C_{13} + C_{55}) \cdot u_{z,xz} &= 0 \\ (C_{12} + C_{66}) \cdot u_{x,xy} + C_{66} \cdot u_{y,yy} + C_{22} \cdot u_{y,yy} + C_{44} \cdot u_{y,zz} + (C_{23} + C_{44}) \cdot u_{z,yz} &= 0 \\ (C_{13} + C_{55}) \cdot u_{x,xz} + (C_{23} + C_{44}) \cdot u_{y,yz} + C_{55} \cdot u_{z,xx} + C_{44} \cdot u_{z,yy} + C_{33} \cdot u_{z,zz} &= 0 \end{aligned} \quad (\text{A.3})$$

The queried solution of equation A.3 has to satisfy the interlaminar stress and displacement boundary conditions (see Tab. 3.2), the laminate displacement boundary conditions (see Eqs. 3.12 and 3.13) and the following laminate stress boundary conditions:

$$\begin{aligned} \sigma_z \left(z = +\frac{t}{2} \right) &= q_0(x, y) ; \quad \sigma_z \left(z = -\frac{t}{2} \right) = 0 \\ \tau_{xz} \left(z = \pm\frac{t}{2} \right) &= \tau_{yz} \left(z = \pm\frac{t}{2} \right) = 0 \end{aligned} \quad (\text{A.4})$$

The following ansatz – one product term for each of the three orthogonal displacements – fulfils all boundary conditions mentioned above [113]:

$$\begin{aligned} u_x &= U(z) \cdot \cos(px) \cdot \sin(qy) = 0 \\ u_y &= V(z) \cdot \sin(px) \cdot \cos(qy) = 0 \\ u_z &= W(z) \cdot \sin(px) \cdot \sin(qy) = 0 \end{aligned} \quad (\text{A.5})$$

$$\text{with } U(z) = U^* \cdot e^{s \cdot z} ; \quad V(z) = V^* \cdot e^{s \cdot z} ; \quad W(z) = W^* \cdot e^{s \cdot z}$$

$$\text{and } p = \frac{\pi}{a} ; \quad q = \frac{\pi}{b}$$

Differentiated and put into equation A.3 the resulting equation system defines the parameter s introduced above:

$$\begin{bmatrix} C_{11} p^2 + C_{66} q^2 - C_{55} s^2 & (C_{12} + C_{66}) p q & -(C_{13} + C_{55}) p s \\ (C_{12} + C_{66}) p q & C_{22} q^2 + C_{66} p^2 - C_{44} s^2 & -(C_{23} + C_{44}) q s \\ (C_{13} + C_{55}) p s & (C_{23} + C_{44}) q s & C_{55} p^2 + C_{44} q^2 - C_{33} s^2 \end{bmatrix} \cdot \begin{bmatrix} U^* \\ V^* \\ W^* \end{bmatrix} = \begin{bmatrix} 0 \\ 0 \\ 0 \end{bmatrix} \quad (\text{A.6})$$

The following simplified term leads to the solutions of s which represent the eigenvalues of the matrix in equation A.6:

$$-A \cdot s^6 + B \cdot s^4 + C \cdot s^2 + D = 0 \quad (\text{A.7})$$

The abbreviations A , B , C , and D result from a parameter comparison with equation A.6 and depend on the material parameters C_{ij} , p and q only, thus are constants for the respective lamina.

By means of the substitution $\gamma = s^2 - \frac{B}{3A}$ equation A.7 becomes

$$\gamma^3 + d \cdot \gamma + f = 0 \quad (\text{A.8})$$

$$\text{with } d = -\frac{C}{A} - \frac{1}{3} \left(\frac{B}{A} \right)^2 ; \quad f = -\frac{2}{27} \left(\frac{B}{A} \right)^3 - \frac{1}{3} \frac{B \cdot C}{A^2} - \frac{D}{A}.$$

In the case of $\frac{f^2}{4} + \frac{d^3}{27} < 0$, which was the case for all composite materials analysed by Pagano, the results for γ are

$$\begin{aligned} \gamma_1 &= 2 \cdot \sqrt{\frac{|d|}{3}} \cdot \cos\left(\frac{\Phi}{3}\right) \\ \gamma_2 &= -2 \cdot \sqrt{\frac{|d|}{3}} \cdot \cos\left(\frac{\Phi}{3} + \frac{\pi}{3}\right) \\ \gamma_3 &= -2 \cdot \sqrt{\frac{|d|}{3}} \cdot \cos\left(\frac{\Phi}{3} - \frac{\pi}{3}\right) \end{aligned} \quad (\text{A.9})$$

$$\text{with } \cos \Phi = \frac{-f\sqrt{27}}{2\sqrt{|d|^3}}.$$

After a re-substitution there are three pairs of eigenvalues

$$s_j = \pm \sqrt{\gamma_j + \frac{B}{3A}} \quad \text{for } j = 1, 2, 3; \quad s_j \in \mathfrak{R}, \mathfrak{I} \quad (\text{A.10})$$

which may partly be imaginary. Now there is the basis on which the eigenvectors can be formed whereas the procedure varies whether s_j is positive and real, negative and real, positive an imaginary or negative and imaginary. This is a lengthy algebraic procedure which produces the solution for the queried displacement field by a linear combination of the eigenvectors [112]. During this procedure it turns out that it is convenient to present the solution based on

$$m_j = \left| \gamma_j + \frac{B}{3A} \right|^{\frac{1}{2}} \quad \text{for } j = 1, 2, 3 \quad (\text{A.11})$$

in combination with a case differentiation between $\gamma_j + \frac{B}{3A} > 0$ and $\gamma_j + \frac{B}{3A} < 0$ rather than based on s_j .

The displacement field of equation A.5 is now completely described by

$$\begin{aligned} U(z) &= \sum_{j=1}^3 U_j(z) \\ V(z) &= \sum_{j=1}^3 L_j \cdot U_j(z) \\ W(z) &= \sum_{j=1}^3 R_j \cdot W_j(z) \end{aligned} \quad (\text{A.12})$$

with

$$\begin{aligned} U_j(z) &= F_j \cdot C_j(z) + G_j \cdot S_j(z) \\ W_j(z) &= G_j \cdot C_j(z) + \alpha_j \cdot F_j \cdot S_j(z) \end{aligned} \quad (\text{A.13})$$

and

$$\begin{aligned} C_j(z) &= \begin{cases} \cosh(m_j \cdot z) & \text{for } \gamma_j + \frac{B}{3A} > 0 \\ \cos(m_j \cdot z) & \text{for } \gamma_j + \frac{B}{3A} < 0 \end{cases} \\ S_j(z) &= \begin{cases} \sinh(m_j \cdot z) & \text{for } \gamma_j + \frac{B}{3A} > 0 \\ \sin(m_j \cdot z) & \text{for } \gamma_j + \frac{B}{3A} < 0 \end{cases} \\ \alpha_j &= \begin{cases} 1 & \text{for } \gamma_j + \frac{B}{3A} > 0 \\ -1 & \text{for } \gamma_j + \frac{B}{3A} < 0 \end{cases} \end{aligned} \quad (\text{A.14})$$

and the lamina's material specific constants

$$\begin{aligned} L_j &= \frac{p q}{J_j} \{ \alpha_j m_j^2 [C_{33} (C_{12} + C_{66}) - (C_{23} + C_{44}) (C_{13} + C_{55}) - (C_{12} + C_{66}) (C_{55} p^2 + C_{44} q^2)] \} \\ R_j &= \frac{p m_j}{J_j} [\alpha_j m_j^2 C_{44} (C_{13} + C_{55}) - (C_{13} + C_{55}) (C_{66} p^2 + C_{22} q^2) + q^2 (C_{23} + C_{44}) (C_{12} + C_{66})] \\ J_j &= C_{33} C_{44} m_j^4 + \alpha_j m_j^2 [-p^2 (C_{44} C_{55} + C_{33} C_{66}) + q^2 (C_{23}^2 - C_{22} C_{33} + 2C_{23} C_{44})] \\ &\quad + (C_{66} p^2 + C_{22} q^2) (C_{55} p^2 + C_{44} q^2) . \end{aligned} \quad (\text{A.15})$$

The displacement field \bar{u}_i of the respective lamina i now contains six free parameters F_{j_i} and G_{j_i} by which it is adjusted to the required boundary conditions. It is furthermore defined by the lamina-specific parameters m_{j_i} , L_{j_i} , R_{j_i} and J_{j_i} and the lamina specific parameter functions $C_{j_i}(z)$ and $S_{j_i}(z)$ (three values/functions each).

The stress components can now be derived by putting the displacement field into equations A.2 and A.1:

$$\sigma_x(x, y, z) = \sin(px) \cdot \sin(qy) \cdot \sum_{j=1}^3 M_{x_j} \cdot U_j(z) \quad (\text{A.16})$$

$$\text{with } M_{x_j} = -p C_{11} - q C_{12} L_j + \alpha_j m_j R_j C_{13}$$

$$\sigma_y(x, y, z) = \sin(px) \cdot \sin(qy) \cdot \sum_{j=1}^3 M_{y_j} \cdot U_j(z) \quad (\text{A.17})$$

$$\text{with } M_{y_j} = -p C_{12} - q C_{22} L_j + \alpha_j m_j R_j C_{23}$$

$$\sigma_z(x, y, z) = \sin(px) \cdot \sin(qy) \cdot \sum_{j=1}^3 M_{z_j} \cdot U_j(z) \quad (\text{A.18})$$

$$\text{with } M_{z_j} = -p C_{13} - q C_{23} L_j + \alpha_j m_j R_j C_{33}$$

$$\tau_{yz}(x, y, z) = \sin(px) \cdot \sin(qy) \cdot \sum_{j=1}^3 N_j \cdot W_j(z) \quad (\text{A.19})$$

$$\text{with } N_j = m_j L_j + q R_j$$

$$\tau_{xz}(x, y, z) = \sin(px) \cdot \sin(qy) \cdot \sum_{j=1}^3 T_j \cdot W_j(z) \quad (\text{A.20})$$

$$\text{with } T_j = m_j + p R_j$$

$$\tau_{xy}(x, y, z) = \sin(px) \cdot \sin(qy) \cdot \sum_{j=1}^3 Q_j \cdot U_j(z) \quad (\text{A.21})$$

$$\text{with } Q_j = q + p L_j$$

Regarding a laminate consisting of n layers, there are $6n$ unknown free parameters. The displacement boundary conditions regarding the support (see Eqs. 3.12 and 3.13) are fulfilled by the ansatz (see Eq. A.5) automatically, but there are six (6) laminate stress boundary conditions (see Eq. A.4). According to table 3.2 each of the $n - 1$ interlaminar interfaces provides three (3) displacement boundary conditions

$$\begin{aligned} u_{x_i}^{top} &= u_{x_{i+1}}^{bottom} \\ u_{y_i}^{top} &= u_{y_{i+1}}^{bottom} \\ u_{z_i}^{top} &= u_{z_{i+1}}^{bottom} \end{aligned} \quad (\text{A.22})$$

and three stress boundary conditions

$$\begin{aligned} \sigma_{z_i}^{top} &= \sigma_{z_{i+1}}^{bottom} \\ \tau_{xz_i}^{top} &= \tau_{xz_{i+1}}^{bottom} \\ \tau_{yz_i}^{top} &= \tau_{yz_{i+1}}^{bottom} . \end{aligned} \quad (\text{A.23})$$

The sum of $6 + (n - 1) \cdot 6$ boundary conditions allows the unambiguous determination of the $6n$ free parameters of all the involved laminae.

B WWFE-II test cases

B.1 Given Instructions

Excerpt of the original instructions provided for the WWFE-II:

INSTRUCTIONS TO CONTRIBUTORS

The following provides general guidelines and instructions that you may find helpful when writing your paper and making your submission.

1. The in-plane loads (section stresses) should be applied in the x and y directions defined in the diagrams provided for each laminate.
2. The through-thickness stresses should be applied in the z-direction.
3. The section stresses σ_x and σ_y are defined in the usual way as the in-plane loads per unit width divided by the total thickness of the laminate.
4. Unless otherwise stated, please assume that the loads are increased monotonically, keeping any combination of the following ratios $\sigma_x/\sigma_y/\sigma_z/\tau_{xy}/\tau_{xz}/\tau_{yz}$ constant¹.
5. Please, record and tabulate the magnitude of the stresses (and if appropriate the type and location of failure as well as the mode of failure) at which each failure is predicted.
6. Repeat the calculation to cover the range of stress ratios (2 or 4 quadrants) indicated by the graphs provided for each laminate.
7. If possible, please plot the results using the scales provided for each laminate.
8. Draw curves through the results to represent the initial (inner), and final (outer) failure envelopes. Indicate any intermediate failure points/curves. Figure 13 shows a schematic of failure envelopes representing various stages of failure. The aim of this figure is to illustrate what a failure envelope is. It is possible that not all the envelopes will be closed and, in this case, please indicate the stress ratios and stress regime where the envelope is open.
9. For the stress strain curves, please plot the section stress versus strain curves as requested for particular laminates using the scales provided.
10. It would be extremely helpful if you would also send us your tables of results, but these will probably not be included in the paper. Results in the form of data files sent to us by E-mail or other accessible forms (e.g. CD) would be appreciated.
11. We are asking all of the contributors to use the same material properties even if you have reservations about the values provided.
12. Your theory may not require all the lamina properties provided (e.g. some models and computer programs assume linear elastic properties). In that case please employ your

¹ For Test Cases No 4 and 9, please refer to the notes below Table No 4.

usual assumptions and neglect any information which is not needed.

13. If your theory requires additional (or different) information from that provided, please let us know as soon as possible and we will endeavour to provide that information. If you have default values for any missing parameters (e.g. interaction coefficients), we prefer you to use those.
14. In some cases the theory employed may not be intended to be applied to the whole range of laminates specified here. In that case, you may opt to analyse only some of the laminates but please explain the reasons for not analysing the other laminates in your paper.
15. The paper should describe your failure theory and method of application to laminates in sufficient detail to allow your predictions to be reproduced by others, comment on the nature and the effects of the failures predicted and, if appropriate, how your predictions could be used for design.

After receiving all the theoretical papers for publications, the experimental results will be superimposed on the theoretical predictions. The superimposed graphs will be sent back to you together with tables of the experimental results for your future use and information on how the experimental results were obtained.

The second paper (Part B) would present graphs of superimposed results with any comment you may wish to make on the correlation between experiment and theory. You may choose to add a figure (or figures) and appropriate sections to demonstrate refinement or particular features of your approach. You could indicate any future development to your theory which would allow you to consider a wider variety of laminates than those you are able to analyse immediately.

For those participants who have integrated failure analyses and structural analysis packages, details of the specimen geometries that you may opt to analyse as part of the second paper, will be sent as soon as you request them.

B.2 Given material parameters

Excerpt of the original instructions provided for the WWFE-II:

Table (1) Mechanical properties for four unidirectional laminae

Fibre type	IM7	T300	A-S	S2-glass	E-Glass
Matrix	8551-7	PR-319	Epoxy1	Epoxy2	MY750
Fibre volume fraction V_f (%)	60	60	60	60	60
Longitudinal modulus E_1 (GPa)	165*	129	140*	52	45.6
Transverse modulus E_2 (GPa)	8.4	5.6+	10	19	16.2
Through-thickness modulus E_3 (GPa)	8.4	5.6+	10	19	16.2
In-plane shear modulus G_{12} (GPa)	5.6*	1.33+	6*	6.7*	5.83*
Transverse shear modulus G_{13} (GPa)	5.6*	1.33+	6*	6.7*	5.83*
Through-thickness shear modulus G_{23} (GPa)	2.8	1.86	3.35	6.7	5.7
Major Poisson's ratio ν_{12}	0.34	0.318	0.3	0.3	0.278
Major transverse Poisson's ratio ν_{13}	0.34	0.318	0.3	0.3	0.278
Through-thickness Poisson's ratio ν_{23}	0.5	0.5	0.49	0.42	0.4
Longitudinal tensile strength X_T (MPa)	2560	1378	1990	1700	1280
Longitudinal compressive strength X_C (MPa)	1590	950	1500	1150	800
Transverse tensile strength Y_T (MPa)	73	40	38	63	40
Transverse compressive strength Y_C (MPa)	185**	125**	150**	180**	145**
Through-thickness tensile strength Z_T (MPa)	63	40	38	50	40
Through-thickness compressive strength Z_C (MPa)	185**	125**	150**	180**	145**
In-plane shear strength S_{12} (MPa)	90**	97**	70**	72**	73**
Transverse shear strength S_{13} (MPa)	90**	97**	70**	72**	73**
Through-thickness shear strength S_{23} (MPa)	57	45	50	40	50
Longitudinal tensile failure strain ϵ_{1T} (%)	1.551	1.07	1.42	3.27	2.807
Longitudinal compressive failure strain ϵ_{1C} (%)	1.1	0.74	1.2	2.21	1.754
Transverse tensile failure strain ϵ_{2T} (%)	0.87	0.43	0.38	0.33	0.246
Through-thickness compressive failure strain ϵ_{2C} (%)	3.2	2.8	1.6	1.5	1.2
Transverse tensile failure strain ϵ_{3T} (%)	0.755	0.43	0.38	0.263	0.246
Through-thickness compressive failure strain ϵ_{3C} (%)	3.2	2.8	1.6	1.5	1.2
In-plane shear failure strain γ_{12u} (%)	5	8.6	3.5	4	4
Transverse shear failure strain γ_{13u} (%)	5	8.6	3.5	4	4
Through-thickness shear failure strain γ_{23u} (%)	2.1	1.5	1.5	0.59	0.88
Longitudinal thermal coefficient α_1 ($10^{-6}/^\circ\text{C}$)	-1	-1	-1	8.6	8.6
Transverse thermal coefficient α_2 ($10^{-6}/^\circ\text{C}$)	18	26	26	26.4	26.4
Through-thickness thermal coefficient α_3 ($10^{-6}/^\circ\text{C}$)	18	26	26	26.4	26.4
Stress free temperature ($^\circ\text{C}$)	177	120	120	120	120

* Initial modulus

** Nonlinear behaviour and stress strain curves and data points are provided

+ Please note that values are considered to be low, compared with typical data for the same material published somewhere else or quoted by the manufacturers. We have not attempted to change them in order to facilitate a comparison with test data in Part B of the exercise.

Table (2) Mechanical properties of fibres

Fibre type	IM7	T300	AS	S2-glass	E-Glass
Longitudinal modulus E_{f1} (GPa)	276	231	231	87	74
Transverse modulus E_{f2} (GPa)	19	15	15	87	74
Transverse modulus E_{f3} (GPa)	19	15	15	87	74
In-plane shear modulus G_{f12} (GPa)	27	15	15	36	30.8
Major Poisson's ratio ν_{f12}	0.2	0.2	0.2	0.2	0.2
Major Poisson's ratio ν_{f13}	0.2	0.2	0.2	0.2	0.2
Transverse shear modulus G_{f23} (GPa)	7	7	7	36	30.8
Longitudinal tensile strength X_{f1T} (MPa)	5180	2500	3500	2850	2150
Longitudinal compressive strength X_{f1C} (MPa)	3200	2000	3000	2450	1450
Longitudinal tensile failure strain ϵ_{f1T} (%)	1.87	1.086	1.515	3.27	2.905
Longitudinal compressive failure strain ϵ_{f1C} (%)	1.16	0.869	1.298	2.82	1.959
Longitudinal thermal coefficient α_{f1} ($10^{-6}/^{\circ}\text{C}$)	-0.4	-0.7	-0.7	5	4.9
Transverse thermal coefficient α_{f2} ($10^{-6}/^{\circ}\text{C}$)	5.6	12	12	5	4.9
Through-thickness thermal coefficient α_{f3} ($10^{-6}/^{\circ}\text{C}$)	5.6	12	12	5	4.9

Table (3) Mechanical properties of various matrices

Matrix type	8551-7 epoxy	PR319 epoxy	Epoxy1	Epoxy2	MY750
Elastic Modulus E_m (GPa)	4.08	0.95+	3.2	3.2	3.35
Elastic Shear modulus G_m (GPa)	1.478	0.35+	1.2	1.2	1.24
Elastic Poisson's ratio ν_m	0.38	0.35	0.35	0.35	0.35
Tensile strength Y_{mT} (MPa)	99	70	85	73	80
Compressive strength Y_{mC} (MPa)	130	130	120	120	120
Shear strength S_m (MPa)	57	41	50	52	54
Tensile failure strain ϵ_{mT} (%)	4.4	7.3	2.65	2.5	2.7
Compressive failure strain ϵ_{mC} (%)	9	13.6	3.75	5	5
Shear failure strain γ_m (%)	5.1	11.5	4.16	6	6
Thermal expansion coefficient α_m ($10^{-6}/^{\circ}\text{C}$)	46.7	60	58	58	58

+ These values are considered to be low, compared with typical data for the same material published somewhere else or quoted by the manufacturers. We have not attempted to change them in order to facilitate a comparison with test data in Part B of the exercise.

The behaviour of materials PR319 and Epoxy1 is taken as linear

B.3 Given load cases

Excerpt of the original instructions provided for the WWFE-II:

Table (4) Details of the Test Cases

Test Case	Laminate lay-up	Material	Description of Required Prediction
1	Resin	MY750 epoxy	σ_x versus σ_z (with $\sigma_y = \sigma_z$) envelope
2	0°	T300/PR319	τ_{12} versus σ_2 (with $\sigma_1 = \sigma_2 = \sigma_3$) envelope
3	0°	T300/PR319	γ_{12} versus σ_2 (with $\sigma_1 = \sigma_2 = \sigma_3$) envelope
4(a)	0°	T300/PR319	Shear stress strain curves (τ_{12} - γ_{12}) (for $\sigma_1 = \sigma_2 = \sigma_3 = -600\text{MPa}$)
5	90°	E-glass/MY750 epoxy	σ_2 versus σ_3 (with $\sigma_1 = \sigma_3$) envelope
6	0°	S-glass/epoxy	σ_1 versus σ_3 (with $\sigma_2 = \sigma_3$) envelope
7	0°	A-S carbon/epoxy	σ_1 versus σ_3 (with $\sigma_2 = \sigma_3$) envelope
8	$\pm 35^\circ$	E-glass/MY750 epoxy	σ_y versus σ_z (with $\sigma_x = \sigma_z$) envelope
9(b)	$\pm 35^\circ$	E-glass/MY750 epoxy	Stress-strain curves (σ_y - ϵ_x and σ_y - ϵ_y) at $\sigma_z = \sigma_x = -100\text{MPa}$
10	(0°/90°/ $\pm 45^\circ$)s	IM7/8551-7	τ_{yz} versus σ_z (with $\sigma_y = \sigma_x = 0$) envelope
11	(0°/90°)s	IM7/8551-7	τ_{yz} versus σ_z (with $\sigma_y = \sigma_x = 0$) envelope
12	(0°/90°)s	IM7/8551-7	Stress-strain curves (σ_z - ϵ_z , σ_z - ϵ_x and σ_z - ϵ_y) for $\sigma_y = \sigma_x = 0$

(a) Please first apply $\sigma_1 = \sigma_2 = \sigma_3 = -600\text{MPa}$ to the lamina. Then apply the shear loading till final failure takes place.

Please first apply $\sigma_y = \sigma_z = \sigma_x = -100\text{MPa}$ and record the resulting strain values. Then increase the stress σ_y (beyond -100MPa) gradually till final failure takes place. Please plot the full stress-strain curves (σ_y - ϵ_x and σ_y - ϵ_y).

C Material data of HexPly 8551-7 (IM7)

	$[N/mm^2]$ or $[-]$
E_1	165000
E_2	8400
E_3	8400
G_{12}	5600
G_{13}	5600
G_{23}	2800
ν_{12}	0.34
ν_{13}	0.34
ν_{23}	0.5

Table C.1: Material data of HexPly 8551-7 (IM7) from [114] used for the Pagano analytical solution (see Sec. 3.4) and the RVE studies of discrete cracks (see Sec. 5.6).

Bibliography

- [1] G. Marsh. Composites lift off in primary aerostructures. *Reinforced Plastics*, 48(4):22–27, 2004.
- [2] M.J. Hinton, A.S. Kaddour, and P.D. Soden (Eds.). *Failure Criteria in Fibre Reinforced Polymer Composites: The World-Wide Failure Exercise*. Elsevier, 2004.
- [3] G. Busse, B.-H. Kröplin, and F.K. Wittel (Eds.). *Damage and its Evolution in Fiber-Composite Materials*. ISD Verlag, 2006.
- [4] M. Knops. *Analysis of Failure in Fiber Polymer Laminates: The Theory of Alfred Puck*. Springer, 2008.
- [5] A. Puck and H. Schürmann. Failure analysis of FRP laminates by means of physically based phenomenological models. *Composites Science and Technology*, 58(7):1045–1067, 1998.
- [6] A. Puck and H. Schürmann. Failure analysis of FRP laminates by means of physically based phenomenological models. *Composites Science and Technology*, 62(12/13):1633–1662, 2002.
- [7] A. Puck. Festigkeitsberechnung an Glasfaser/Kunststoff-Laminaten bei zusammengesetzter Beanspruchung: Bruchhypothese und schichtenweise Bruchanalyse. *Kunststoffe*, 59:780–787, 1969.
- [8] ABAQUS Inc. *ABAQUS Analysis User's manual*, v6.61 edition, 2006.
- [9] H.M. Deuschle, W. Lutz, H. Gerger, and S. Schmauder. Simulation of Photoelasticity in a Glass Fibre Polymer Matrix Composite. In G. Busse, B.-H. Kröplin, and F.K. Wittel, editors, *Damage and its Evolution in Fiber-Composite Materials*. ISD Verlag, Stuttgart, 2006.
- [10] H.M. Deuschle, F.K. Wittel, H. Gerhard, G. Busse, and B.-H. Kröplin. Investigation of progressive failure in composites by combined simulated and experimental photoelasticity. *Computational Materials Science*, 38(1):1–8, 2006.
- [11] F. Raischel, F. Kun, R.C. Hidalgo, and H.J. Herrmann. Statistical Damage Models: Fibre Bundle Models. In G. Busse, B.-H. Kröplin, and F.K. Wittel, editors, *Damage and its Evolution in Fiber-Composite Materials*. ISD Verlag, Stuttgart, 2006.

- [12] R.M. Jones. *Mechanics of Composite Materials*. McGraw-Hill, 1975.
- [13] A. Puck. Zur Beanspruchung und Verformung von GFK-Mehrschichtverbund-Bauelementen – Teil 1: Grundlagen der Spannungs- und Verformungsanalyse. *Kunststoffe*, 57(4):284–293, 1967.
- [14] L.J. Gibson and M.F. Ashby. *Cellular Solids: Structure and Properties*. Cambridge University Press, 2nd edition, 1999.
- [15] R. Talreja (Ed.). *Comprehensive Composite Materials*. Elsevier, 2000.
- [16] J. Aboudi. *Mechanics of Composite Materials – A Unified Micromechanical Approach*. Elsevier, 1991.
- [17] M. Paley and J. Aboudi. Micromechanical Analysis of Composites by the Generalized Cells Model. *Mechanics of Materials*, 14:127–139, 2006.
- [18] J. Lemaitre and J.L. Chaboche. *Mechanics of Solid Materials*. Cambridge University Press, 1990.
- [19] J. Lemaitre. *A Course on Damage Mechanics*. Springer, 2nd edition, 1996.
- [20] D. Raabe. *Computational Material Science: The Simulation of Material's Microstructures and Properties*. Wiley-WCH, 1998.
- [21] A. Puck. Should Fibre-Plastics Composites be designed with Strain or Stress Criteria. *Kunststoffe - German Plastics*, 82(5):34–38 & 431–434, 1992.
- [22] B. Schlehöfer and A. Mattern. Research of the suitability of GRP pipes for long distance hot water transportation. *Fernwärme Int.*, 10(4):194–198, 1981.
- [23] J.W. Kopp. *Contribution to the Stress and Strength Analysis of Unidirectionally Fibre Reinforced Plastics*. PhD thesis, RWTH Aachen, Institut für Kunststoffverarbeitung (IKV), 2000.
- [24] W. Michaeli, M. Knops, O. Fischer, and D. Eifel. Investigations on the fiber fracture behaviour of carbon fiber reinforced plastics. In *Proceedings of Intern. SAMPE Symposium & Exhibition*. Long Beach, CA, 2002.
- [25] O. Fischer. *Fibre Fracture Behaviour in Fibre Reinforced Plastics*. PhD thesis, RWTH Aachen, Institut für Kunststoffverarbeitung (IKV), 2003.

- [26] M. Mannigel. *Influence of Shear Stresses on the Fibre Failure Behaviour in Carbon Fibre Reinforced Plastics (CFRP)*. PhD thesis, RWTH Aachen, Institut für Kunststoffverarbeitung (IKV), 2007.
- [27] L.J. Hart-Smith. Predictions of a generalized maximum-shear-stress failure criterion for certain fibrous composite laminates. *Composites Science and Technology*, special issue 58:1179–1208, 1998.
- [28] L.J. Hart-Smith. Predictions of the original and truncated maximum strain failure models for certain fibrous composite laminates. *Composites Science and Technology*, special issue 58:1151–1178, 1998.
- [29] S. Lütze. Confocal laser scanning photoelasticity: Improvement of precision for quantitative photoelastic studies on model composite materials. *SCANNING The J. of Scanning Microscopies*, 23(4):273–278, 2001.
- [30] F.K. Wittel, F. Kun, and H.J. Herrmann. Simulation of Damage and Fracture in Composites using a Discrete Element Approach. In G. Busse, B.-H. Kröplin, and F.K. Wittel, editors, *Damage and its Evolution in Fiber-Composite Materials*. ISD Verlag, Stuttgart, 2006.
- [31] S. Predak, H. Gerhard, I. Solodov, O. Bullinger, N. Davidson, and W. Lutz. Short fibre reinforced thermoplastics. In G. Busse, B.-H. Kröplin, and F.K. Wittel, editors, *Damage and its Evolution in Fiber-Composite Materials*. ISD Verlag, Stuttgart, 2006.
- [32] D. Huybrechts. *Ein erster Beitrag zur Verifikation des wirkebenebezogenen Zwischenfaserbruchkriteriums nach Puck*. Verlagshaus Mainz, Aachen, 1996. Technisch-wissenschaftlicher Bericht IKV, vol.44.
- [33] R. Krüger. *Delaminationswachstum in Faserverbundlaminate*. PhD thesis, Universität Stuttgart, ISD, 1996.
- [34] S. Essebier. *Berechnung dynamischer Delaminationsvorgänge in Faserverbundplatten*. PhD thesis, Universität Stuttgart, ISD, 1999.
- [35] M. D’Ottavio and M. König. Numerical Models for Delamination. In G. Busse, B.-H. Kröplin, and F.K. Wittel, editors, *Damage and its Evolution in Fiber-Composite Materials*. ISD Verlag, Stuttgart, 2006.
- [36] N.J. Pagano (Ed.). *Interlaminar Response of Composite Materials*. Elsevier, 1989.

- [37] P.P. Camanho and C.G. Davila. Mixed-Mode Decohesion Finite Elements for the Simulation of Delamination in Composite Materials. *NASA/TM*, 211737(4):1–37, 2002.
- [38] ABAQUS Inc. *ABAQUS Analysis User's manual*, v6.5 edition, 2004. Sec. 18.5.
- [39] A. Puck. *Festigkeitsanalyse von Faser-Matrix-Laminaten: Modelle für die Praxis*. Hanser Verlag, 1996. available online at <http://www.klub.tu-darmstadt.de/forschung/download.php>.
- [40] J. Garbe and A. Puck. Erfahrungen mit Bruchkriterien an schwellend belasteten GFK-Drehfedern. *Kunststoffe*, 83(5):406–411, 1993.
- [41] ZF Friedrichshafen AG. Focus on ultralight chassis. Technical report, 25.06.2009. press release.
- [42] P. Gall. FE-Analyse einer Fahrzeugachse aus Faserverbund. Master's thesis, ISD Universität Stuttgart, 2009.
- [43] S. Fell, T. Güll, R. Immel, T. Schütz, V. Schultheis, M. Shubert, and W. Oelerich. CAE-Prozesskette zur Festikeits- und Crashanalyse von Hochdrucktanks aus nassgewickeltem Faser-Kunststoff-Verbund. *NAFEMS Magazin*, 9(1):20–33, 2008.
- [44] I.M. Daniel and O. Ishai. *Engineering Mechanics of Composite Materials*. Oxford University Press, 1994.
- [45] A. Puck and M. Mannigel. Physically based nonlinear stress-strain relations for the inter-fibre fracture analysis of FRP laminates. *Composites Science and Technology*, 67(9):1955–1964, 2007.
- [46] M. D'Ottavio. *Advanced Hierarchical Models of Multilayered Plates and Shells Including Mechanical and electrical Interfaces*. PhD thesis, Universität Stuttgart, Institut für Statik und Dynamik der Luft- und Raumfahrtkonstruktionen (ISD), 2008.
- [47] K. Washizu. *Variational Methods in Elasticity and Plasticity*. Pergamon Press, 3rd edition, 1982.
- [48] A.J.M. Spencer. *Deformation of Fibre-reinforced Materials*. Oxford University Press, 1972.
- [49] E. Carrera. C_z^0 -Requirements – models for the two-dimensional analysis of multi-layered structures. *Composite Structures*, 37:373–383, 1997.

- [50] J.N. Reddy. *Energy Principles and Variational Methods in Applied Mechanics*. John Wiley, 2002.
- [51] H. Kraus. *Thin Elastic Shells*. John Wiley & Sons, 1967.
- [52] E. Reissner. The effect of transverse shear deformation on the bending of elastic plates. *J. of Applied Mechanics*, 12:69–76, 1945.
- [53] R.D. Mindlin. Influence of rotatory inertia and shear on flexural vibrations of isotropic, elastic plates. *J. of Applied Mechanics*, 18:31–38, 1951.
- [54] Y.M. Ghugal and R.P. Shimpi. A review of refined shear deformation theories of isotropic and anisotropic laminated plates. *J. of Reinforced Plastics and Composites*, 21:775–813, 2002.
- [55] K.P. Saldatos. A redefined laminated plate and shell theory with applications. *Journal of Sound and Vibration*, 144:109–129, 1991.
- [56] P.R. Hildebrand, E. Reissner, and G.B. Thomas. *Notes on the foundations of theory of small displacements of orthotropic shells*. National Advisory Committee for Aeronautics, 1949. Technical Report 1833.
- [57] K.H. Lo, R.M. Christensen, and E.M. Wu. A high-order theory of plate deformation – Part 1: Homogeneous plates, Part 2: Laminated Plates. *J. of applied Mechanics*, 44:663–668 & 669–676, 1978.
- [58] A.K. Noor and W.S. Burton. Assessment of computational models for multilayered shells. *Applied Mechanics Review*, 43:67–97, 1990.
- [59] J.N. Reddy and D.H. Robbins Jr. Theories and computational models for composite laminates. *Applied Mechanics Review*, 47:147–169, 1994.
- [60] E. Carrera. An assessment of mixed and classical theories on global and local response of multilayered orthotropic plates. *Composite Structures*, 50:183–198, 2000.
- [61] K.H. Lo, R.M. Christensen, and E.M. Wu. Stress solution determination for high order plate theory. *Int. J. of Solids and Structures*, 14:655–662, 1978.
- [62] J.M. Whitney. The effect of transverse shear deformation on the bending of laminated plates. *J. of Composite Material*, 3:534–547, 1969.
- [63] E. Carrera. Historical review of zig-zag theories for multilayered plates and shells. *Applied Mechanics Review*, 56:287–308, 2003.

- [64] S.A. Ambartsumyan. *Theory of Anisotropic Plates*. Technomic Publishing Company, 1970.
- [65] E. Reissner. On a certain mixed variational theorem and a proposed application. *Int. J. of Numerical Methods in Engineering*, 20(7):1366–1368, 1984.
- [66] E. Reissner. On a mixed variational theorem and on shear deformable plate theory. *Int. J. of Numerical Methods in Engineering*, 23(2):193–198, 1986.
- [67] N.J. Pagano. Exact Solutions for Rectangular bidirectional Composites and Sandwich Plates. *Journal of Composite Materials*, 4:20–34, 1969.
- [68] K. Girkmann. *Flächentragwerke*. Springer, 1946.
- [69] A.S. Kaddour and M.J. Hinton. 3D properties of unidirectional composite laminae and test problems used in WWFE-II. to be published.
- [70] W. Michaeli, D. Huybrechts, and M. Wegener. *Dimensionieren mit Faserverbundkunststoffen*. Hanser, 1995.
- [71] J.R. Vinson and R.L. Sierakowski. *The Behaviour of Composite Materials*. Martinus Nijhoff Publishers, 1986.
- [72] S.W. Tsai. *Composite Design – Think Composites*. Dayton, 1988.
- [73] K. Moser. *Faser-Kunststoff-Verbund*. VDI-Verlag, 1992.
- [74] R. Hill. Elastic properties of reinforced solids: Some theoretical principles. *J. of the Mechanics and Physics of Solids*, 11:352–372, 1963.
- [75] S. Nemat-Nasser and M. Hori. *Micromechanics: Overall properties of heterogeneous materials*. North-Holland, 1998.
- [76] M. D’Ottavio, F.K. Wittel, and J.Reiser. Mechanisms based Toolbox: Prototypical Implementation of Tools. In G. Busse, B.-H. Kröplin, and F.K.Wittel, editors, *Damage and its Evolution in Fiber-Composite Materials*. ISD Verlag, Stuttgart, 2006.
- [77] M. Willamowski. Untersuchung des Degradationsverhaltens von unidirektional verstärkten Faserverbundschichten im Fall von Zwischenfaserbrüchen. Master’s thesis, Institut für Statik und Dynamik der Luft- und Raumfahrtkonstruktionen (ISD), Universität Stuttgart, 2008.

- [78] J. Loose. Bestimmung der mechanischen Eigenschaften inhomogener Werkstoffe mit Hilfe des Konzeptes der repräsentativen Volumenelemente. Master's thesis, Institut für Statik und Dynamik der Luft- und Raumfahrtkonstruktionen (ISD), Universität Stuttgart, 2007.
- [79] P. Ludwik. *Elemente der technologischen Mechanik*. J. Springer, 1909.
- [80] L. Issler, H. Ruoff, and P. Häfele. *Festigkeitslehre – Grundlagen*. Springer, 2nd edition, 2003.
- [81] S.W. Tsai and E. Wu. A General Theory of Strength for Anisotropic Materials. *Journal of Composite Materials*, 5(1):58–80, 1971.
- [82] K.S. Liu and S.W. Tsai. A Progressive quadratic failure criterion for a laminate – Part A. *Composites Science and Technology*, 58:1023–1032, 1998.
- [83] M. Knops. Die wirkebenenbezogenen Bruchkriterien von Puck. In *Proc. of Dimensionieren mit Faserverstärkten Kunststoffen – IKV Fachtagung zur Kunststoffverarbeitung*. Aachen, 2008.
- [84] C.A. Coulomb. Sur une Application des Règles de Maximis et Minimis a quelques Problemes de Statique relatives a l'Architecture. In *Memoires de Mathematique et de Physique: Anné 1773*. Academie Royal des Sciences par divers Savans, Paris, France, 1776.
- [85] O. Mohr. Welche Umstände bedingen die Elastizitätsgrenze und den Bruch eines Materials. *Zeitschrift des VDI*, 24(45/46):1524–1541 & 1572–1577, 1900.
- [86] B. Paul. A Modification of the Coulomb-Mohr Theory of Fracture. *Journal of Applied Mechanics*, 28:259–268, 1961.
- [87] G. Lutz. The Puck theory of failure in laminates in the context of the new guideline VDI2014 Part 3. In *Proceedings of Conference on Damage in Composite Materials*. Stuttgart, 2006. available online at <http://www.ndt.net/v11n12.htm>.
- [88] VDI 2014/3. Development of Fibre-Reinforced Plastics components: Analysis. Technical report, Verein Deutscher Ingenieure e.V., Düsseldorf, 2006.
- [89] A. Puck, J. Kopp, and M. Knops. Guidelines for the determination of the parameters in Puck's action plane strength criterion. *Composites Science and Technology*, 62(3 & 9):371–378 & 1275, 2002.

- [90] P.P. Camanho, P. Maimí, and C.G. Dávila. Prediction of size effects in notched laminates using continuum damage mechanics. *Composites Science and Technology*, 67:2715–2727, 2007.
- [91] I.V. Papadopoulos. Critical plane approaches in high-cycle fatigue: On the definition of amplitude and mean value of shear stress acting on the critical plane. *Fatigue and Fracture of engineering Materials and Structures*, 21(3):269–285, 1998.
- [92] Institut für Kunststoffverarbeitung (IKV), RWTH Aachen. *COMPOSITOR: Hilfsmittel zur Analyse von Laminaten aus Faserverbundkunststoffen*, 3.0 edition, 2007.
- [93] S. Weihe, B. Kröplin, and R. de Borst. Classification of smeared crack models based on material and structural properties. *Int. Journal of Solids and Structures*, 35(12):1289–1308, 1998.
- [94] L. Lambrecht. Numerische Experimente zur Analyse der Einflussgrößen auf die Degradation von mehrschichtigem GFK-Laminat. Master's thesis, Institut für Kunststoffverarbeitung (IKV), RWTH Aachen, 2003.
- [95] M. Knops. *Gradual failure process in fibre/polymer laminates*. PhD thesis, RWTH Aachen, Institut für Kunststoffverarbeitung (IKV), 2003.
- [96] M. Knops and C. Bögle. Gradual failure process in fibre/polymer laminates. *Composites Science and Technology*, 66(5):616–625, 2006.
- [97] A. Matzenmiller, J. Lubliner, and R.L. Taylor. A constitutive model for anisotropic damage in fiber-composites. *Mechanics of Materials*, 20:125–152, 1995.
- [98] A. Puck and H.M. Deuschle. A simple physically based degradation model for FRP-UD laminate after onset of cracking caused by inter fibre fracture. 2009. short note submitted to *Composites Science and Technology*.
- [99] H. Schürmann. *Konstruieren mit Faser-Kunststoff-Verbunden*. Springer, 2nd edition, 2007.
- [100] A.L. Highsmith and K.L. Reifsnider. Damage in Composite Materials. In K.L. Reifsnider, editor, *ASTM STP 775*. American Society for Testing and Materials, Philadelphia, PA, 1982.
- [101] R. Talreja. Transverse cracking and stiffness reduction in cross ply laminates of different matrix toughness. *Journal of Composite Materials*, 26:1644–1663, 1992.

- [102] J.W. Hoover, D. Kujawski, and F. Ellyin. Transverse cracking of symmetric and unsymmetric glass-fibre/epoxy-resin laminates. *Composites Science and Technology*, 57:1513–1526, 1997.
- [103] C. Li, F. Ellyin, and A. Wharmby. On matrix crack saturation in composite laminates. *Composites Part B. Engineering*, 34:473–480, 2003.
- [104] E. Hinton and D.R.J. Owen. *An introduction to finite element computations*. Pineridge Press, 1981.
- [105] G.D. Smith. *Numerical solution of partial differential equations: finite difference methods*. Oxford University Press, 1985.
- [106] K.H. Huebner, D.L. Dewhurst, D.E. Smith, and T.G. Byrom. *The Finite Element Method for Engineers*. John Wiley & Sons, 4th edition, 2001.
- [107] D. Quabis. FEM-based Failure Analysis of UD Composites following Puck. Master's thesis, Institut für Statik und Dynamik der Luft- und Raumfahrtkonstruktionen (ISD), Universität Stuttgart, 2009.
- [108] T. Lindemann. Analytische Verfeinerungen der Puckschen Versagenshypthesen für Faserverbundmaterial. Master's thesis, Institut für Statik und Dynamik der Luft- und Raumfahrtkonstruktionen (ISD), Universität Stuttgart, 2009.
- [109] H.M. Deuschle and B.-H. Kröplin. FE Implementation of Puck's Failure Theory for Fibre Reinforced Composites under 3D-Stress. 2009. submitted to *Composites Science and Technology*.
- [110] F.K. Wittel. *Diskrete Elemente - Modelle zur Bestimmung der Festigkeitsevolution in Verbundwerkstoffen*. PhD thesis, Universität Stuttgart, ISD, 2006.
- [111] P.J. Hine, R.A. Duckett, A.S. Kaddour, M.J. Hinton, and G.M. Wells. The effect of hydrostatic pressure on the mechanical properties of glass fibre/epoxy unidirectional composites. *Composites Part A*, 36:279–289, 2005.
- [112] M. Hahn. 3D Spannungsanalyse von Faserverbundlaminaten: Vergleich von Finiten Volumen- und Schalenelementen mit der analytischen Lösung nach Pagano. Master's thesis, Institut für Statik und Dynamik der Luft- und Raumfahrtkonstruktionen (ISD), Universität Stuttgart, 2008.
- [113] C. Navier. Mémoires sur les lois de l'équilibre et du mouvement des corps solides élastiques. *Mém. Acad. Sci. Inst. Fr.*, 7:375–393, 1824.

- [114] Hexcel Company. Product Data HexPly 8551-7 (IM7).
http://www.hexcel.com/NR/rdonlyres/C7264B73-64EE-4CA1-ADC2-5573E6E98FB4/0/HexPly_8551_7_us.pdf, 2009.

Vita

Particulars:

Name	Heiko <u>Matthias</u> Deuschle
Date / place of birth	July 18, 1977 in Karlsruhe
Marital status	married
Nationality	German

Schools:

1984 – 1988	Pestalozzi Grundschule Rheinstetten
1988 – 1997	Walahfrid-Strabo-Gymnasium Rheinstetten
	Allgemeine Hochschulreife 05/1997

Civilian Service:

1997 – 1998	Arbeiter-Samariter-Bund Rheinstetten
-------------	--------------------------------------

Studies:

1998 – 2004	Aero- and astronautics engineering at the Universität Stuttgart
	Diplom-Ingenieur aer. 09/2004
	Doktor-Ingenieur aer. 09/2010

Professional activity:

since 09/2004	Research associate with the Institut für Statik und Dynamik der Luft- und Raumfahrtkonstruktionen at the Universität Stuttgart
since 01/2007	Teaching assistant with the Institut für Statik und Dynamik der Luft- und Raumfahrtkonstruktionen at the Universität Stuttgart
since 09/2010	FEM Calculation Engineer with Kolt Engineering, Böblingen, Germany

ISBN 3-930683-99-7